Chapter 1 Introduction

1.1 Dengue virus

Dengue viruses (DVs) are human pathogens and the infections affect up to 100 million individuals per year (McBride and Bielefeldt-Ohmann, 2000).

They belong to the genus Flavivirus within the family of *Flaviviridae*. Members of the genus are typically transmitted to vertebrates by mosquitoes or ticks and frequently cause significant human morbidity and mortality. In addition to DV, other human pathogens such as Japanese encephalitis virus (JEV), tick borne encephalitis virus, West Nile virus (WNV), yellow fever virus (YFV), and Kunjin virus (KUNV) are classified to this family (Beeck *et al.*, 2004).

DVs are comprised of four distinct serotypes, DV1 through DV4, which are transmitted from human to human by the mosquitoes *Adeds aegypti* and cause infections mostly in tropical and subtropical regions worldwide. They cause dramatic variations in clinical symptom varying from asymptomatic to dengue fever (DF), or even more severe infection with bleeding and shock, known as the dengue hemorrhagic fever (DHF), and dengue shock syndrome (DSS) (McBride and Bielefeldt-Ohmann, 2000). DF is a self-limited debilitating illness characterized by fever, headache, retro-orbital pain, myalgia, arthralgia, and rash. DHF is marked by increased vascular permeability (plasma leakage), thrombocytopenia, and hemorrhagic manifestations; DSS occurs when fluids leakage into the interstitial spaces results in shock, which without appropriate treatment may lead to death (Clyde *et al.*, 2006). The case-fatality rate of DHF/DSS in most countries is about 5% (CDC, USA, 2005).

In 2005, dengue viral infection is one of the most important mosquito-borne viral diseases affecting humans. In the 1950s, there were only nine countries reporting the clinical manifestations of dengue. Today the geographic distribution includes more than 100 countries worldwide (Fig. 1.1). Many of these countries had no dengue reported for over 20 years and

several countries have no known history of the diseases. The World Health Organization estimates that more than 2.5 billion people are at risk of dengue infection. First recognized in the 1950s, DHF/DSS has become a leading cause of child mortality in several Asian and South American countries (Guha-Sapir and Schimmer, 2005).

In 2007 the four serotypes of DVs were estimated to cause 50-100 million annual human infections and 22000 deaths worldwide. The number of dengue fever cases per year is increasing steadily, including in the United States where DVs has spread to 36 states since 1985, and the risk of an outbreak is recognized (Zhou *et al.*, 2008; Morens *et al.*, 2008).

Nevertheless, there are no known antiviral compounds and no therapeutic treatment against dengue virus. Safe vaccines against the yellow fever virus exist, and progress toward a dengue virus vaccine has being made, but the availability of vaccines is often limited. Therefore, the development of new antiviral drugs and a safe vaccine become imperative (Solomon *et al.*, 2001; Zhou *et al*., 2008).

1.2 Replication of dengue virus

The intracellular life cycles of the flaviviruses are very similar (Fig. 1.2). Infection with one of the arthropod-borne flaviviruses begins when the vector takes a blood meal and the virus is introduced into the host. The virus attaches to the cell surface, mediated by the E protein, and enters the cell by receptor-mediated endocytosis. Low pH in the endosomal compartment triggers fusion of the viral and host cell membrane mediated by structural reorganization of E, which leads to the release of the nucleocapsid and viral RNA into the cytoplasm. Translation of the input strand takes place; then the virus switches from translation to synthesis of a negative-strand intermediate, which serves as a template for the production of multiple copies of positive-strand viral RNA (vRNA). Successive rounds of translation produce high levels of viral proteins; the structural protein capsid (C), premembrane (prM), and envelope (E) proteins, along with vRNA, are assembled into progeny virions, which are

transported through the Golgi compartment and secreted (Fields *et al.*, 2001; McBride and Bielefeldt-Ohmann, 2000; Clyde *et al.*, 2006; Aruna *et al.*, 2009).

1.3 Genome of dengue virus

DV possesses a positive sense, single-stranded RNA wrapped in a nucleocapsid protein within an envelope. The whole genome is approximately 10.8 kb in length and contains a single open reading frame. A single polyprotein translated from the viral RNA is cleaved co- and post-translationally by the virus-encoded serine protease, NS2B/NS3, and by host-encoded proteases, including signalase and furin, to produce the three structural proteins, capsid (C), membrane protein (M, which is expressed as prM, the precursor to M), and envelope (E) – that constitute the virus particle and seven nonstructural proteins (NS) that are essential for viral replication encoded by the remainder of the genome. The reported gene order is 5'-C-prM/M-E-NS1-NS2A-NS2B-NS3-NS4A-NS4B-NS5-3' (Fig. 1.3) (Gubler *et al.*, 1997; Chao *et al.*, 2005; Mukhopadhyay *et al.*, 2005; Sampath *et al.*, 2009).

1.4 Four small non-structural proteins of dengue virus

DV has seven non-structural proteins: NS1, NS2A, NS2B, NS3, NS4A, NS4B, and NS5 (Fig. 1.4). Except for enzymatic activities contained within NS3 and NS5, the roles of the other proteins in virus replication and pathogenesis are not well defined.

NS2A, 2B, 4A, and 4B are four small non-structural proteins encoded by flavivirus genome. All four proteins are poorly conserved in sequence but exhibit conserved hydrophobicity profiles among flaviviruses, which suggests that they may be membrane-associated (Gublur *et al.*, 1997). The crude membrane fractions of WNV-infected cells contain a set of viral encoding proteins as major constitutes after weak or stringent salt washes. The NS2A, NS2B, and NS4B are membrane or integral membrane proteins that are separated from the membranes after stringent salt washes. In addition, expression in human

A549 cells of the DV nonstructural proteins NS2A, NS4A, or NS4B enhances replication of an IFN-sensitive virus. Moreover, expression of NS4B and, to a lesser extent, of NS2A and NS4A proteins results in down-regulation of IFN-α/β-stimulated gene expression (Munoz-Jordan *et al.*, 2003). This phenomenon is also observed in WNV and KUNV (Liu *et al.*, 2005).

1.5 Properties of NS2A

NS2A of DV is a small hydrophobic protein of about 24 kDa that migrates anomalously by SDS-polyacrylamide gel electrophoresis (SDS-PAGE). It is about 20 kDa in KUNV (Mackenzie *et al.*, 1998) and 22 kDa in YFV (Lindenbach *et al.*, 1999). Its N-terminus is generated via NS1–2A cleavage by an unknown ER-resident host enzyme (Falgout *et al.*, 1995) and cytosolic cleavage at the NS2A/2B junction by the NS2B-NS3 serine protease. Two forms of NS2A are found in YFV-infected cells. Full-length NS2A (224 amino acids) is the product of cleavage at the NS1/2A and NS2A/2B sites. NS2Aα, a C-terminally truncated form of 190 amino acids, was resulted from partial cleavage by the viral NS2B-NS3 serine protease at the sequence QK↓T within NS2A. Changing lysine to serine at this site (QKT→QST) blocks the production of both NS2Aα and infectious virus, but a mutation in NS2A that blocks virus production can be suppressed by a second mutation on the surface of the NS3 helicase domain (Kummerer *et al.*, 2002). In addition, an upstream mutation in KUNV NS2A has also been shown to block virus assembly (Liu *et al.*, 2003). Therefore, mutations at the YFV and KUNV NS2A provided evidence that NS2A is involved in virus assembly (Lindenbach *et al.*, 2007). In addition, studies in RNA replication with KUNV have shown that NS2A co-localizes with double-strand RNA in discrete cytoplasmic foci and interacts with the 3' untranslated region of Kunjin viral RNA, as well the proposed replicase components NS3 and NS5 in cell lysates. The result indicates that the flavivirus replication complex includes NS2A (Mackenzie *et al.*, 1998). Thus, NS2A is an attractive candidate for

coordinating the shift between RNA packaging and RNA replication, processes that have been shown to be linked (Khromykh *et al.*, 2001).

Besides its apparent roles in RNA replication and virus assembly, DV2 NS2A has also been shown to act as an interferon (IFN) antagonist by inhibiting IFN signaling (Munoz-Jordan *et al.*, 2003) and specific mutations in KUNV and WNV NS2A have been identified that diminish this inhibitory activity (Liu *et al.*, 2004) and attenuate WNV virulence in mice (Liu *et al.*, 2006). However, the small hydrophobic protein NS2A is poorly characterized, and its specific function for viral replication cycle is still unknown.

1.6 Properties of NS2B

NS2B is a small (≈14 kDa) membrane-associated protein. NS2B forms a stable complex with NS3 and acts as a cofactor for the NS2B-NS3 serine protease. This protease complex catalyzes autocleavage (*cis*) at the junction between NS2A and NS2B as well as between NS2B and NS3. It also catalyzes the *trans* cleavage at the junctions between NS3 and NS4A as well as NS4B and NS5 (Clum *et al.*, 1997; Falgout *et al.*, 1991). The initial characterization of the cofactor requirement for the DV NS3 protease revealed that the minimal region required for protease activity was located in a 40-residue central hydrophilic segment of NS2B spanning residues Leu54 to Glu93 (Falgout *et al.*, 1993). Although the hydrophobic regions of NS2B are dispensable for protease activity, they are required for cotranslational membrane insertion of full length NS2B and its efficient activation of the NS3 protease domain (Yusof *et al.*, 2000). Modeling of the putative interactions between the DV2 NS3 protease and its cofactor, NS2B, suggests that a 12 amino acid hydrophobic region within this sequence (^{70}GSSPILSITISE^{81}) may associate directly with NS3 (Fig. 1.5) (Brinkworth *et al.*, 1999).

The alanine substitutions at residues Trp62, Leu75, and Ile79 in the DV NS2B cofactor result in marked effects on autoprocessing at the NS2B/NS3 site (Niyomrattanakit *et al.*,

2004). Also, mutagenesis experiments with YFV NS2B protein demonstrated that specific residues within this core sequence are critical for protease activation. Deletion of residues 51 to 55, 53 to 55, and 56 to 93 within the conserved central domain of YFV NS2B yielded no detectable processing of an NS2B-NS3pro polyprotein precursor, whereas a four-amino-acid deletion of the sequence ^{67}ISGS^{70} generated a protease with significantly reduced cleavage efficiency (Chambers *et al.*, 1993). In all, mutation of conserved residues in NS2B can have dramatic effects on autoproteolytic cleavage at the NS2B/NS3 junction and transcleavage activities (Chambers *et al.*, 2005; Niyomrattanakit *et al.*, 2004).

Besides, although the DV NS3 protease exhibits NS2B-independent activity with model substrates for serine proteases such as N-a-benzoyl-arginine-p-nitroanilide, enzymatic cleavage of dibasic peptides is markedly enhanced with the NS2B-NS3 cocomplex, and the presence of the NS2B cofactor was shown to be an absolute requirement for *trans* cleavage of a cloned polyprotein substrate (Niyomrattanakit *et al.*, 2004). The cofactor, NS2B, is also essential for proper domain motion that contributes to substrate binding (Zuo *et al.*, 2009).

1.7 Properties of NS4A

NS4A is a small hydrophobic protein about 16 kDa. The N-terminus of NS4A is generated in the cytoplasm by the viral two-component protease NS2B/NS3, whereas the C-terminal 23 amino acid residues of NS4A seem to act as a signal sequence for the translocation of NS4B into the lumen of the ER (Fig. 1.6). This signal sequence (designated the 2K fragment) is removed from the N terminus of NS4B by the host signalase in the ER lumen. In a previous study, KUNV NS4A-2K precursor can induce intracellular membrane rearrangements, which may form the scaffold for the viral replication complex (Roosendaal *et al.*, 2006).

The observations that KUNV NS4A localizes to the presumed sites of RNA replication and polyprotein processing (Mackenzie *et al.*, 1998) and that an interaction between NS4A and NS1 is required for RNA replication (Lindenbach *et al.*, 1999) suggest that flavivirus

NS4A was involved in some steps of viral RNA amplification.

Recently, it was reported that DV NS4A associates with membranes via 4 internal hydrophobic regions, which are all able to mediate membrane targeting of a cytosolic reporter protein. It was also developed a model for the membrane topology of NS4A in which the N-terminal third of NS4A localizes to the cytoplasm, while the remaining part contains three transmembrane segments, with the C-terminal end localized in the ER lumen (Fig. 1.7). Subcellular localization experiments in DV-infected cells revealed that NS4A resides primarily in ER-derived cytoplasmic that also contain double-strained RNA (dsRNA) and other DV proteins, suggesting that NS4A is a component of membrane-bound viral replication complex. Besides, the individual expression of DV NS4A lacking the 2K fragment resulted in the induction of cytoplasmic membrane alternations resembling virus-induced structures, whereas expression of full-length NS4A does not. Thus, proteolytic removal of the 2K peptide appears to be important for induction of membrane alternations that may harbor the viral replication complex (Miller *et al.*, 2007). However, the small hydrophobic protein NS4A is poorly characterized, and its proper function for viral replication cycle is still unknown.

1.8 Properties of NS4B

NS4B is the largest of the four small hydrophobic nonstructural proteins and comprises 248 amino acid residues. In DV2-infected cells, NS4B is first produced as a peptide of apparent size of 30 kDa; NS4B is then post-translationally modified, in an unknown way, to produce a polypeptide of apparent size 28 of kDa. The modification of NS4B is found to be cell-dependent and most likely mediated by a cellular enzyme (Preugschat *et al.*, 1991). NS4B proteins of DV serotypes share 78-85 % amino acid sequence identity, whereas those of YFV, WNV and DV share 35 % identity. Hepatitis C virus (HCV) NS4B has only negligible sequence identity to the flavivirus NS4B proteins. Despite this divergence, the topology of NS4B, containing several ER and cytoplasmic domains separated by transmembrane regions

(Fig. 1.8; Miller *et al.*, 2006), is strikingly similar among members of the flaviviridae, suggesting a conserved function of NS4B in the viral life cycle (Lundin *et al.*, 2003).

NS4B of the DV, the WNV, and also the YFV was recently identified as an inhibitor of the IFN-α/β response. Expression of DV NS4B blocks the IFN-α/β-induced signal transduction cascade by interfering with STAT1 (transducer and activator of transcription) phosphorylation. Deletion analyses suggest that the first 125 amino acids of DV 2K-NS4B are sufficient for the inhibition of IFN-α/β signaling, and that proper viral polyprotein processing is required for anti-IFN function (Munoz-Jordan *et al.*, 2005). Likewise NS4A and, to a lesser extent NS2A, appear to block IFN signaling, and the cumulative effect of the three proteins results in robust inhibition of IFN signaling (Munoz-Jordan *et al.*, 2003, 2005).

A number of publications have described mutations in the NS4B protein in attenuated or passage-adapted mosquito-born flaviviruses suggesting this protein plays a vital role in replication and pathogenesis. A single coding mutation (P101L) in DV4 NS4B conferred a small-plaque phenotype in C6/36 cells while at the same time increasing plaque size in Vero cells two-fold and Huh7 cells three-fold. The opposing effects of the NS4B P101L mutation in mosquito and vertebrate systems suggest that the NS4B protein is involved in maintaining the balance between efficient replication in the mosquito vector and the human host (Hanley *et al.*, 2003).

Miller *et al.* found that NS4B colocalizes with NS3 and double-stranded RNA (dsRNA), an intermediate of viral replication, arguing that NS4B is part of the membrane-bound viral replication complex (Miller *et al.*, 2006). Besides, an interaction between the DV NS4B and NS3 was identified by using a yeast two-hybrid assay and validated in pull-down and immunoprecipitation studies. Furthermore, recombinant NS4B dissociated single-strained RNA (ssRNA) from NS3 and consequently enhanced the overall helicase activity of NS3 in an *in vitro* unwinding assay. It suggests that NS4B modulates DV replication via its interaction with NS3 (Umareddy *et al.*, 2006). However, the actual role of NS4B in dengue

replication cycle is not clear.

1.9 Properties of E protein

The DV envelope (E) protein is 495 amino acids in length, forms oligomers, and along with the M protein, constitutes most of the accessible virion surface that is covered by the envelope membrane. The DV E protein mediates host cell binding and is essential for infection via a conformation-induced membrane fusion event between the host cell and the virion. In addition, it is also the primary antigen that induces protective immunity and the major antigen for virus neutralization (Monath *et al.*, 1996).

The X-ray crystallographic structures of ectodomains of TBEV E and DV2 E proteins have been determined (Modis *et al,* 2003, 2004). Each monomer of the crystallized dimeric E protein contains three domains (Fig. 1.9): domain I is a centrally located β barrel, domain II contains a dimerization region and fusion peptide, and domain III harbors the receptor-binding activity.

The glycosylated E protein mediates both receptor binding and fusion activities (Anderson *et al.*, 1992; Guirakhoo *et al.*, 1991). Infectious entry occurs within the endosome, following uptake of intact virus particles through receptor-mediated endocytosis. Protonation of histidines in the low-pH environment of the endosome is the likely trigger for the conformational change that leads to the reversible dissociation of virion surface E dimmers into monomers, followed by an irreversible transition to homotrimers (Modis *et al,* 2004; Kampmann *et al.*, 2006). A hydrophobic stretch of amino acids, referred to as the "fusion peptide", is exposed during this conformational change and interacts with the target membrane, initiating the fusion process and ultimately the merging of the two bilayers (Heinz *et al.*, 2001; Yennamalli *et al.*, 2009).

Furthermore, crystallization of a DV2 E protein fragment in the presence of the detergent β-N-octylglucoside (β-OG) has led to structures with and without occupation of the hinge

pocket by β-OG. Occupation of the pocket by β-OG requires an altered conformation of the *kl* loop toward an "open" position, and the angle that domain II makes with domain I-domain III also differs between two crystal structures with and without β-OG. The β-OG pocket (Fig. 1.10) may therefore represent an ideal target for structure-based design of potential antiviral agents because ligands that bind there could alter the conformational equilibrium associated with the hinge angle and inhibit virus entry (Modis *et al.*, 2003, 2004).

1.10 The β-OG pocket of E as a target

Flavivirus E proteins have been shown to play a pivotal role in virus assembly, morphogenesis, and infection of host cells. A crystal structure of the soluble ectodomain of E from DV2 reveals a hydrophobic pocket, the β-OG pocket, lined by residues that influence the pH threshold for fusion. The β-OG pocket, which accepts a hydrophobic ligand, opens and closes through a conformational shift in a β-hairpin at the interface between domain I and domain II. Therefore, the opening up of the β-OG pocket just at the locus of a likely hinge suggests that compounds inserted at this position might hinder further conformational change and hence inhibit the fusion transition (Modis *et al.*, 2003). It opens up a new avenue for identifying antiviral agents against early steps of dengue virus infection.

Recently, this pocket has been targeted using virtual screening, and tetracycline derivatives and the other small molecules with antiviral inhibitory activity have been identified (Yang *et al.*, 2007; Zhou *et al.*, 2008; Wang *et al.*, 2009). First, Yang *et al.* has identified the tetracyclic ring structure compounds, tetracycline derivatives with the help of a molecular docking platform using the detergent ligand (β-OG) binding site on the DV2 E protein as target and performing virtual screening with comprehensive medical chemistry database (Yang *et al.*, 2007). Among the tetracycline derivatives, rolitetracycline and doxycycline displayed significant inhibitory effects on the propagation of DV2 PL046 strain in cell cultures. Next, Zhou *et al.* used a hierarchical four-stage computational HTS to identify

small-molecule compounds that bind to the β-OG pocket of the E protein of DV. Among the 23 top-ranked compounds, which were tested for antiviral activity in biological assays, P02 (Fig. 1.11) was demonstrated both to bind E protein and to have antiviral activity. Moreover, P02 was shown by STD NMR to compete with β-OG for binding to E protein, which unambiguously demonstrates association of P02 with E protein and supports a binding site that overlaps the β-OG pocket targeted by computational screening (Zhou *et al.*, 2008). This year, Wang *et al.* found a small compound, labeled compound 6 (Fig. 1.12), which was identified as one of the inhibitors with an average EC_{50} of 119 nanomolar against DV2 in a human cell line. Mechanism of action studies demonstrate that compound 6 acts at early stage during DV infection. It arrests DV in vesicles co-localizing with endocytosed dextran, and inhibits NS3 expression (Wang *et al.*, 2009).

In addition to DV, arrays of 23 compounds were selected for antiviral testing against YFV replication. Bioassay results identified a class of thiazole compounds with antiviral potency in cell-based assays. Modification of these lead compounds led to a series of analogues with improved antiviral activity and decreased cytotoxicity (Li *et al.*, 2008).

Furthermore, the pre-fusion and post-fusion structures of DV E protein were analyzed to identify potential novel sites that could bind small molecules, which could interfere with the conformational transitions that mediate the fusion process. Seven structurally diverse molecules were selected to test experimentally for inhibition of DV propagation. The best compound showed an IC_{50} in the micromolar range against DV2 (Yennamalli *et al.*, 2009).

1.11 The overview of the experimental design

(I) Functional expression of nonstructural proteins NS2A, NS2B, NS4A, and NS4B of dengue virus type 2 PL046 strain.

Since the functions of these four small nonstructural proteins regarding to dengue viral replication have not been well-studied, it was decided to construct expression clones of

individual genes for protein production, functional study, subunit vaccine development, and, for the construction of DNA vaccines in the future.

Here, I started with constructing the expression clones of these four nonstructural proteins from DV2 PL046 strain with the enhanced green fluorescence protein gene (EGFP) as tags. Then, I expressed the four nonstructural proteins in mammalian cells, BHK-21, to select for the stable cell lines. Finally, I have initiated the functional study with plaque assay.

(II) Biological assay of inhibitor candidates to dengue virus type 2 and dengue virus type 3.

The incidence of dengue fever epidemics has increased dramatically over the last few decades. However, no commercial vaccine or antiviral therapy is available. Therefore, a need for the search of safe and effective antiviral drugs becomes imperative. Entry of DV into a host cell is mediated by its major envelope protein, E. The crystal structure of the ectodomain of DV2 revealed a hydrophobic pocket, the β-OG pocket, which was proposed as a suitable target site for small-molecule inhibitors of the fusion process. Previously, research in the lab has identified certain tetracyclic ring structure compounds, tetracycline derivatives as inhibitor candidates, targeting the detergent ligand (β-OG) binding site on the DV2 E protein from comprehensive medical chemistry database.

In this study, I attempted to assess (1) whether other tetracycline derivatives and other ringed compounds have inhibitory effect on DV and (2) whether the sequence variations of E protein between DV2 and DV3 affect the specificity of the candidate compounds. Therefore, I performed plaque formation assay using the compounds with different concentrations against DV2 and DV3 separately.

Chapter 2 Materials and Methods

2.1 Materials

2.1.1 Virus

Dengue virus type 2 PL046 strain (Taiwan local strain)

Dengue virus type 3 H87 strain

2.1.2 Cell lines

BHK-21 (baby hamster kidney cell)

C6/36 (*Aedes albopictus* larva cell)

2.1.3 Bacterial strains

Escherichia coli DH5α strain: for general cloning (Invitrogen)

2.1.4 Plasmids

Plasmid	Description	Reference
pcDNA3.0	T7 promoter and CMV promoter. (selection marker: Ampicillin) (Appendix 1)	Invitrogen
pNS2A-HAHis pNS2B-HAHis pNS4A-HAHis pcDNA3-D24B-HAHis	*Bam*HI-*Xba*I fragment containing 2A,2B, 4A, and 4B with C-terminal HA and His tag in pcDNA3 (Appendix 2)	徐婕琳,2003, 楊馥嘉,2006 交大碩士論文; Yang laboratory collection

pNS2A-EGFP pNS2B-EGFP pNS4A-EGFP pcDNA3-D24B-EGFP	*Bam*HI-*Xba*I fragment containing 2A,2B, 4A, and 4B with C-terminal EGFP tag in pcDNA3	This study
pEGFP-N2	pEGFP-N2 encodes a red-shifted variant of wild-type GFP which has been optimized for brighter fluorescence and higher expression in mammalian cells.	Clontech
pNS2B-EGFP(pro) pNS4A-EGFP(pro) pcDNA3-D24B-EGFP(pro)	*Bam*HI-*Xba*I fragment containing 2A,2B, 4A, and 4B with C-terminal EGFP tag in pcDNA3 (EGFP tag without ATG)	This study

2.1.5 Primers

Primer	**Primer sequence (5' to 3')**	**Position in Dengue genome***
2AE-F	ATG**GGACATGGGCAGATTGACAACTTCTCA** start codon	3478-3504
2BE-F	**GAGCTGGCCACTAAATGAGGCTAT**	4131-4154
4AE-F	**CCCTGACCCTGAACCTAATCACA**	6377-6399
4BE-F	TCCATG**AACGAGATGGGTTTCCTGGA** start codon	6826-6845
4BE-FP	G**AACGAGATGGGTTTCCTGGAA**	6826-6846

*According to the sequence of Dengue virus type 2, PL046 strain (GenBank: AJ968413.1)

Boldface: the genes on the dengue virus genome; underline: start codon or restriction site.

Primer	Primer sequence (5' to 3')	Position in EGFP genome*
2AE-R	**TGTACAGCTCGTCCATGCCGAGAGTGATC**	1369-1397
EGFP-F	CCG<u>CTCGAG</u>**ATGGTGAGCAAGGG** (*XhoI*)	683-696
EGFP-R	GC<u>TCTAGA</u>**TTACTTGTACAGCTCGTCCATG** (*XbaI*)	1381-1402
EGFP-F2	CCG<u>CTCGAG</u>**GTGAGCAAGGGCG** (*XhoI*)	686-698
EGFP-R2	GC<u>TCTAGA</u>**TTACTTGTACAGCTCGTCCATGCCG** (*XbaI*)	1378-1402

*According to the sequence of cloning vector pEGFP-N2 with enhanced green fluorescent protein gene (GenBank: U57608.1). Boldface: the genes on the dengue virus genome; underline: start codon or restriction site.

2.1.6 Chemicals, enzymes and reagents

Chemical	Source	Catalog number	Application
1 kb DNA ladder	SibEnzyme	SEM11C001	DNA electrophoresis
2-propanol	Sigma	I 9516	RNA extraction
9-amino-1,2,3,4-tetrahydroacridine hydrochloride hydrate	Sigma	A79922	Plaque assay
Acetic acid	Fluka	33209	Western Blot
Acryl/Bis 37.5:1 solution	AMRESCO	0245	Western Blot
Agarose	VEGONIA	9201-05	DNA/RNA electrophoresis

Ampicillin	Applichem	A0839	Bacterial culture
APS	Bio-Rad	161-0700	Western Blot
B-mercaptoethanol	MERCK	1.1543.0100	Reducing reagent
Berberine	Sigma	B3251	Plaque assay
Chloroform	Riedel-de Haën	32211	Genomic DNA extraction
Chlortetracycline	Sigma	C-4881	Plaque assay
Coomassie Brilliant Blue R-250	J.T.Baker	F792-01	Protein-staining
Crystal Violet	Sigma	C-3886	Cell staining
DEPC	Sigma	D 5758	RNase inactivation for RT-PCR
DMSO	Sigma	D-8418	Freeze cells
DNA Polymerase I, Large (Klenow) Fragment	BioLabs	M0210S	Klenow fill in
Doxycycline	Sigam	D-9891	Plaque assay
ECL substrate	PIERCE	34079	Western Blot
EDTA	AMRESCO	0105	TE buffer
EtBr	Sigma	E-7637	DNA/RNA staining
Fetal Bovine Serum	Biological industries	04-001-1A	Cell culture
Formaldehyde	Riedel-de Haën	33220	Cell fixation
G418 (GENETICIN)	GIBCO	11811-031	Cell culture
Kanamycin	Sigma	K4000	Antibiotics and

			plaque assay
LB agar	Alpha Biosciences	L12-111	Bacterial medium
LB broth	Scharlau	02-385	Bacterial medium
Lipofectamine 2000	Invitrogen	11668-019	Transfection
MEM	GIBCO	41500-034	Cell culture medium
Methanol	Mallinckrodt	3016-08	Western Blot
Methylcellulose	Sigma	M 0512	Plaque assay
NaCl	AMRESCO	0241	Buffer
$NaHCO_3$	Sigma	S-5761	Cell culture
NaOH	Riedel-de Haën	30620	Buffer
Nitrocellulose Transfer Membrane	Schleicher & Schuell	10401396	Western Blot
Nonfat powdered milk	New Zealand Milk Brands Ltd	EMB 53048-D	Western Blot
Oxytetracycline	Sigma	O-5750	Plaque assay
Phenol saturated solution	Amresco	0945	Genomic DNA extraction
PMSF	Fluka	78830	Protein inhibitor
Protein marker	Fermentas	SM0671	SDS-PAGE
Restriction enzyme	TakaRa, BioLabs	---	Plasmid construction

Rolitetracycline	Sigma	R-2253	Plaque assay
SDS	Riedel-de Haën	62862	Western Blot
T4 DNA ligase	Fermentas	1812	Plasmid construction
TEMED	Sigma	T-9281	Western Blot
Tetracycline	Sigma	T-3258	Plaque assay
Tris (Base)	AMRESCO	0826	Western Blot
Trypsin	GIBCO	12605-010	Cell culture
Tween-20	Sigma	P-1379	Western Blot
Urea	Fluka	SK-2644U	Denature reagent
X-ray film	Midwest Scientific	LA7111	Western Blot

2.1.7 Antibodies

Antibody	**source**	**Catalog number**
Calnexin (H-70) (from rabbit)	Santa Cruz	SC-11397
Alexa flour 594 goat anti-rabbit IgG	Invitrogen	A11037
Goat Polyclonal anti-GFP, conjugated HRP	NOVUS	NB600-313

2.1.8 Kits

Kit	Source	Catalog number	Application
ExcelPure™ Plasmid Miniprep Purification Kit	Premier	N-PM050	Plasmid extraction
QIAGEN Plasmid Midi Kit	QIAGEN	12143	Plasmid extraction
PCR Clean-up/Gel Extraction Kit	Premier	N-DCE050	DNA purification
RNeasy Mini Kit	QIAGEN	74104	RNA extraction
QIAshredderTM	QIAGEN	79654	RNA extraction
SuperScript One-Step RT-PCR with Platinum *taq*	Invitrogen	10928-042	RT-PCR

2.1.9 Buffers

- 0.25% Coomassive blue stain solution

  2.5 g Coomassive brilliant blue，50% methanol，10% acetic acid added ddH_2O to 1000 ml

- 0.5% crystal violet solution (500 ml)

  2.5 g crystal violet，25 ml 37% formaldehyde，250 ml EtOH，4.25 g NaCl

- 10X SDS-PAGE running buffer

  0.25 M Tris base，1.92 M Glycin，1% SDS

- 10X transfer buffer

  39 mM Glycin，48 mM Tris base，10% SDS， 20% methanol

- 1X PBS (pH 7.4)

  137 mM NaCl，10 mM Na_2HPO4，2.7 mM KCl，1.8 mM KH_2PO4

- 2X SDS-PAGE loading buffer

0.5% bromphenol blue，0.5 MTris-HCl (pH 6.8)，10% SDS，100% glycerol

- 5% Blocking buffer

  2.5 g nonfat powdered milk dissolved in 50 ml 1X TBS buffer

- 50X TAE buffer

  48.4 g Tris base，0.5 M EDTA (pH 8.0) 20 ml，11.42 ml acetic acid added ddH_2O to 200 ml

- Cell lysis buffer (RIPA buffer)

  0.1% SDS，1% Triton X-100，1% NP-40，10 mM Tris-HCl (pH 7.4)，1 mM $MgCl_2$，1 mM PMSF

- Digestion buffer

  100 mM NaCl，10 mM Tris-Cl pH8，25 mM EDTA pH8，0.5% SDS，0.1 mg/ml proteinase K

- TBS buffer (Tris-buffered saline)

  10 mM Tris (pH 8.0)，150 mM NaCl

- TBST buffer

  10 mM Tris (pH 8.0)，150 mM NaCl，0.05% Tween 20

2.1.10 Media

- LB (Luria-Bertani) / Ampicillin agar

  1% tryptone，0.5% yeast extract，1% NaCl，1.5% agar，50 μg/ml Ampicillin

- LB (Luria-Bertani) / Kanamycin agar

  1% tryptone，0.5% yeast extract，1% NaCl，1.5% agar，50 μg/ml Kanamycin

- LB broth

  1% tryptone，0.5% yeast extract，1% NaCl

2.1.11 Equipments

- -20℃ low temperature refrigerator (WHITE-WESTINGHOUSE)
- -80℃ low temperature refrigerator 925/926 (FIRSTEK SCIENTIFIC)
- 4℃ refrigerator KS-101MS (MINI KINGCON)
- Auto dry box DX100 (Taiwan Dry Tech Co. Ltd)
- Bench top orbital shaker S101 (FiRSTEK)
- Centrifuge model 5100 (Kubota Corporation)
- CO_2 incubator 5420-0NEW (NAPCO)
- Confocal (OLYMPUS, FV 500)
- Digital scale PB153-S (METTLER TOLEDO)
- Fluorescence microscope
- GeneQuant pro DNA/RNA calculator (AMERSHAM PHARMACIA BIOTECH)
- Gene Cycler™ (BIO-RAD)
- Hemacytomete (MARIEMFELD)
- Image system GEL DOC 2000 (BIO-RAD)
- Microcentrifuge MICRO 240A (DENVILLE SCIENTIFIC INC.)
- Mini-Protein electrophoresis cell 3 (BIO-RAD)
- Mini Trans-Blot Electrophoretic Transfer Cell (BIO-RAD)
- Orbital shaker IKA-VIBRAX-VXR
- pH meter F 360 (BACKMAN)
- SHORTER MINI Horizontal Gel electrophoresis Apparatus MJ-105 (MEDCLUB)
- Thermal Cycler PTC-100RT (MJ RESEARCH INC.)
- Vertical acrylamide electrophoresis unit (BIO-RAD)
- VORTEX-GENIE2 G560 (SCIENTIFIC INDUSTRICS)
- Water bath B206-T1 (FIRSTEK SCIENTIFIC)

2.2 Methods

2.2.1 Transformation of *E. coli*

2.2.1.1 Preparation of competent cells (for chemical method)

A single colony of *E. coli* was inoculated in 5 ml of LB broth and grew overnight at 37℃ with vigorous shaking (~180 rpm). 2 ml of the overnight culture was transferred into 100 ml LB broth (containing 5% glucose and 2 mM $MgCl_2$) and was then incubated at 37℃ with shaking until the OD_{600} is between 0.4 and 0.7. The cultures were stored on ice for 20 minutes. The cells were recovered by centrifugation at 1620×g for 10 minutes and then resuspended in 50 ml ice-cold 0.1 M $CaCl_2$. The cells were let stand on ice for 30 minutes and were pelleted by centrifugation at 720×g for 10 minutes at 4℃. The pellet was resuspended in 10 ml ice-cold 0.1 M $CaCl_2$. The cells were incubated at 4℃ for 18 hours and were then recovered by centrifugation at 720×g for 10 minutes. The pellet was resuspended in 10 ml ice-cold 0.05 M $CaCl_2$ (containing 15 % glycerol). The cells were dispensed as 100 µl per eppendorf tube and then were stored at -80℃.

2.2.1.2 Transformation

Stored competent cells were thawed on ice. 0.1~1 µg of plasmid DNA was mixed with 50 µl competent cells and was then set on ice for 30 minutes. The mixture was incubated in a preheated 42℃ circulation water bath for 1 minute and then on ice for 1 minute. Then 500 µl of LB broth was added to the cells. The culture was incubated at 37℃ with shaking (180 rpm) for 1 hour. 100 µl of the culture was plated on LB agar plate with 50 µg/ml ampicillin or kanamycin. The plate was set at room temperature until the liquid had been absorbed. The plate was inverted and was then incubated at 37℃ for 12~18 hours.

2.2.2 Plasmid DNA extraction

Plasmid DNA in *E. coli* was extracted with ExcelPure™ Plasmid Miniprep Purification Kit (Premier, Cat. N-PM050). The procedure is as following:

A single colony of *E. coli* was inoculated in 5 ml of LB broth (with antibiotics) and grew overnight at 37℃ with vigorous shaking (180 rpm). The cells were recovered by centrifugation at 1037×g for 12 minutes and then resuspended in 200 µl Solution I buffer (Premier, Inc.; San Diego, USA). The *E. coli* solution was transferred to an eppendorf. 200 µl of Solution II buffer (Premier, Inc.; San Diego, USA) was added and mixed gently. 200 µl of Solution III buffer (Premier, Inc.; San Diego, USA) was added to the mixture and mixed gently again. Cells were spun at 16100×g for 5 minutes at room temperature (RT). The supernatant was transferred to Mini-M™ Column. The solution was centrifuged at 16100×g for 1 minute, and the filtrate in the collection tube was discarded. 700 µl of Washing solution (Premier, Inc.; San Diego, USA) was added in and the column was spun for 1 minute. This step was repeated once again. After the filtrate was discarded, the column was centrifuged at 16100×g for 3 minutes to remove residual ethanol. Mini-M™ Column was transferred to a new eppendorf and incubated at 60℃ for 5 minutes to evaporate the ethanol. Finally, DNA was eluted by 30-50 µl Elution Solution (Premier, Inc.; San Diego, USA) and centrifuged at 16100×g for 1 minute. Plasmid DNA was stored at -20℃.

2.2.3 Restriction enzyme digestion

0.5~1 µg of DNA was dissolved in appropriate volume of water and was digested with restriction enzyme (following the commercial protocol). Generally, 1 µg DNA was digested with 1 unit of restriction enzyme in a 10 µl reaction at 37℃ for 1 hour or longer. The reaction was stopped by heat inactivation (65℃ for 10 minutes in general).

2.2.4 Cell culture

BHK-21 cells were grown in Minimum Essential Medium (MEM; Gibco) supplemented with 5% fetal bovine serum (FBS) and 0.22% $NaHCO_3$. Cells were incubated in tissue culture incubator at 37℃ with 5% CO_2. C6/36 cells were grown at 28℃ in MEM medium (Gibco) supplemented with 0.22% NaHCO3 and 10% FBS.

2.2.5 Transfection of mammalian cell

Cells were transfected with different expression plasmid with Lipofectamine™ 2000 (Invitrogen, Cat. 11668-019) and appropriate amount of plasmids according to the manufacturer's instructions. For example, in a 35 mm culture dish, 4 μg DNA was diluted in 250 μl serum-free medium and mixed gently. 10 μl Lipofectamine™ 2000 was gently mixed with 250 μl serum-free medium and incubated for 5 minutes at RT. The diluted DNA was combined with diluted Lipofectamine™ 2000 and incubated for 20 minutes at RT. The mixture was added to 90-95% confluent cells and incubated at 37℃ in CO_2 incubator for 4-6 hours. The medium was replaced with fresh 5% FBS-MEM medium. Cells were incubated at 37℃ in CO_2 incubator for 24 hours prior to the following assay.

2.2.6 Immunofluorescence and confocal microscopy.

BHK-21 cells were grown on coverslips, 24 hours after transfection, fixed in 4% paraformaldehyde for 30 minutes, followed by washing 2 times for 5 minutes in PBS, and permeabilized with 0.5% Triton X-100 for 10 minutes at room temperature. After the cells were washed as described above, the cells were blocked with 1% bovin serum albumin (BSA) at RT for 1 hour. Then cells were incubated with polyclonal anti-calnexin antibody (1:100) to stain the ER for 1 hour, and then washed 3 times for 5 minutes. Goat anti-rabbit IgG secondary antibody (1:1000) incubation was performed for 1 hour in the dark, and the cells were then washed 3 times for 5 minutes each. Subsequently, coverslips were mounted on

glass slides and the cells were analyzed by confocal laser scanning microscopy (OLYMPUS, FV 500).

2.2.7 Selection of stable transfected cells

24 hours after transfection, transfected BHK-21 cells were passaged down by trypsin. A culture of 1/500 cells were seeded in 6 cm dishes with MEM medium containing 5% FBS and 800 μg/ml G418 for ten days. Then the single colonies were selected to 24 well dishes with MEM medium containing 5% FBS and 800 μg/ml G418 and the medium was changed every four days until the cells were confluent. After that, the cells were passaged to 6 cm dishes for amplification with 500 μg/ml G418. The cell colonies were selected for other experiments.

2.2.8 Preparation of proteins from mammalian cells

The transfectants, 24 hours after transfection, or the stable transfected cells were lysed with 100~200 μl RIPA buffer (containing 1 mM PMSF) at RT. The lysates were sedimented by centrifugation at 12000×g for 5 minutes at 4℃. The supernatant and pellet were respectively mixed with 1 volumn 2X SDS-PAGE loading dye (containing 8 M urea, 200 mM DTT, and 200 mM β-mercaptoethanol) and analyzed by Western blotting.

2.2.9 Western blot analysis

Mammalian cells expressed proteins were separated by SDS-PAGE (12% gel) using a Mini-Protein electrophoresis cell 3 (Bio-Rad) and electrophoretically transferred to Nitrocellulose membrane (Schleicher&Schuell) using Mini Trans-Blot Electrophoretic Transfer Cell (Bio-Rad) at 0.09A for 37 minutes. The membrane was blocked for 12-14 hours at 4℃ with 5% nonfat powdered milk (New Zealand Milk Brands Ltd) in TBS buffer. Then, the membrane was incubated with Goat Polyclonal anti-GFP, conjugated HRP for 1 hour at RT and washed in PBST 3 times for 5 minutes. Finally, the blots were developed by ECL and

then exposed to an X-ray film.

2.2.10 Plaque formation of stable cell lines

MEM without FBS was mixed with virions of DV2 PL046 strain in the amount of 200-250 PFU/well. The mixtures were mixed gently and added onto the stable transfected BHK-21 cells in 35mm dishes and then incubated at 37℃ with 5% CO_2 for 1 hour. MEM containing 5% FBS and 1.1% methylcellulose were added to the well and incubated at 37℃ with 5% CO_2 for 5-7 days. The medium was discarded before the cells were fixed with 3.7% formaldehyde. After 30 minutes, the solution was removed and the cells were stained with 0.5% crystal violet in 3.7% formaldehyde. The plated were washed with water before the plaque numbers were scored.

2.2.11 Statistical analysis

Analysis of variance (ANOVA) of the data was evaluated by the Statistics Package for Social Science (SPSS 10.0). Scheffe test was employed to determine the statistical significance of the differences between the means (P<0.05).

2.2.12 Preparation of genomic DNA from mammalian tissue

The stable transfected cells of BHK-21 were trypsinized, and collected cells from the flask. The cells were then centrifuged at 500×g for 5 minutes and the supernatant was discarded. The cell pellet was resuspended with 1 to 10 ml ice-cold PBS then centrifuged for 5 minutes at 500×g and the supernatant was discarded. This step was then repeated once. Then, 0.3 ml digestion buffer was added to resuspend cells and the samples were incubated with shaking at 50℃ for 12-18 hours in tightly capped tubes. Then samples were extracted by adding an equal volume of phenol/chloroform/isoamyl alcohol and then centrifuged for 10 minutes at 1080×g at 4℃. The aqueous (top) layer were transferred to a new tube and 1/2 volume of 7.5 M

ammonium acetate and 2 (original) volume of 100% ethanol were added. The DNA should immediately form a stringy precipitate and recovered by centrifugation at 16100×g 4℃ for 10 minutes. The pellet was rinsed with 70% ethanol and centrifuged at 16100×g for 10 minutes to decant ethanol and air dry. Finally, DNA was resuspended with autoclaved water until dissolved. It can be shaken gently at room temperature or at 65℃ for several hours to facilitate solubilization. The extracted genomic DNA was stored at -20℃.

2.2.13 RNA extraction

RNA in mammalian cells was extracted with RNeasy Mini Kit (Qiagen). The procedure is as following:

After the media were removed, the stable transfected cells were lysed directly in the cell culture dish (10 cm diameter) by adding 350 μl Buffer RLT (QIAGEN) to the cell culture dish and then pipetting the lysate well into a microcentrifuge tube to ensure that no cell clumps are visible. To homogenize the lysate, it was pipetted directly into a QIAshredder spin column (QIAGEN) placed in a 2 ml collection tube (QIAGEN). Then, the whole set up was centrifuged for 2 minutes at 16100×g. 350 μl (1 volume) 70% ethanol was added to the homogenized lysate, and it was mixed well by pipetting. The samples were transferred, including any precipitate that may be formed, to an RNeasy spin column (QIAGEN) placed in a 2 ml collection tube (QIAGEN) and centrifuged for 30 seconds at ≧8000×g. Then the flow through was discarded. 350 μl buffer RW1 (QIAGEN) was added to the RNeasy spin column, and the whole set up was centrifuged for 30 seconds at ≧8000×g to wash the spin column membrane and then the flow through was discarded. 80 μl DNase I incubation mix (10 μl DNase I stock and 70 μl buffer RDD, QIAGEN) was added directly to the RNeasy spin column membrane, and the whole set up was placed on the benchtop (20-30℃) for 15 minutes. 350 μl buffer RW1 was added to the RNeasy spin column and the whole set up was centrifuged for 30 seconds at ≧8000×g to wash the spin column membrane. 500 μl buffer

RPE was added to the RNeasy spin column, which was centrifuged for 30 seconds at ≧ 8000×g to wash the spin column. 500 μl buffer RPE was added to the RNeasy spin column, which was centrifuged for 2 minutes at ≧ 8000×g to wash the spin column. The RNeasy spin column was then transferred to a new 2 ml collection to centrifuge at 16100×g for 1 minute. Finally, the RNeasy spin column was placed in a new 1.5 ml collection tube and 30-50 μl RNase-free water was added directly to the spin column membrane for centrifugation 1 minute at ≧ 8000×g to elute the RNA. The extracted RNA was stored at -80℃.

2.2.14 Semi-quantitative RT-PCR-Superscript™ One-Step RT-PCR

The SuperScript™ One-Step RT-PCR with PlatinumR *Taq* System is designed for the convenient, sensitive, and reproducible detection and analysis of RNA molecules by RT-PCR. Components for both cDNA synthesis and PCR are combined in a single tube, using gene-specific primers and target RNAs from either total RNA or mRNA. Reverse transcription automatically follows PCR cycling without additional steps (Invitrogen).

The extracted RNA was performed with SuperScrip™ One-Step RT-PCR, the procedure is as following:

The template RNA and components, including 2X reaction mix, sense primers, anti-sense primers, RT/platinum *Taq* mix, and autoclaved distilled water were prepared as depicted in table 1 (Invitrogen) and added to the microcentrifuge tubes on the ice. The mixture was gently mixed to make sure that all the components are at the bottom of the amplification tube. The mixture was then centrifuged briefly if needed. The thermal cycle was performed according to the program in table 2 (Invitrogen Cat. 10928-042).

2.2.15 Amplification of Dengue virus

DVs used in this study were prepared by inoculating monolayers of C6/36 cells grown in

MEM medium with 10% FBS. Infection of C6/36 cells with DV2 PL046 strain or DV3 H87 strain was carried out at multiplicity of infection 0.1 (M.O.I.) in 10% FBS MEM medium at 37℃ in 5% CO_2 for 2 hours and then cultured in 28℃ in the absence of CO_2. After incubating at 28℃ for 4-5 days, cell culture supernatant was collected after clarification of cell debris, and stored at -80℃.

2.2.16 Plaque formation assay for the inhibitory effects of compounds in DV2 and DV3 propagation

Mammalian BHK-21 host cells were cultured at 37℃ with 5% CO_2 in MEM medium (Gibco) supplemented with 0.22% sodium bicarbonate and 5% fetal bovine serum (FBS) (Gibco). BHK-21 cells were plated at a density of 3×10^5 cells per well in 6-well plates and incubated at 37℃ with 5% CO_2 for 24 hours. Different dilutions of the compounds were added to the 6-well plates incubated at 37℃ with 5% CO_2 for 1 hour, following by 0.5 ml of medium containing 200 PFUs of the DV2 PL046 strain or DV3 H87 strain per well for 1 hour incubated at 37℃ with 5% CO_2. Then a 1:1 mixture of 10% MEM medium: 2.2% methylcellulose was added to the cultures. The cultures were then incubated at 37℃ with 5% CO_2 for 6~7 days. The medium was aspirated prior to fixation of the cells with 3.7% formaldehyde for 30 minutes. Then, the fixing solution was removed and the cells were stained with 1% crystal violet in 3.7% formaldehyde. Finally, the plates were washed with water prior to scoring of plaques.

Chapter 3 Functional expression of nonstructural proteins NS2A, NS2B, NS4A, and NS4B of dengue virus type 2 PL046 strain

(I) Results

3.1 Construction of pNS2A-EGFP, pNS2B-EGFP, pNS4A-EGFP, and pcDNA3-D24B-EGFP expression plasmids

pEGFP-N2 (Clontech) encodes a red-shifted variant of wild-type GFP (Prasher *et al.*, 1992; Chalfie *et al.*, 1994; Inouye *et al.*, 1994) which has been optimized for brighter fluorescence and higher expression in mammalian cells (Fig. 3.1). The EGFP fragment was obtained by polymerase chain reaction (PCR) amplification with primers EGFP-F and EGFP-R on pEGFP-N2 as the template. The contents of the PCR reaction mixture are listed in table 3 and the condition of the PCR reaction was performed with the program described in table 4. The PCR products were gel-purified after being digested with restriction enzyme *Xho*I at the 5'-end and *Xba*I at the 3'-end. pNS2A-HAHis, pNS2B-HAHis, pNS4A-HAHis (徐婕琳, 2003, 交大碩士論文), and pcDNA-D24B-HAHis (楊馥嘉, 2006, 交大碩士論文) were also treated with the same restriction enzyme digestion to remove the HA-His tag and then to be gel purified. The *Xho*I-*Xba*I fragment containing EGFP was ligated to the *Xho*I-*Xba*I vector fragments of pNS2A-HAHis, pNS2B-HAHis, pNS4A-HAHis, and pcDNA3-D24B-HAHis (pcDNA3 based). Thus the four nonstructural genes in pcDNA3 carried the C-terminal EGFP tag and the new constructs were named pNS2A-EGFP, pNS2B-EGFP, pNS4A-EGFP, and pcDNA3-D24B-EGFP (Fig. 3.2 A, B, C, and D), respectively. These constructs were assessed by *BsrG*I and *Nde*I digestions. pNS2A-EGFP was digested into 1.8 kb and 5 kb fragments (Fig. 3.3). pNS2B-EGFP was digested into 1.5 kb and 5 kb fragments (Fig. 3.3). pNS4A-EGFP was digested into 1.6 kb and 5 kb fragments (Fig. 3.3). pcDNA3-D24B-EGFP was digested into 1.9 kb and 5 kb fragments (Fig. 3.3).

3.2 Expression and subcellular localization of pNS2A-EGFP, pNS2B-EGFP, pNS4A-EGFP, and pcDNA3-D24B-EGFP in mammalian cells, BHK-21

3.2.1 Confocal fluorescence microscope analysis

pNS2A-EGFP, pNS2B-EGFP, pNS4A-EGFP, pcDNA3-D24B-EGFP, and the control pEGFP-N2 were transfected into BHK-21 to investigate the expression of the recombinant proteins by IF assay (immunofluorescence assay) and confocal fluorescence microscopy. Those four constructs all exhibited the green fluorescence through the C-terminal EGFP tag (enhanced green fluorescence protein) as shown in Fig. 3.4 (D, G, J, and M), which confirmed the expression of NS2A-EGFP, NS2B-EGFP, NS4A-EGFP, and NS4B-EGFP.

Additionally, a colocalization study with the cellular marker protein calnexin, a marker for the reticular subdomain of rough ER was performed. And the green fluorescence of the four proteins displayed at the same location as the red fluorescence, from calnexin, in cytoplasm (Fig. 3.4 E, H, K, and N). While the EGFP displayed the green fluorescence around whole cells (Fig. 3.4 A.). The merged were shown in Fig. 3.4 (C, F, I, L, and O).

3.2.2 Assay of the transient expression of pNS2A-EGFP, pNS2B-EGFP, pNS4A-EGFP, and pcDNA3-D24B-EGFP in BHK-21 by Western blot analysis

Expression of four nonstructural protein constructs, pNS2A-EGFP, pNS2B-EGFP, pNS4A-EGFP, and pcDNA3-D24B-EGFP were driven by CMV immediate-early gene promoter on vector pcDNA3 in BHK-21 cells. BHK-21 cells transfected with these four plasmids separately were harvested 24 hours posttransfection and were lysed by RIPA buffer. The cell lysates were analyzed by SDS-PAGE with Coomassie blue staining and Western blot with antibody against the C-terminal EGFP tag (Fig. 3.5). The predicted molecular weights of NS2A-EGFP, NS2B-EGFP, NS4A-EGFP, and NS4B-EGFP are 50.9, 41.2, 43.7, 54 kDa, respectively. Compared with cells transfected with vector only, there was no extra band on the Coomassie blue stained gel (Fig. 3.5 A). Next, the blots were examined with Western blot

analysis. For cells transfected with pNS2A-EGFP, the dominant band was between 34 and 26 kDa which was the same as EGFP positive control (Fig. 3.5 B *b*). There was also a band at about 43 kDa, which was a little smaller than the predicted 50.9 kDa by Western blot (Fig. 3.5 B *a*).For cells transfected with pNS2B-EGFP, there were two bands at about 43 kDa (Fig. 3.5 B *c*). For cells transfected with pNS4A-EGFP, a band was detected at about 43 kDa, which was as expected (Fig. 3.5 B *d*) but the dominant band was between 34 and 26 kDa which was the same as EGFP control (Fig. 3.5 B *e*). As for NS4B, there was a band at about 55 kDa, as expected (Fig. 3.5 B *f*).

3.3 Selection of stable transfected cells of pNS2A-EGFP, pNS2B-EGFP, pNS4A-EGFP, pcDNA3-D24B-EGFP, and pEGFP-N2

3.3.1 Fluorescence microscopy and Western blot analysis of the selected stable cell lines

pNS2A-EGFP, pNS2B-EGFP, pNS4A-EGFP, pcDNA3-D24B-EGFP, and pEGFP-N2 were transfected into BHK-21 for stable clone selection by G418. The selected colonies were analyzed by Western blot with anti-GFP-HRP antibody against the C-terminal EGFP tag and were observed by fluorescence microscope.

There were fluorescence signals in the selected cells including EGFP, NS2A-EGFP, NS2B-EGFP, NS4A-EGFP, and NS4B-EGFP (Fig. 3.6 B, 3.7 B, 3.8 B, 3.9 B, and 3.10 B). The predicted molecular weights of EGFP, NS2A-EGFP, NS2B-EGFP, NS4A-EGFP, and NS4B-EGFP are 27, 50.9, 41.2, 43.7, and 54 kDa, respectively. For all the selected colonies, only the pellets and the supernatants of EGFP had the expected bands at 27 kDa (Fig. 3.6 C and D), and the NS2A-EGFP had the bands at about 43 kDa (Fig. 3.7 C) in the pellet and the supernatant, which was a little smaller than the expected. The others all had the unexpected bands at 27 kDa just as the molecular weight of EGFP (Fig. 3.8 C, 3.9 C, and 3.10 C).

3.3.2 PCR analysis on the genomic DNA of the selected stable cell lines of NS2A-EGFP, NS2B-EGFP, NS4A-EGFP, and NS4B-EGFP

Because of the bands in Western blot of NS2A-EGFP, NS2B-EGFP, NS4A-EGFP, and NS4B-EGFP were smaller than expected, I decided to check the constructs by PCR amplification of the genomic DNA extracted from the stable transfected cell lines.

The PCR amplification of the genomic DNA of the stable cell line NS2A-EGFP was performed with primers 2AE-F and 2AE-R to obtain a band of 1.4 kb, which was consistent with the expected 1377 bp (indicated by a in Fig. 3.11 A). The negative control was the stable transfected cells of pcDNA3 and the positive control was the pNS2A-EGFP plasmid, indicated by b in Fig. 3.11 A. The PCR amplification of the genomic DNA of the stable cell line, NS2B-EGFP, was performed with primers 2BE-F and 2AE-R to obtain a band of 1.1 kb, which is consistent with the expected 1111 bp (indicated by c in Fig. 3.11 B). The negative control was the stable transfected cells of pcDNA3 and the positive control was the pNS2B-EGFP plasmid, indicated by d in Fig. 3.11 B. For NS4A-EGFP genomic DNA, the PCR primers were 4AE-F and 2AE-R, and a fragment of 1169 bp was obtained, which was as expected (indicated by e in Fig. 3.11 C) when compared with the negative control (stable transfected cells of pcDNA3) and the positive control (pNS4A-EGFP plasmid, indicated f in Fig. 3.11 C). As for NS4B-EGFP, the PCR amplification was with primers 4BE-F and 2AE-R. But no band was detected when compared with the negative control (stable transfected cells of pcDNA3) and the positive control (pcDNA3-D24B-EGFP plasmid, indicated by g in Fig. 3.11 D).

3.3.3 RNA expression of the stable cell lines of 2A-EGFP, 2B-EGFP, 4A-EGFP, and 4B-EGFP

The total RNAs were extracted from selected stable cell lines of NS2A-EGFP, NS2B-EGFP, NS4A-EGFP, NS4B-EGFP, and pcDNA3 by RNeasy Mini Kit. The extracted

RNAs were used for performing superscript one-step RT-PCR with individual primers. For NS2A-EGFP, the primers were 2AE-F and 2AE-R and a fragment of 1.4 kb was obtained, which was as the expected 1377 bp (indicated by a in Fig. 3.12) when compared to the negative control (stable transfected cells pcDNA3, Fig. 3.12 lane 4). For NS2B-EGFP, the primers were 2BE-F and 2AE-R and a fragment of 1.1 kb was obtained, which was as the expected 1111 bp (indicated by b in Fig. 3.12) when compared to the negative control (stable transfected cells pcDNA3, Fig. 3.12 lane 5). As for NS4A-EGFP, the primers were 4AE-F and 2AE-R and a fragment of 1.2 kb was obtained, which was as the expected 1169 bp (indicated by c in Fig. 3.12) when compared to the negative control (stable transfected cells pcDNA3, Fig. 3.12 lane 6). But for NS4B-EGFP with primers 4BE-FP and 2AE-R, no band was detected (Fig. 3.12 lane 7). In conclusion, the expressions of mRNAs of NS2A-EGFP, NS2B-EGFP, and NS4A-EGFP in the stable lines were detected but not NS4B-EGFP.

3.4 Construction of pNS2B-EGFP(pro), pNS4A-EGFP(pro), and pcDNA3-D24B-EGFP(pro) expression plasmids

The EGFP' fragment without the start codon ATG was obtained by polymerase chain reaction (PCR) amplification with primers EGFP-F2 and EGFP-R2 on pEGFP-N2 as the template. The PCR products were digested with restriction enzymes *Xho*I at the 5'-end and *Xba*I at the 3'-end and followed by gel purification. pNS2B-EGFP, pNS4A-EGFP, and pcDNA-D24B-EGFP were also treated with the same restriction enzyme digestions to remove the EGFP tag with the start codon, and gel purified. The *Xho*I-*Xba*I fragment containing EGFP' was ligated to the larger *Xho*I-*Xba*I fragments of pNS2B-EGFP, pNS4A-EGFP, and pcDNA3-D24B-EGFP (Fig. 3.13). Thus I replaced the original EGFP tag with the EGFP' tag, which did not contain the start codon. They were named pNS2B-EGFP(pro), pNS4A-EGFP(pro), and pcDNA3-D24B-EGFP(pro) (Fig. 3.14 A, B, C).

pNS2B-EGFP(pro) was assessed by *BsrG*I and *Nde*I digestions. There were fragments of

1.5 kb (1534 bp) and 5 kb (4958 bp) (Fig. 3.14 D). pNS4A-EGFP(pro) was assessed by *BsrG*I and *Nde*I. There were fragments of 1.6 kb (1594 bp) and 5 kb (4958 bp) (Fig. 3.14 D). pcDNA3-D24B-EGFP(pro) was assessed by *BsrG*I and *Nde*I. There were fragments of 1.9 kb (1888 bp) and 5 kb (4958 bp) (Fig. 3.14 D). Besides, pNS2B-EGFP(pro), pNS4A-EGFP(pro), and pcDNA3-D24B-EGFP(pro) were sequenced to confirm the deletion of the EGFP start codon, ATG, in Fig. 3.15.

3.5 Expression of pNS2B-EGFP(pro), pNS4A-EGFP(pro), and pcDNA3-D24B-EGFP(pro) in mammalian cells, BHK-21

BHK-21 cells transfected with pNS2B-EGFP(pro), pNS4A-EGFP(pro), and pcDNA3-D24B-EGFP(pro) separately were harvested 24 hours posttransfection and were lysed by RIPA buffer. The cell lysates were analyzed by SDS-PAGE with Coomassie blue staining and Western blot with antibody against the C-terminal EGFP tag (Fig. 3.16 A, B). The predicted molecular weights of NS2B-EGFP(pro), NS4A-EGFP(pro), and NS4B-EGFP(pro) are 41.1, 43.6, and 53.9 kDa, respectively. Compared with cells transfected with vector only, there was no extra band on the Coomassie blue stained gel in the lanes (Fig. 3.16 A). With Western analysis, for cells transfected with pNS2B-EGFP(pro), there was a dominant band at about 43 kDa (Fig. 3.16 B, a). For cells transfected with pNS4A-EGFP(pro), a band was detected at about 43 kDa, which was as expected (Fig. 3.16 B, b) but the dominant band was between 34 and 26 kDa, which was the same as the EGFP control (Fig. 3.16 B, c). As for NS4B, there was a band at about 55 kDa, which was as expected (Fig. 3.16 B, d).

3.6 Selection of stable transfected cells of pNS2B-EGFP(pro), pNS4A-EGFP(pro), and pcDNA3-D24B-EGFP(pro).

pNS2B-EGFP(pro), pNS4A-EGFP(pro), and pcDNA3-D24B-EGFP(pro) were transfected into BHK-21 for stable clone selection by G418. The selected cells were analyzed by Western

blot analysis with anti-GFP-HRP antibody against the C-terminal EGFP tag and were observed by fluorescence microscope. There was fluorescence signal in the selected cells NS4A-EGFP(pro) (Fig. 3.17 F), but the fluorescence signals of NS2B-EGFP(pro) and NS4B-EGFP(pro) were not prominent (Fig. 8. D, H), compared to the BHK-21 cells (Fig. 3.17 J).

The predicted molecular weights of NS2B-EGFP(pro), NS4A-EGFP(pro), and NS4B-EGFP(pro) are 41.1, 41.2, and 53.9 kDa, respectively. For stable cell line NS2B-EGFP(pro), a band was detected below 43 kDa by Western blot analysis, which was as expected (Fig. 3.17 A b). For stable cell line NS4B-EGFP(pro), a band was detected at about 55 kDa, which was as expected (Fig. 3.17 B. c). But NS2B-EGFP(pro) and NS4A-EGFP(pro) also had a band at the same position (Fig. 3.17 A d), at about 55 kDa. For NS4A-EGFP(pro), no band at the predicted position was detected instead, but there was the unexpected band at about 27 kDa, the same as the molecular weight of EGFP (Fig. 3.17 A a).

3.7 Plaque formation on stable cell lines

The selected stable cell lines NS2A-EGFP, NS2B-EGFP(pro), NS4B-EGFP(pro), EGFP, and pcDNA3 were infected with DV2 virus PL046 strain. Seven days post-infection, the cells were fixed and stained with crystal violet. The number of plaques of BHK-21 was defined as 100% and the relative percentage of plaque numbers of the stable cell lines were recorded in Table 5 and Fig. 3.18. The data were analyzed by ANOVA and Scheffe test. For NS2A-EGFP, there was a 44% reduction (down to 81.46% from that of control EGFP, 126.32%) with significance ($P<0.05$). Whereas, the differences of the percentage of plaque numbers between NS2B-EGFP(pro), NS4B-EGFP(pro) and controls, pcDNA3, and EGFP, were not significant.

(II) Discussion

3.8 Construction of pNS2A-EGFP, pNS2B-EGFP, pNS4A-EGFP, and pcDNA3-D24B-EGFP expression plasmids

Previously, researchers in the laboratory have cloned the four nonstructural genes of DV2 PL046 strain into the expression vector pcDNA3 along with C-terminal HA and His tags (徐婕琳，2003，交大碩士論文；楊馥嘉，2006，交大碩士論文). They were named pNS2A-HAHis, pNS2B-HAHis, pNS4A-HAHis, and pcDNA3-D24B-HAHis (Appendix 2). Therefore, it was convenient to investigate the expression and to select the stable cell lines of these four nonstructural genes by the C-terminal EGFP tag. I replaced the HA-His tags with the EGFP tag and obtained the expression clones of the four nonstructural genes on the pcDNA3 backbone, named pNS2A-EGFP, pNS2B-EGFP, pNS4A-EGFP, and pcDNA3-D24B-EGFP. These four constructs were assessed by restriction digestions (Fig. 3.3) and confirmed by sequencing.

3.9 Expression of pNS2A-EGFP, pNS2B-EGFP, pNS4A-EGFP, and pcDNA3-D24B-EGFP in mammalian cells, BHK-21

3.9.1 Confocal fluorescence microscopy analysis

The EGFP gene has been optimized for brighter fluorescence and higher expression in mammalian cells (excitation maximum= 488 nm; emission maximum=507 nm). To confirm the expression of pNS2A-EGFP, pNS2B-EGFP, pNS4A-EGFP, and pcDNA3-D24B-EGFP, these four expression plasmids and pEGFP-N2 were transfected into BHK-21. All have the green fluorescence expression through the C-terminal EGFP tag in BHK-21 (Fig. 3.4 A, D, G, J, and M). Additionally, the four nonstructural proteins were colocalized against the ER, using calnexin as the marker. 2A-EGFP, 2B-EGFP, 4A-EGFP, and 4B-EGFP proteins co-localized with the ER markers in the cytoplasm of BHK-21, compared to EGFP proteins displayed the

whole cells (Fig. 3.4 A). It suggested that the constructs of the four nonstructural genes could express in mammalian cells.

3.9.2 Transient expression of pNS2A-EGFP, pNS2B-EGFP, pNS4A-EGFP, and pcDNA3-D24B-EGFP in BHK-21

The predicted molecular weights of NS2A-EGFP, NS2B-EGFP, NS4A-EGFP, and NS4B-EGFP are 50.9, 41.2, 43.7, and 54.0 kDa, respectively. The nonstructural proteins NS2B and NS4B could be detected both in the supernatants of the cells with the expected size by Western blot (Fig. 3.5 B c, f). For NS4A, even though there was a band at about 43 kDa, the dominant band was between 34 and 26 kDa (Fig. 3.5 B c). For NS2A, the dominant band was between 34 and 26 kDa, and there was a band at about 43 kDa which was smaller than expected. This was perhaps due to the protein charge affecting mobility or a partial cleavage at the N-terminal of NS2A. All in all, the transient expression of nonstructural proteins NS2B and NS4B in mammalian cells were confirmed by Western blot clearly, but NS2A and NS4A were not. Nevertheless, I proceeded to select the stable cell lines expressing these four proteins.

3.10 Selection of stable transfected cells of pNS2A-EGFP, pNS2B-EGFP, pNS4A-EGFP, pcDNA3-D24B-EGFP, and pEGFP-N2

3.10.1 Western blot analysis of the selected stable cell lines

pNS2A-EGFP, pNS2B-EGFP, pNS4A-EGFP, pcDNA3-D24B-EGFP, and pEGFP-N2 were transfected into BHK-21 for stable clone selection by G418. The selected cells were analyzed by Western blot analysis with anti-GFP-HRP antibody against the C-terminal EGFP tag and were observed by fluorescence microscope (Fig. 3.6. b; 3.7. b; 3.8. b; 3.9. b; 3.10. b). The predicted molecular weights of NS2A-EGFP, NS2B-EGFP, NS4A-EGFP, NS4B-EGFP, and EGFP are 50.9, 41.2, 43.7, 54.0, and 27 kDa, respectively. The EGFP were detected in the

supernatants and pellets of the cells with the expected size by Western blot (Fig. 3.6 c, d). The 2A-EGFP was detected at about 43 kDa in the supernatants and pellets which was smaller than the expected 50.9 kDa (Fig 3.7. c). It was similar with the transient expression of NS2A-EGFP (Fig. 3.5 B. a). The smaller size may be due to the protein charge affecting mobility or a partial cleavage at the N-terminal of NS2A. For NS2B-EGFP, NS4A-EGFP, and NS4B-EGFP, no expected bands were detected but a band at about 27 kDa, which was the same as the molecular weight of EGFP (Fig. 3.8. c, 3.9. c, 3.10. c).

3.10.2 Materials and RNA expression confirmation of the selected stable cell lines of NS2A-EGFP, NS2B-EGFP, NS4A-EGFP, and NS4B-EGFP

Because of the incorrect bands in Western blot of NS2A-EGFP (smaller than expected), NS2B-EGFP, NS4A-EGFP, and NS4B-EGFP, first I tried to examine the materials by PCR amplification of the genomic DNA extracted from the stable cell lines. The PCR amplification of the genomic DNA extracted from the stable cell lines of NS2A-EGFP, NS2B-EGFP, NS4A-EGFP, and NS4B-EGFP were performed with forward primers 2AE-F, 2BE-F, 4AE-F, and 4BE-F and reverse primers 2AE-R located at the C-terminal of EGFP tag. For NS2A-EGFP, NS2B-EGFP, and NS4A-EGFP, expected bands were obtained by PCR amplification, but no band was detected with NS4B-EGFP. It showed that the DNA in the selected stable cell lines of NS2A-EGFP, NS2B-EGFP, and BS4A-EGFP were correct while NS4B-EGFP was not.

Second, I isolated the total RNA of the selected stable cell lines NS2A-EGFP, NS2B-EGFP, NS4A-EGFP, and NS4B-EGFP by using RNeasy Mini Kit. The extracted RNAs were subjected to superscript one-step RT-PCR (Invitrogen) with individual primers to amplify the full length RNA of NS2A-EGFP, NS2B-EGFP, NS4A-EGFP, and NS4B-EGFP, separately. According to the results in Fig. 3.12, RNAs of NS2A-EGFP, NS2B-EGFP, and NS4A-EGFP were detected in the stable lines but not NS4B-EGFP. Therefore, genomic DNA

and RNA expression of NS2A-EGFP, NS2B-EGFP, and NS4A-EGFP were verified by PCR and RT-PCR except for NS4B-EGFP. Thus, I presumed that the transient and long-term expressions of NS2A-EGFP were achieved but the smaller size in Western blot perhaps due to the protein charge. Nevertheless, the selection of stable cell lines of NS2B-EGFP and NS4A-EGFP could not be achieved.

There were two possible reasons: (1) The C-terminal EGFP tag of NS2B-EGFP and NS4A-EGFP clones had its own start codon, ATG. Overexpression of NS2B and NS4A proteins is toxic to cells, therefore, the translation starts at the ATG of the EGFP sequence. (2) The sequence of NS2B and NS4A may contain internal ribosome entry sites (IRESs). Many pathogenic viruses, for example HCV and piconavirus, use an alternative, cap-independent mechanism that substitutes RNA structure for the cap and proteins involved in translation initiation. The RNA structure driving this process is called internal ribosome entry sites (IRESs) (Jeffrey *et al.*, 2008; Baird *et al.*, 2006).

Therefore, I decided to solve the problem by deleting the ATG start codon at the N-terminal of the EGFP tag of pNS2B-EGFP, pNS4A-EGFP, and pcDNA3-D24B-EGFP. Thus, I re-cloned 2B-EGFP, 4A-EGFP, and 4B-EGFP constructs as described in the next section.

3.11 Construction of pNS2B-EGFP(pro), pNS4A-EGFP(pro), and pcDNA3-D24B-EGFP(pro) expression plasmids

The possible reason why the stable cell line selection of NS2B-EGFP, NS4A-EGFP, and NS4B-EGFP could not be carried out maybe because cells selectively expressed the C-terminal EGFP gene, which had its own start codon. Thus I obtained the EGFP fragment without the start codon by PCR amplification. This fragment is named EGFP'. The EGFP fragments of pNS2B-EGFP, pNS4A-EGFP, and pcDNA3-D24B-EGFP were then replaced by the EGFP' fragments. The constructs were named pNS2B-EGFP(pro), pNS4A-EGFP(pro),

and pcDNA3-D24B-EGFP(pro) (Fig. 3.14 A, B, C). All constructs were assessed by *BsrG*I and *Nde*I to expected results (Fig. 3.14 D). The constructs were further confirmed by sequencing to ensure that the ATG at the EGFP tag of pNS2B-EGFP(pro), pNS4A-EGFP(pro), and pcDNA3-D24B-EGFP(pro) were actually deleted (Fig. 3.15).

3.12 Expression of pNS2B-EGFP(pro), pNS4A-EGFP(pro), and pcDNA3-D24B-EGFP(pro) in mammalian cells, BHK-21

The predicted molecular weights of NS2B-EGFP(pro), NS4A-EGFP(pro), and NS4B-EGFP(pro) are 41.1, 43.6, and 53.9 kDa, respectively. The nonstructural proteins NS2B and NS4B could be detected both in the supernatants of the cells with the expected size by Western blot (Fig. 3.16 B a, d). For NS4A, the dominant band was between 34 and 26 kDa (Fig. 3.16 B c), even though the expected band was detected at about 43 kDa (Fig. 3.16 B b).

All in all, the transient expression of nonstructural proteins NS2B-EGFP(pro) and NS4B-EGFP(pro) in mammalian cells were confirmed by Western blot but NS4A-EGFP(pro) was not. The sequence of NS4A may contain internal ribosome entry sites (IRESs) or a partial cleavage at the end of NS4A (Preugschat *et al.*, 1991). Nevertheless, these three re-cloned constructs were proceeded to the stable cell line selection.

3.13 Selection of stable transfected cells of pNS2B-EGFP(pro), pNS4A-EGFP(pro), and pcDNA3-D24B-EGFP(pro)

pNS2B-EGFP(pro), pNS4A-EGFP(pro), and pcDNA3-D24B-EGFP(pro) were transfected into BHK-21 for stable clone selection by G418. First the selected cells were observed by fluorescence microscope. The fluorescence signal of NS4A-EGFP(pro) was observed (Fig. 3.17 F), but NS2B-EGFP(pro) and NS4B-EGFP(pro) were not observed obviously (Fig. 3.17 D, H), compared to the BHK-21 cells (Fig. 3.17 J). It was a possibility that the fluorescence signals were too weak to be observed. Besides, I further confirmed the expression by Western

blot with anti-GFP-HRP antibody against the C-terminal EGFP tag.

The predicted molecular weights of NS2B-EGFP(pro), NS4A-EGFP(pro), and NS4B-EGFP(pro) are 41.1, 41.2, and 53.9 kDa, respectively. The expected band was detected in the stable cell line NS2B-EGFP(pro) by Western blot (Fig. 3.17 A b). For NS4B-EGFP(pro), there was an expected band at about 55 kDa (Fig. 3.17 B c) but NS2B-EGFP(pro) and NS4A-EGFP(pro) also had a band at the same position (Fig. 3.17 A d). According to this, the expression of NS4B-EGFP(pro) in the stable lines still needed to be examined further. For NS4A-EGFP(pro), no expected band was detected but a band between 34 and 26 kDa was detected, which was the same as the molecular weight of EGFP (Fig. 3.17 A a). It was a possibility that NS4A sequence may fold into a distinct structure to be the internal ribosome entry sites (IRESs) (Jeffrey *et al.*, 2008; Baird *et a*l., 2006). The other possibility was that the NS4A-EGFP protein was cleavaged in BHK-21 cells. The 4A/4B cleavage site was preceded by a stretch of hydrophobic amino acids, 2K region, which suggested that this cleavage was mediated by a signalase-like enzyme (von Heijne, 1986; Speight *et al.*, 1988; Preugschat *et al.*, 1991).

3.14 Plaque formation on stable cell lines

The number of plaques in an assay plate indicates the numbers of successful virion infection events (Chiu and Yang, 2003). Thus, reducing number of plaques implies the decreased infectivity. According to the results, the stable cell lines NS2A-EGFP showed a significant 44% reduction of plaque numbers compared to the negative controls, EGFP. But NS2B-EGFP(pro) and NS4B-EGFP(pro) had no significant difference compared to the negative controls. Therefore, it suggested that the overexpression of NS2A in BHK-21 cells may decrease infectivity of DV2.

(III) Conclusion

The four nonstructural proteins of DV2 were expressed as EGFP (enhanced green fluorescence protein) fusion proteins in mammalian cells. The expressions of NS2A, NS2B, NS4A, and NS4B in mammalian cells, BHK-21, were observed by confocal fluorescence microscopy. Additionally, transient expressions of NS2A, NS2B, and NS4B in mammalian cells, BHK-21, were also confirmed by Western blot analysis. Furthermore, the stable cell lines of NS2A and NS2B were successfully selected by G418 and confirmed by Western blot analysis. As for NS4B, it was also detected by Western blot analysis but NS2B and NS4A also had a background band at the same position as the one of NS2B. Thus it still needed to be examined further. The transient expression and long-term expression of NS4A were not detected by Western blot analysis. This perhaps due to the NS4A sequence folding into a distinct structure to be an internal ribosome entry site (IRES) or a signalase cleavage at the end of NS4A.

Functional assay of stable cell lines NS2A-EGFP, NS2B-EGFP(pro), and NS4B-EGFP(pro) was attempted with plaque assay. The results showed that NS2A-EGFP effected a 44% reduction of plaque numbers compared to the negative control. It suggested that the overexpression of NS2A in BHK-21 cells may decrease infectivity of dengue virus type 2.

Chapter 4 Biological assay of inhibitor candidates to dengue virus type 2 and dengue virus type 3

(I) Result

4.1 Candidate compounds on DV propagation

The dengue virus enters a host cell when the E protein binds to the virus receptor on the host cell surface and activates its conformational rearrangement, causing the E protein in its dimeric pre-fusion form to transform into a trimeric post-fusion structure. This essentially irreversible conformational change induces the fusion between the viral envelope membrane and the host cell membrane, allowing entry to be completed (Modis *et al.*, 2004). The key difference between pre-fusion form and post-fusion form is a local rearrangement of the "*kl*" β-hairpin and the concomitant opening up of a hydrophobic pocket for ligand binding, for example, the detergent β-N-octylglucoside, β-OG (Modis *et al.*, 2003). Additionally, mutations that affect the pH threshold for membrane fusion have been mapped to this hydrophobic pocket (Lee *et al.*, 1997; Rey *et al.*, 1995). Therefore, this pocket was proposed to be a hinge point in the fusion-activating conformational change and suggested that it could be a target site for development of fusion inhibitors that could disrupt or even block the correct conformational changes necessary for DV entry (Modis *et al.*, 2003; Modis *et al.*, 2004). Based on these, previously, the lab has worked with Dr. J.M. Yang's lab to perform structure-based virtual screening to dock small molecules into the hydrophobic pocket of the detergent ligand (β-OG) binding site on DV2 E protein. The result indicated tetracyclic ring structure compounds may block or interrupt the essential conformational change of E protein for membrane fusion. Hence, several tetracycline derivatives that contain tetracyclic ring structure were subjected to further test. In this study, four tetracycline derivatives (tetracycline, doxycycline, chlortetracycline, and rolitetracycline), kanamycin, 9-amino-1,2,3,4-tetrahydroacridine hydrochloride hydrate, and berberine were subjected to

plaque formation assay to assess their effect on the DV propagation, especially to determine whether the ring structure is sufficient for the effect.

4.2 Sequence analysis of the detergent-binding pocket in envelope protein between DV2 PL046 strain and DV3 H87 strain

A crystal structure of the soluble ectodomain of E from DV2 reveals a hydrophobic pocket lined by residues that influence the pH threshold for fusion (Modis *et al*, 2003). Previously in the lab, the tetracyclic ring structure was identified by docking small molecules into the β-OG binding pocket on DV2 E protein in a virtual screening (Yang *et al.*, 2007). Alignment and comparison of the amino acids lined the hydrophobic pocket (residues 48-52, 126-128, and 268-279) between DV2 and DV3 revealed that there were variations in the sequences of the hydrophobic pocket at residues 51, 272, 274, 276, 277, and 278 (table 6 and Fig. 4.1). To assess whether this variation has effect on the inhibitory effect of the tetracycline derivatives, I performed plaque formation assay using different concentrations of compounds against DV2 and DV3 separately.

4.3 *In vivo* plaque formation assay

To assess whether those individual tetracycline derivatives could indeed affect the DV propagation as predicted, different concentrations of the compounds were added separately to cultures of BHK-21 cells, followed by the addition of DV2 PL046 strain or DV3 H87 strain at a fixed number of plaque formation units (PFUs). The reduction in the number of plaques reflected the portion of the virion infection that was inhibited by the presence of the particular compound. Therefore, using the number of PFUs from the culture plates added the solvent of the compound (0 μM) as 100%, the relative percentage of the PFUs from the culture plates with compounds was calculated (PFU %).

4.3.1 Tetracycline

The concentrations of tetracycline in the culture were 0 μM, 10 μM, 50 μM, 100 μM, 300 μM, 500 μM, 700 μM, and 1000 μM. Using the number of PFUs from the culture plates added 0 μM tetracycline as 100%, the relative percentage of the PFUs was calculated as PFU %. The PFU % of the culture plates with DV2 PL046 strain were 106.44% (10 μM), 121.55% (50 μM), 119.45% (100 μM), 85.55% (300 μM), 40.52% (500 μM), 23.47% (700 μM), and 12.86% (1000 μM), yielding the estimated IC_{50} value of 457.89 μM (Fig 4.2).

The PFU % of the culture plates with DV3 H87 strain were 95.61% (10 μM), 100.46% (50 μM), 100.46% (100 μM), 54.79% (300 μM), 26.49% (500 μM), 27.99% (700 μM), and 11.33% (1000 μM), yielding the estimated IC_{50} value of 333.85 μM (Fig. 4.3).

4.3.2 Doxycycline

The concentrations of doxycycline in the culture were 0 μM, 10 μM, 50 μM, 100 μM, 200 μM, 300 μM, 500 μM, and 700 μM. Using the number of PFUs from the culture plates added 0 μM doxycycline as 100%, the relative percentage of the PFUs was calculated as PFU %. The PFU % of the culture plates with DV2 PL046 strain were 126.82% (10 μM), 45.20% (50 μM), 14.83% (100 μM), 5.90% (200 μM), 1.69% (300 μM), 0.57% (500 μM), and 0% (700 μM), yielding the estimated IC_{50} value of 47.64 μM (Fig. 4.4).

The PFU % of the culture plates with DV3 H87 strain were 116.25% (10 μM), 156.28% (50 μM), 84.48% (100 μM), 48.94% (200 μM), 25.48% (300μM), 16.40% (500 μM), and 6.58% (700 μM), yielding the estimated IC_{50} value of 197.02μM (Fig. 4.5).

4.3.3 Chlortetracycline

The concentrations of chlortetracycline in the culture were 0 μM, 10 μM, 50 M, 100 μM, 200 μM, 300 μM, 500 μM, and 700 μM. Using the number of PFUs from the culture plates added 0 μM chlortetracycline as 100%, the relative percentage of the PFUs was calculated as

PFU %. The PFU % of the culture plates with DV2 PL046 strain were 101.13% (10 μM), 48.91% (50 μM), 27.81% (100 μM), 13.34% (200 μM), 6.94% (300 μM), 6.39% (500 μM), and 2.16% (700 μM), yielding the estimated IC_{50} value of 49.17 μM (Fig. 4.6).

The PFU % of the culture plates with DV3 H87 strain were 98.67% (10 μM), 60.11% (50 μM), 59.52% (100 μM), 34.60% (200 μM), 17.81% (300 μM), 12.04% (500 μM), and 3.95% (700 μM), yielding the estimated IC_{50} value of 138.20 μM (Fig. 4.7).

4.3.4 Rolitetracycline

The concentrations of rolitetracycline in the culture were 0 μM, 10 μM, 50 μM, 100 μM, 200 μM, 300 μM, 500 μM, and 700 μM. Using the number of PFUs from the culture plates added 0 μM rolitetracycline as 100%, the relative percentage of the PFUs was calculated as PFU %. The PFU % of the culture plates with DV2 PL046 strain were 128.38% (10 μM), 171.93% (50 μM), 160.02% (100 μM), 54.41% (200 μM), 26.14% (300 μM), 5.26% (500 μM), and 0.92% (700 μM), yielding the estimated IC_{50} value of 215.60 μM (Fig. 4.8).

The PFU % of the culture plates with DV3 H87 strain were 100.99% (10 μM), 119.13% (50 μM), 110.74% (100 μM), 68.95% (300 μM), 40.28% (500 μM), and 13.34% (700 μM), yielding the estimated IC_{50} value of 432.19 μM (Fig. 4.9).

4.3.5 Kanamycin

The concentrations of kanamycin in the culture were 0 μM, 10 μM, 50 μM, 100 μM, 200 μM, 300 μM, 500 μM, and 700 μM. Using the number of PFUs from the culture plates added 0 μM kanamycin as 100%, the relative percentage of the PFUs was calculated as PFU %. The PFU % of the culture plates with DV2 PL046 strain were 103.19% (10 μM), 100.06% (50 μM), 107.75% (100 μM), 111.28% (300 μM), 104.34% (500 μM), 122.10% (700 μM),and the IC_{50} was not determined (Fig. 4.10).

The PFU % of the culture plates with DV3 H87 strain were 88.05% (10 μM), 85.84% (50

μM), 90.48% (100 μM), 83.70% (200 μM), 91.75% (300 μM), 87.50% (500 μM), and 86.06% (700 μM), and the IC_{50} was not determined (Fig. 4.11).

4.3.6 9-amino-1,2,3,4-tetrahydroacridine hydrochloride hydrate

The concentrations of 9-amino-1,2,3,4-tetrahydroacridine hydrochloride hydrate in the culture were 0 μM, 10 μM, 50 μM, 100 μM, 200 μM, 300 μM. Using the number of PFUs from the culture plates added 0 μM 9-amino-1,2,3,4-tetrahydroacridine hydrochloride hydrate as 100%, the relative percentage of the PFUs was calculated as PFU %. The PFU % of the culture plates with DV2 PL046 strain were 99.05% (10 μM), 93.72% (50 μM), 69.23% (100 μM), 68.59% (200 μM), and 53.68% (300 μM), and the IC_{50} was not determined (Fig. 4.12).

The PFU % of the culture plates with DV3 H87 strain were 88.81% (10 μM), 86.60% (50 μM), 74.41% (100 μM), 74.09% (200 μM), 68.33% (300 μM), and 63.22% (500 μM), and the IC_{50} was not determined (Fig. 4.13).

4.3.7 Berberine

The concentrations of Berberine in the culture were 0 μM, 10 μM, 50 μM, 10 μM, 200 μM, 300 μM. Using the number of PFUs from the culture plates added 0 μM Berberine as 100%, the relative percentage of the PFUs was calculated as PFU %. The PFU % of the culture plates with DV2 PL046 strain were 105.26% (10 μM), 132.49% (50 μM), 153.91% (100 μM), 125.94% (200 μM), and 70.13% (300 μM), and the IC_{50} was not determined (Fig. 4.14).

The PFU % of the culture plates with DV3 H87 strain were 94.38% (10 μM), 113.37% (50 μM), and 95.68% (100 μM), and the IC_{50} was not determined (Fig. 4.15).

(II) Discussion

There were two main purposes for this study: (1) to assess whether those individual compounds, tetracycline derivatives and others, could indeed affect the DV propagation. (2) To assess whether the sequence variations between DV2 and DV3 affect the specificity of the candidate compounds.

Of the seven compounds, all tetracycline derivatives showed inhibitory effects on DV2 and DV3, compared with kanamycin, 9-amino-1,2,3,4-tetrahydroacridine hydrochloride hydrate, and berberine. The results also revealed that doxycycline and chlortetracycline had dramatic inhibitory effects on DV2 and DV3. For doxycycline on DV2, the IC_{50} value was 47.64 μM and there were only 14.83% of the PFUs remaining at 100 μM; on DV3, the IC_{50} value was 197.02 μM and 16.40% of the PFUs were retained at 500 μM. As for chlortetracycline on DV2, the IC_{50} value was 49.17 μM and there were only 13.34% of the PFUs remaining at 200 μM; on DV3, the IC_{50} value was 138.20 μM and 17.81% of the PFUs were retained at 300 μM. For rolitetracycline on DV2 and DV3, the IC_{50} values were 215.6 μM and 432.19 μM. As for tetracycline on DV2 and DV3, the IC_{50} values were 457.89 μM and 333.85 μM. But, previously, the result of tetracycline on DV2 showed that it had no inhibitory effect on the DV propagation carried out by Y.Y. Tu in the lab (appendix 3). This may be due to the way the tetracycline solution was made. In Tu's study, the tetracycline might be dissolved in water. The solubility of tetracycline in alcohol is better than that in water. For kanamycin, it showed no inhibitory effect on DV2 and DV3 at concentrations ranging from 10 μM to 700 μM. For 9-amino-1,2,3,4-tetrahydroacridine hydrochloride hydrate and berberine on DV2 and DV3, no IC_{50} value was available. 9-amino-1,2,3,4-tetrahydroacridine hydrochloride hydrate and berberine have cellular toxicity effects at higher concentrations (9-amino-1,2,3,4-tetrahydroacridine hydrochloride hydrate from 500 μM, berberine from 200 μM), which would affect cellular morphology and cell

growth (Fig. 4.16, 4.17, 4.18), whereas the tetracycline derivatives would not. Nevertheless, in comparison with tetracycline, doxycycline, chlortetracycline, and rolitetracycline at concentrations ranged from 10 μM to 500 μM, 9-amino-1,2,3,4-tetrahydroacridine hydrochloride hydrate and berberine showed no significant inhibitory effect. It showed that the tetracycline derivatives, which contained the tetracyclic ring structure, had distinct inhibitory effects on DV2 and DV3 compared to kanamycin, 9-amino-1,2,3,4-tetrahydroacridine hydrochloride hydrate, with three connected rings structure , and berberine, with five connected rings structure (Table 8).

Therefore, the compounds showed inhibitory effects as long as they contained the tetracyclic ring (Table 7). The tetracyclic ring structure may be the core factor of showing inhibitory effects on the propagation of DV2 and DV3. Additionally, doxycycline and chlortetracycline revealed more obvious inhibitory effects than tetracycline and rolitetracycline, even though they all shared the core tetracyclic ring structure. The comparison of the 3D structures (Table 8) showed that the angles between the fourth ring and the third ring and the length of the side chain could confer the enhanced anti-dengue virus activity. The pharmacokinetic results of the tetracycline derivatives were showed in table 9. The peak plasma concentrations (C_{max}) of tetracycline, doxycycline, chlortetracycline, and rolitetracycline were 11.3 μM, 30 μM, 2.72 μM, and 11.4 μM, separately. When compared the C_{max} (table 9) with the IC_{50} value of the tetracycline derivatives (table 7), it was found that doxycycline has the potential to be a therapeutic drug against dengue virus.

Zhou *et al.* used a hierarchical four-stage computational HTS to identify small-molecule compounds that bind to the β-OG pocket of the E protein of DV2. In biological assays, candidate compound P02 was demonstrated both to bind E protein and to have antiviral activity (Fig. 1.11). Additionally, Wang *et al.* performed docking on the β-OG pocket of the E protein of DV2 and found a small compound, labeled compound 6, which was identified as one of the inhibitors against DV2 (Fig. 1.12). When compared the tetracycline derivatives

with P02 and compound 6, it is found that they all have the hydrophobic properties and no similar basic structure was shared. Maybe the hydrophobic interaction is the factor to interfere the membrane fusion and conformational change of the E protein. Or there is other mechanism or reason not noticed.

Besides, in comparison with the inhibitory effects between DV2 and DV3, tetracycline showed no obvious difference while doxycycline, chlortetracycline and rolitetracycline showed more inhibitive effects on DV2 than on DV3. This suggested that the inhibitory effects may differ from E proteins of different serotype viruses. The alignment of the E protein hydrophobic pocket between DV2 and DV3 (Fig. 4.1; Table 6) showed that they were different at residues 51, 272, 274, 276, 277, and 278. Therefore, it was possible that these residues may affect compound binding and/or the subsequent membrane fusion.

All in all, all the tetracycline derivatives tested showed inhibited plaque formations on DV2 and DV3 in cell culture systems. Although the potencies varied, the compounds showed inhibitory effects as long as they contained the tetracyclic ring structure. Additionally, the angles between the fourth ring and the third ring and the length of the side chain according to the 3D structure may appear to confer the extra anti-dengue virus activity. In comparison, the inhibitory effects on DV2 were better than DV3 (Table 7). Hence, the results demonstrated that the sequence variations at residues 51, 272, 274, 276, 277, and 278 in the β-OG-binding hydrophobic pocket of E protein may affect the specificity of the tetracycline derivatives to DV E protein.

(III) Conclusion

Four tetracycline derivatives (tetracycline, doxycycline, chlortetracycline, and rolitetracycline), kanamycin, 9-amino-1,2,3,4-tetrahydroacridine hydrochloride hydrate, and berberine were subjected to plaque formation assay to assess whether those tetracycline derivatives could indeed affect the dengue virus propagation, as predicted. Of the seven compounds, all tetracycline derivatives showed inhibitory effects on DV2 and DV3, compared with the kanamycin, 9-amino-1,2,3,4-tetrahydroacridine hydrochloride hydrate, and berberine. It also revealed that doxycycline and chlortetracycline had dramatic inhibitory effects on DV2 and DV3. Although the potencies varied, the compounds showed inhibitory effects as long as they contained the tetracyclic ring structure. The tetracyclic ring structure may be the core factor of showing inhibitory effects on propagation of DV2 and DV3.

Additionally, in comparison, the inhibitory effects on DV2 were better than DV3. It demonstrated that the inhibitory effects may differ from the DV2 and DV3, with sequence variation at residues 51, 272, 274, 276, 277, and 278 in the β-OG-binding hydrophobic pocket of E protein. The sequence variations could indeed affect the specificity of the tetracycline derivatives to DV E protein.

Reference

Adadevoh, B.K., Ogunnaike, I.A., Bolodeoku, J.O. 1976. Serum levels of doxycycline in normal subjects after a single oral dose. *Br Med J*. 1: 880.

Agwuh, K.N. and MacGowan, A. 2006. Pharmacokinetics and pharmacodynamics of the tetracyclines including glycylcyclines. *Journal of Antimicrobial Chemotherapy.* 58:256-265.

Beeck, A.O.D., Rouille, Y., Caron, M., Duvet, S., and Dubuisson, J. 2004. The transmembrane domains of the prM and E proteins of yellow fever virus are endoplasmic reticulum localization signals. *J. Virol.* 78: 12591-12602.

Brinkworth, R.I., Fairlie, D.P., Leung, D., and Young, P.R. 1999. Homology model of the dengue 2 virus NS3 protease: putative interactions with both substrate and NS2B cofactor. *J. Gen. Viral.* 80: 1167-1177.

Centers for disease control and prevention (CDC, USA). 2008. Website of CDC, USA <http://www.cdc.gov>

Chambers, T.J., Droll, D.A., Tang, Y., *et al.* 2005. Yellow fever virus NS2BNS3 protease: characterization of charged-to-alanine mutant and revertant viruses and analysis of polyprotein-cleavage activities. *J Gen Virol.* 86(Pt 5): 1403–1413.

Chambers, T.J., Nestorowicz, A., Amberg, S.M., and Rice, C.M. 1993. Mutagenesis of the yellow fever virus NS2B protein: effects on proteolytic processing, NS2B-NS3 complex formation, and viral replication. *J. Viral.* 67 (11): 6797-6807.

Chao, D.Y., Kingi, C.C., Wang, W.K., Chen, W.J. 2005. Strategically examining the full-genome of dengue virus type 3 in the clinical isolates reveals its mutation spectra. *J. Virol.* 2: 72-81.

Clyde, K., Kyle, L.J., and Harris, E. 2006. Recent advances in deciphering viral and host determinants of dengue virus replication and pathogenesis. *J. Virol.* 80: 11418-11431.

Clum, S., Ebner, K.E., Padmanabhan, R. 1997. Cotranslational membrane insertion of the serine proteinase precursor NS2B-NS3(Pro) of dengue virus type 2 is required for efficient in vitro processing and is mediated through the hydrophobic regions of NS2B. *J Biol Chem.* 272(49): 30715–30723.

Erbel, P., Schiering, N., *et al.* 2006. Structural basis for the activation of flaviviral NS3 proteases from dengue and West Nile virus. *Nat Struct Mol Biol.* 13(4): 372–373.

Falgout, B., Pethel, M., Zhang, Y.M., *et al.* 1991. Both nonstructural proteins NS2B and NS3 are required for the proteolytic processing of Dengue virus nonstructural proteins. *J Virol.* 65: 2467–2475.

Falgout, B., Miller, R.H., and Lai, C.J. 1993. Deletion analysis of dengue virus type 4 nonstructural protein NS2B: identification of a domain required for NS2B-NS3 protease activity. *J. Virol.* 67: 2034–2042.

Falgout, B., Markoff, L. 1995. Evidence that flavivirus NS1-NS2A cleavage is mediated by

a membrane-bound host protease in the endoplasmic reticulum. *J Virol.* 69: 7232–7243.

Farshad, G., Franz, X.H., Christian, W.M., Heidemarie, H., and Christian, K. 1991. Fusion activity of flaviviruses: comparison of mature and immature (prM-containing) tick-borne encephalitis virions. *J. General Virology.* 72: 1323-1329.

Fields, B.N., Knipe, D.M., Howley, P.M., and Griffin, D.E. 2001. Fields virology, 4th ed. Lippincott Williams & Wilkins, Philadelphia, Pa.

Gubler, D.J. and Kuno, G. 1997. Dengue and Dengue Hemorrhagic Fever. CAB International, New York, New York.

Guha-Sapir, D. and Schimmer, B. 2005. Dengue fever: new paradigms for a changing epidemiology. Emerg. *Themes Epidemiol.* 2: 1-10.

Hanley, K.A., Manlucu, L.R., Gilmore, L.E., Blaney, J.E., Jr. H., C.T., Murphy, B.R., Whitehead, S.S. 2003. A trade-off in replication in mosquito versus mammalian systems conferred by a point mutation in the NS4B protein of dengue virus type 4. *J. Virol.* 312: 222-232.

Heinz, F.X. and Allison, S.L. 2001. The machinery for flavivirus fusion with host cell membranes. *Curr Opin Microbiol* 4: 450-455.

Khromykh, A.A., Varnavski, A.N., Sedlak, P.L., *et al*. 2001. Coupling between replication and packaging of flavivirus RNA: evidence derived from the use of DNA-based full-length cDNA clones of Kunjin virus. *J Virol.* 75: 4633–4640.

Kummerer, B.M. and Rice, C.M. 2002. Mutations in Yellow Fever Virus nonstructural protein NS2A selectively block production of infectious particles. *J. Virol.* 76 (10): 4773-4784.

Kunin, C., Dornbush, A.C., Finland, M. 1966. Distribution and excretion of four tetracycline analogues in normal young men. J Clin Invest. 38: 1950–9.

Lee, E., Weir, R.C., Dalgarno, L. 1997. Changes in the dengue virus major envelope protein on passaging and their localization on the three-dimensional structure of the protein. *J. Virol.* 232: 281–290.

Lindenbach, B.D. and Rice, C.M. 1999. Genetic interaction of flavivirus nonstructural proteins NS1 and NS4A as a determinant of replicase function. *J. Virol.* 73: 4611-4621.

Lindenbach, B.D., Thiel, H.J., and Rice, C.M. 2007. Flaviviridae: the viruses and their replication. *Fields virology.* 33: 1101-1152.

Li, Z., Khaliq, M., Zhou, Z., Post, C.B., Kuhn, R.J., Cushman, M. 2008. Design synthesis, and biological evaluation of antiviral agents targeting flavivirus envelope proteins. *J. Med. Chem.* 51: 4660-4671.

Liu, W.J., Chen, H.B., Khromykh, A.A. 2003. Molecular and functional analyses of Kunjin virus infectious cDNA clones demonstrate the essential roles for NS2A in virus assembly and for a nonconservative residue in NS3 in RNA replication. *J. Virol.* 77: 7804–7813.

Liu, W.J., Chen, H.B., Wang, X.J., *et al*. 2004. Analysis of adaptive mutations in Kunjin virus replicon RNA reveals a novel role for the flavivirus nonstructural protein NS2A in

inhibition of beta interferon promoter-driven transcription. *J. Virol.* 78: 12225–12235.

Liu, W.J., Wang, X.J., Mokhonov, V.V., Shi, P.V., Randall, R., and Khromykh, A.A. 2005. Inhibition of interferon signaling by the New York 99 strain and Kunjin subtype of West Nile Virus involves blockage of STAT1 and STAT2 activation by nonstructural proteins. *J. Virol.* 79: 1934-1942.

Liu, W.J., Wang, X.J., Clark, D.C., *et al.* 2006. A single amino acid substitution in the West Nile virus nonstructural protein NS2A disables its ability to inhibit alpha/beta interferon induction and attenuates virus virulence in mice. *J. Virol.* 80: 2396–2404.

Lundin, M., Monne, M., Widell, A., Von, H., and Persson, M.A.A. 2003. Topology of the membrane-associated hepatitis C virus protein NS4B. *J. Virol.* 77: 5428-5438.

Mackenzie, J.M., Khromykh, A.A., Jones, M.K., Westaway, E.G. 1998. Subcellular Localization and Some Biochemical Properties of the Flavivirus Kunjin Nonstructural Proteins NS2A and NS4A. *J. Virol.* 245: 203-215.

McBride, W.J., Bielefeldt-Ohmann, H. 2000. Dengue viral infection; pathogenesis and epidemiology. *Microbes Infect* 2: 1041-50.

Miller, S., Kastner, S., Jacomine, K.L., Buhler, S., Bartenschlager, R. 2007. The non-structural protein 4A of dengue virus is an intergral membrane protein inducing membrane alteration in a 2K-regulated manner. *J. Biological Chemistry.* 282(12): 8873-8882.

Monath, T.P., Henize, F.X. 1996. Flavivirus. In: Fields BN, Knipe DM, Howley PM, eds. Fields virology, 3rd ed, vol. 1. Philadelphia, Pa: LipponcottRaven. Pp 961-1034.

Morens, D.M., and Fauci, A.S. 2008. Dengue and hemorrhagic fever: A potential threat to public health in the United States. JAMA, J. Am. Med. Assoc. 299: 214-216.

Modis, Y., Ogata, S., Clements, D., and Harrison, S.C. 2003. A ligandbinding pocket in the dengue virus envelope glycoprotein. Proceedings of the National Academy of Sciences 100: 6986-6991.

Modis, Y., Ogata, S., Clements, D., and Harrison, S.C. 2004. Structure of the dengue virus envelope protein after membrane fusion. *Nature* 427: 313-319.

Munoz-Jordan, J.L., Sanchez-Burgos, G.G., Laurent-Rolle, M., and Garcia-Sastre, A. 2003. Inhibition of interferon signaling by dengue virus. *Proc. Nalt. Acad. Sci.* 100: 14333-14338.

Mukhopadhyay, S., Kuhn, R.J., and Rossmann, M.G. 2005 Structural perspective of the flavivirus life cycle. *Nat. Rev. Microbiol.* 3: 13-22.

Munoz-Jordan, J.L., Laurent-Rolle, M., Ashour, J., Martinez-Sobrido, L., Ashok, M., Lipkin, W.I., and Garcia-Sastre, A. 2005. Inhibition of alpha/beta interferon signaling by the NS4B protein of flaviviruses. *J. Virol.* 79: 8004-8013.

Niyomrattanakit, P., Winoyanuwattikun, P., Chanprapaph, S., *et al.* 2004. Identification of residues in the dengue virus type 2 NS2B cofactor that are critical for NS3 protease activation. *J Virol.* 78(24): 13708–13716.

Preugschat, F. and Strauss, J.H. 1991. Processing of nonstructural proteins NS4A and NS4B of dengue 2 virus *in vitro* and *in vivo*. *J. Virol.* 185: 689-697.

Rey, F.A., Heinz, F.X., Mandl, C., Kunz, C., Harrison, S.C. 1995. The envelope glycoprotein from tick-borne encephalitis virus at 2 A resolution. *Nature* 375: 291–298.

Roosendaal, J., Westaway, E.G., Khromykh, A., Mackenzie, J.M. 2006. Regulated cleavages at the West Nile virus NS4A-2K-NS4B junctions play a major role in rearranging cytoplasmic membranes and Golgi trafficking of the NS4A protein. *J. Virol.* 80: 4623-4632.

Robert, A., Alan, D.K., and Bruce, L.L. 1992. Correlation of E protein binding with cell susceptibility to dengue 4 virus infection. *J. General Virology.* 73: 2155-2159.

Sampath, A. and Padmanabhan, R. 2009. Molecular targets for flavivirus drug discovery. *Antiviral research.* 81: 6-15.

Sjolin-Forsberg G, Hermannson J. 1984. Comparative bioavailability of tetracycline and lymecycline. Br J Clin Pharmacol. 18: 529–33.

Smilack, J.D. 1999. The tetracyclines. Mayo Clinic Proceedings. 74: 729–729.

Solomon, T. and Mallewa, M. 2001. Dengue and other emerging flaviviruses. *J. Infect.* 42: 104-115.

Speight, G., Coia, G., Parker, M.D., and Westaway, E.G. 1988. Gene mapping and positive identification of the non-structural proteins NS2A, NS2B, NS3, NS4B and NS5 of the flavivirus Kunjin and their cleavage sites. *J. Gen. Virol.* 69: 23-34.

Thorsten, K., Daniela, S.M., Alan, E.M., Paul, R.Y., and Bostjan, K. 2006. The Role of Histidine Residues in Hypothesis Low-pH-Mediated Viral Membrane Fusion. Structure. 14: 1481-1487.

Umareddy, I., Chao, A., Sampath, A., Gu, F., Vasudevan, S.G. 2006. Dengue virus NS4B interacts with NS3 and dissociates it from single-stranded RNA. *J. General Virology.* 87: 2605-2614.

von Heijne, G. 1986. A new method for predicting signal sequence cleavage site. *Nucleic Acids Res.* 14: 4683-4690.

Wang, Q.Y., Patel, S.J., Vangrevelinghe, E., *et al.* 2009. A small molecule dengue virus entry inhibitor. Antimicrob. Agents Chemother. 01148-08.

Yang, J.M., Chen, Y.F., Tu, Y.Y., Yen, K.R., Yang, Y.L. 2007. Combinatorial computational approaches to identity tetracycline derivatives as flavivirus inhibitors. *PLoS One* 2: e428.

Yennamalli, R., Subbarao, N., Kampmann, T., McGeary, R.P., Young, P.R., Kobe, B. 2009. Idetification of novel target sites and an inhibitor of the dengue virus E protein. J Comput Aided Mol Des.

Yusof, R., Clum, S., Wetzel, M., Krishna, M., H.M., Padmanabhan, R. 2000. Purified NS2B/NS3 serine protease of dengue virus type 2 exhibits cofactor NS2B dependence for cleavage of substrates with dibasic amino acids in vitro. *J. Biological Chemistry.*

275(14): 9963-9969.

Zhou, Z., Khaliq, M., Suk, J.E., Patkar, C., Li, L., Kuhn, R.J., and Post, C.B. 2008. Antiviral compounds discovered by virtual screening of small-molecule libraries against dengue virus E protein. *ACS Chemical Biology*. 3: 756-775.

Zuo, Z., Liew, O.W., Chen, G., Chong, P.C.J., Lee, S.H. 2009. Mechanism of NS2B-mediated activation of NS3pro in dengue virus: molecular dynamics simulations and bioassays. *J. Viral.* 83(2): 1060-1070.

徐婕琳. 2003. 表現登革熱病毒二型PL046非結構型蛋白: NS2A, NS2B, NS4A及NS4B在大腸桿菌, 哺乳類細胞及真菌*Pichia pastoris*表現系統. 交通大學碩士論文.

楊馥嘉. 2006. 登革熱病毒二型PL046非結構型蛋白: NS2A, NS2B, NS4A及NS4B之功能性研究. 交通大學碩士論文.

杜育穎. 2007. 以四環素及其衍生物為第二型登革熱病毒之抑制劑. 交通大學碩士論文.

Table 1. Contents of the SuperScript™ One-Step RT-PCR reaction

Components	Volume/50 µl	Final Concentration
2X Reaction Mix	25 µl	1X
Template RNA	x µl	10 pg – 1 µg
Sense Primer (10 µM)	1 µl	0.2 µM
Anti-sense Primer (10 µM)	1 µl	0.2 µM
RT/ PlatinumR *Taq* Mix	1 µl	—
Autoclaved distilled water	to 50 µl	—

Table 2. The thermal cycle program

A: cDNA synthesis and pre-denaturation	B: PCR ampification	C: Final-extention
Perform 1 cycle of: 55℃ for 30 minutes 94℃ for 2 minutes	Perform 35 cycles of: Denature, 94℃ 15 s Anneal, 60℃ 30 s Extend, 72℃ for 1min/kb	1 cycle of 72℃ for 10 minutes

Table 3. Contents of the PCR reaction

Reagent	Volume
Fermentas 10X *Taq* buffer	5 µl
dNTP mixture (10 mM)	4 µl
Taq DNA polymerase	1 µl
Forward PCR primer (EGFP-F)	1 µl
Reverse PCR primer (EGFP-R)	1 µl
pEGFP-N2 plasmid	1 µl
Add ddH_2O to a final volume of 50 µl	

Table 4. Condition for the PCR reaction for EGFP

Segment	Cycle	Temperature	Time
1	1	94℃	3 minutes
2	30	94℃	30 seconds
		62℃	30 seconds
		72℃	90 seconds
3	1	72℃	15 minutes

Table 5. The relative percentage of plaque numbers of the stable cell lines

Experiment number	BHK-21 %PFU	pcDNA3 %PFU	EGFP %PFU	2A-EGFP %PFU	2B-EGFP (pro) %PFU	4B-EGFP (pro) %PFU
1	100	112.82	123.08		78.63	134.19
2	100	116.28	138.37		95.35	116.28
3	100	138.89	144.44		102.78	148.61
4	100	101.64	104.10		95.90	143.44
5	100	99.07	123.36		104.67	118.69
6	100	89.81	106.48		119.44	108.33
7	100	127.74	107.3	67.88		
8	100	149.56	150.94	88.68		
9	100	141.59	132.74	82.30		
10	100	125.77	160.82	78.35		
11	100	120.24	110.71	90.48		
12	100	141.89	113.51	81.08		
Mean±S.D.	-	122.11±18.99	126.32±19.04	81.46±8.10*	99.46±13.42	128.26±16.20

The percentage of plaque numbers of each stable cell lines was compared with that of EGFP using analysis of variation (ANOVA) and Scheffe test. * means it was significantly different (P<0.05).

Table 6. Comparison of the amino acids of the β-OG-binding hydrophobic pocket in E protein between dengue virus type 2 PL046 strain and dengue virus type 3 H87 strain

Residue position	Amino acids		Amino acids Changes (DV2→DV3)
	DV2 PL046	DV3 H87	
48	T	T	T48T
49	E	E	E49E
50	A	A	A50A
51	K	T	K51T
52	Q	Q	Q52Q
126	E	E	E126E
127	G	G	G127G
128	K	K	K128K
268	T	T	T268T
269	E	E	E269E
270	I	I	I270I
271	Q	Q	Q271Q
272	M	T	M272T
273	S	S	S273S
274	S	G	S274G
275	G	G	G275G
276	N	T	N276T
277	L	S	L277S
278	L	I	L278I
279	F	F	F279F

Table 7. Chemical structures and IC_{50}s for the tetracycline derivatives.

Name, chemical name; IC_{50}, the 50% inhibitory concentration; NA, not applicable.

Name	Structure	Viral serial type	IC_{50} (μM)
Tetracycline	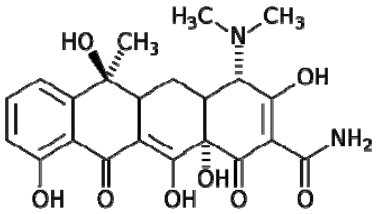	DV 2 DV 3	457.89 333.85
Doxycycline	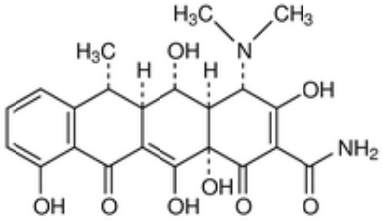	DV 2 DV 3	47.64 197.02
Chlortetracycline	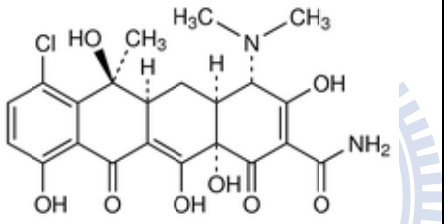	DV 2 DV 3	49.17 138.20
Rolitetracycline	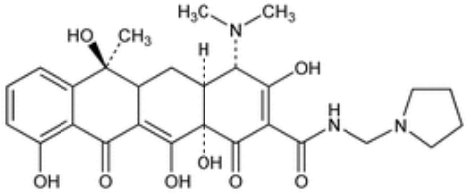	DV 2 DV 3	215.6 432.19
Kanamycin	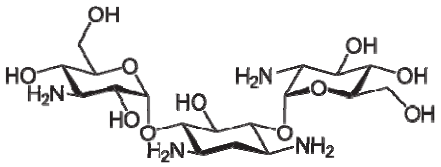	DV 2 DV 3	NA NA
9-amino-1,2,3,4-tetrahydroacridie hydrochloride hydrate	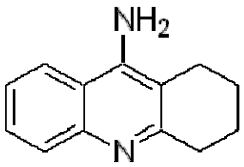	DV 2 DV 3	NA NA
Berberine	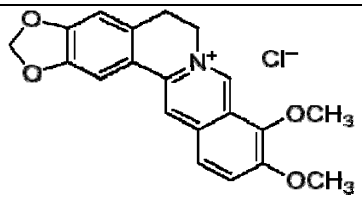	DV 2 DV 3	NA NA

Table 8. 2D and 3D structures for the tetracycline derivatives.

Red: oxygen; blue: nitrogen; green: chloride.

Name	2D-structure	3D-structure
Tetracycline	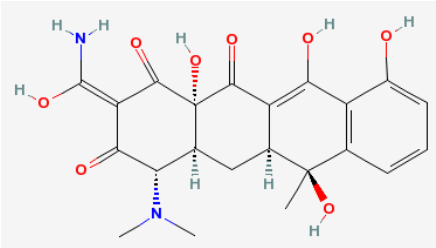	
Doxycycline	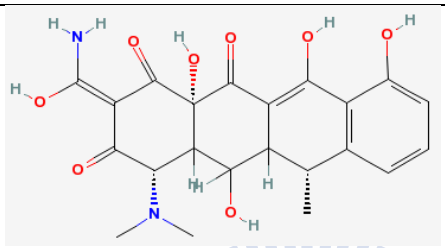	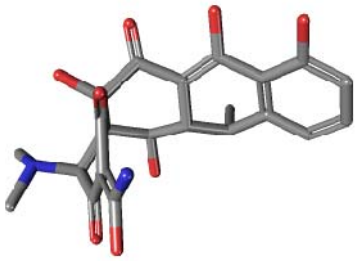
Chlortetracycline	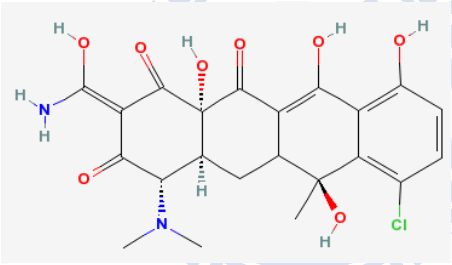	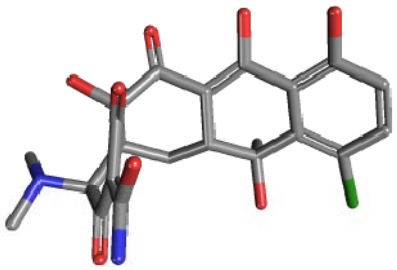
Rolitetracycline	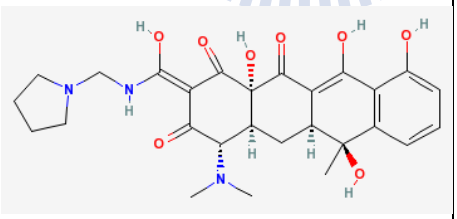	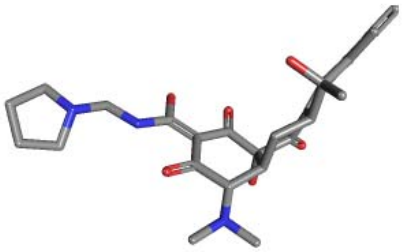
Kanamycin	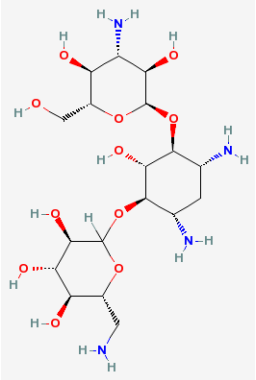	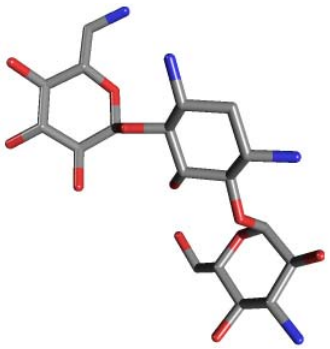

9-amino-1,2,3,4-tetrahydroacridie hydrochloride hydrate	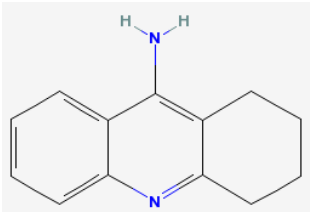	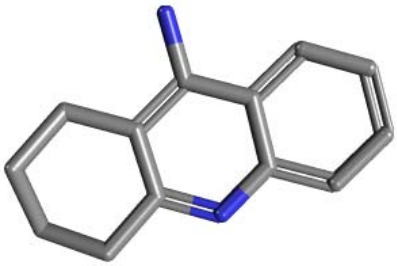
Berberine	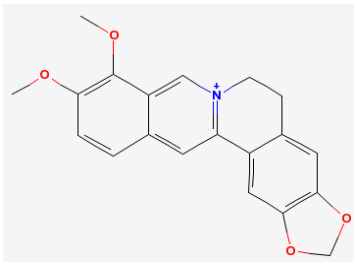	

Form NCBI PubChem compound. http://pubchem.ncbi.nlm.nih.gov/

Table 9. Pharmacokinetics of tetracycline derivatives

Agent	Formulations	Percentage absorption	Dose (mg)	Peak plasma concentration (C_{max}) (mg/L)	Time to peak concentration (t_{max}) (h)
Tetracycline	po/iv[a]	77-88	500	3-5 (11.3 μM)	2
Doxycycline	po	-	500	15.3 (30 μM)	4
Chlortetracycline	po	25-30	500	1.4 (2.72 μM)	3
Rolitetracycline	iv	none	300	4-6 (11.4 μM)	-

a: po: oral; iv: intravenous

(tetracycline MW=444.43; doxycycline MW=512.94; chlortetracycline MW=515.34; rolitetracycline MW=527.57)

(Adadevoh *et al*., 1976; Agwuh *et al*., 2006; Kunin *et al*., 1966; Sjolin-Forsberg G *et al*., 1984; Smilack *et al*., 1999)

World Distribution of Dengue-2008

Fig. 1.1 World distributions of dengue viruses and their mosquito vector, *Aedes aegypti*, in 2008. (CDC, USA, 2008)

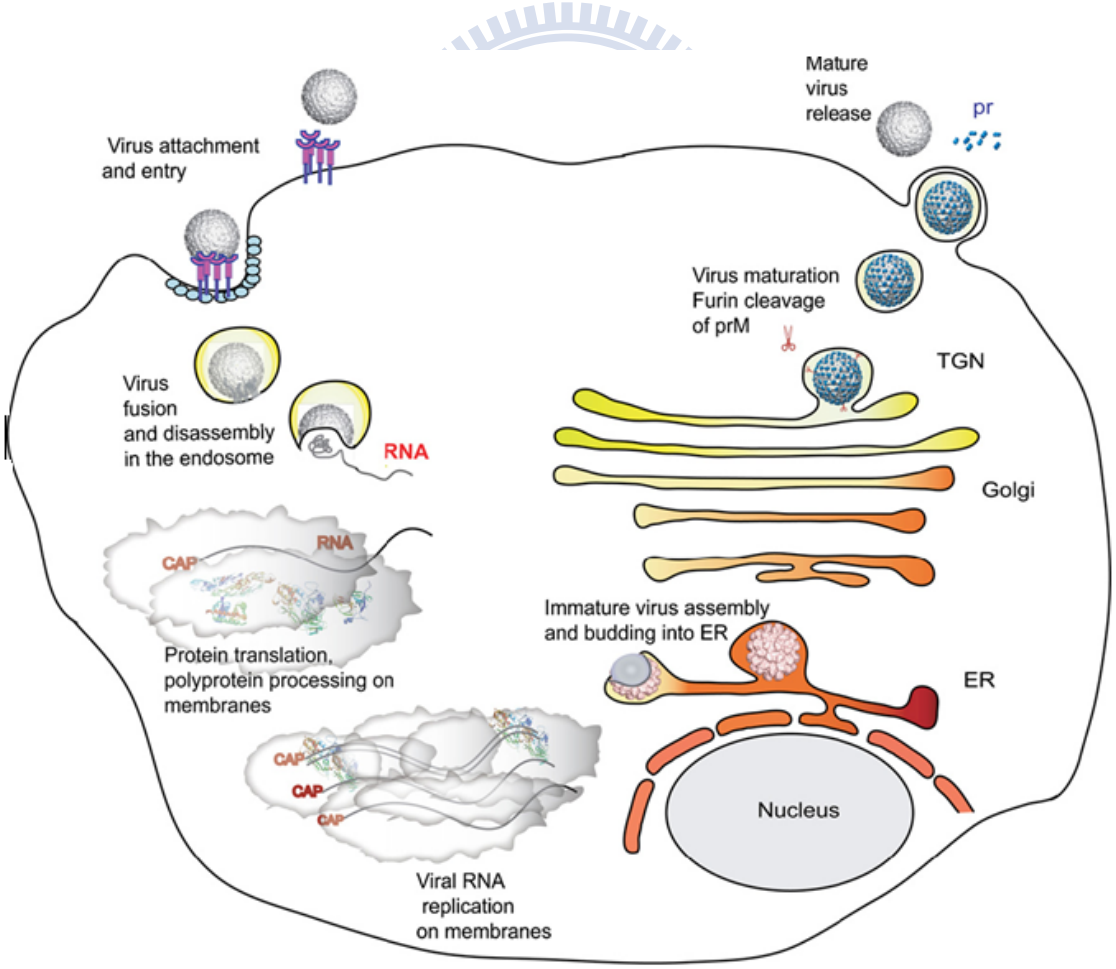

Fig. 1.2 The flavivirus replication cycle. (Sampath *et al.*, 2009)

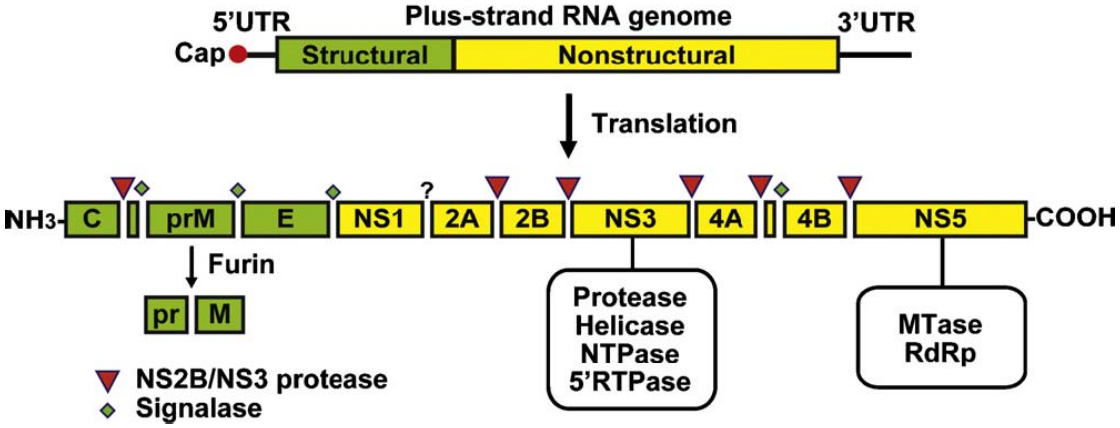

Fig. 1.3 Schematic representation of flavivirus genome organization and polyprotein processing.

The 11 kb positive-sense, single-stranded RNA genome contains a single open reading frame with encodes 3 structural proteins (capsid (C), precursor membrane (prM) and envelope (E)) and 7 non-structural proteins (NS1, NS2A, NS2B, NS3, NS4A, NS4B, and NS5). The open reading frame is flanked by untranslated regions. Sites of polyprotein cleavage mediated by the viral NS2B-NS3 and by host signalase and furin are shown, and the enzymatic activities of NS3 and NS5 are also indicated.

(Sampath *et al.*, 2009)

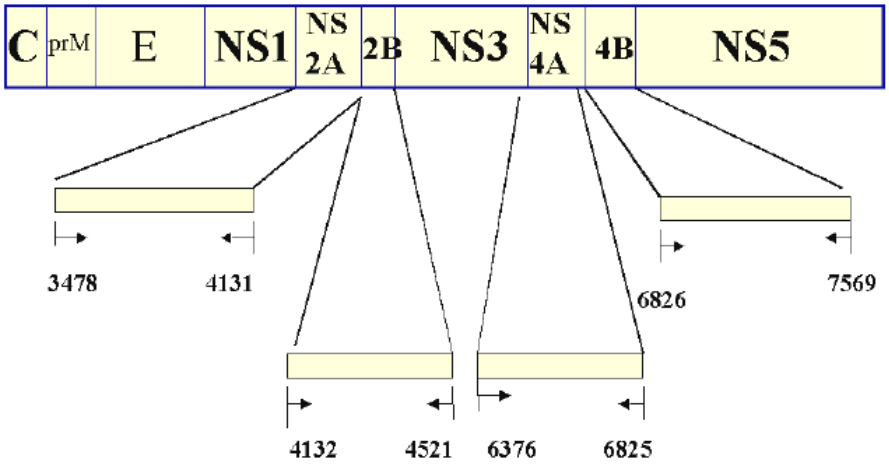

Fig. 1.4 Nucleotide mapping of NS2A, NS2B, NS4A, and NS4B in dengue virus type 2 genome.

Numbers indicate the nucleotide numbers starting from 5' UTR.

(Gubler and Kuno, 1997)

(A)

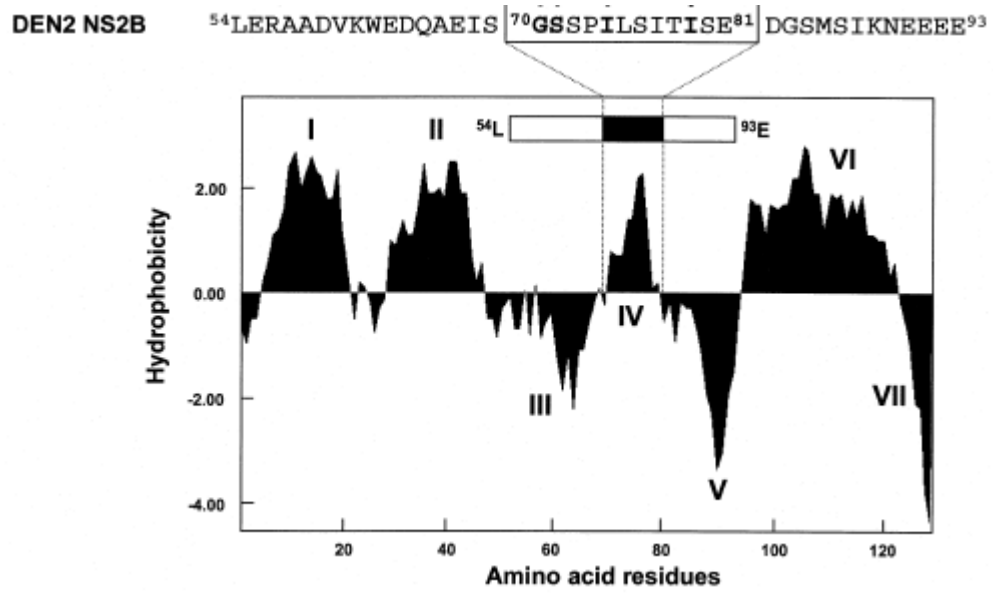

(B)

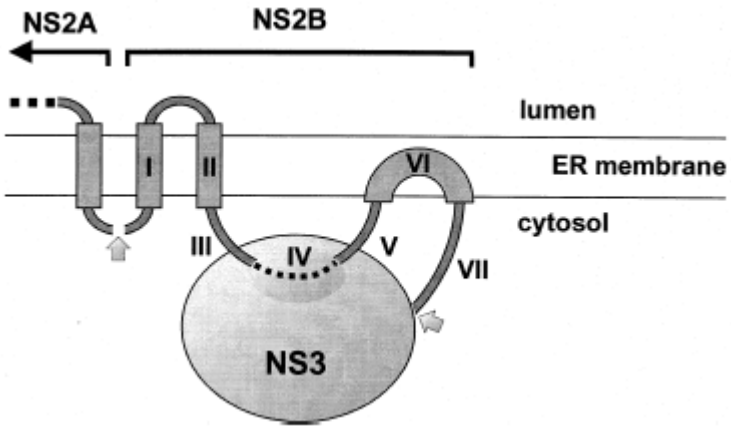

Fig. 1.5 NS2B hydrophobicity plots and a hypothetical model of NS2B-NS3pro association with membranes.

(A)Hydrophobicity profiles [generated by the Kyte & Doolittle algorithm (Kyte & Doolittle, 1982) in the MacVector suite of programs] of the DEN2 cofactor NS2B. I-VII, regions of NS2B with either hydrophobic (I, II, IV and, VI) or hydrophilic (III, V, and VII) character. The 40 amino acid cofactor domain of NS2B (schematically represented as a boxed region) is as indicated, and the central hydrophobic 12 amino acid stretch of NS2B (^{70}GSSPILSITISE^{81}) modeled is also boxed. (B) Schematic representation of potential interactions between specific domains of the NS2B cofactor and either cellular membranes or NS3pro. Domain I-VII correspond to regions of hydrophobicity and hydrophilicity identified in (A). Shaded arrows identify sites of NS2B/NS3 cleavage.

(Brinkworth *et al.*, 1999)

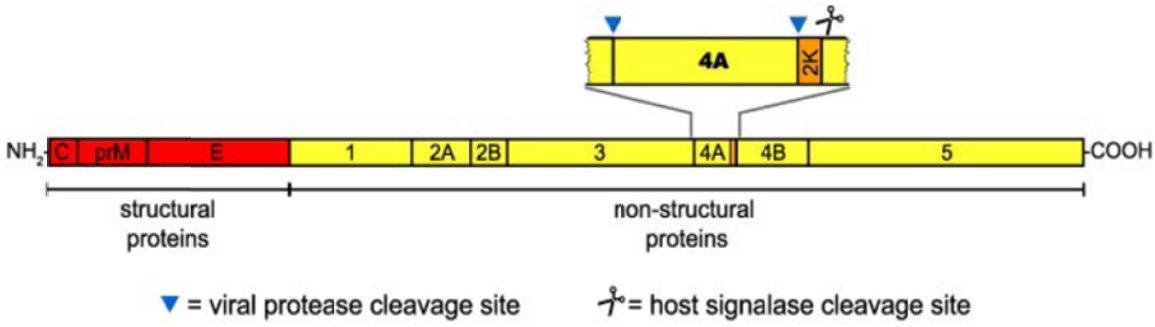

Fig. 1.6 Schematic structure of the DV polyprotein.

Structural proteins (*red*) and non-structural proteins (*yellow*) are indicated. A magnification of the NS4A-2K region is shown in the *top*. Viral protease cleavage sites (*blue arrowhead*) and the host cell signalase cleavage site (*scissors*) are given.

(Miller *et al.*, 2007)

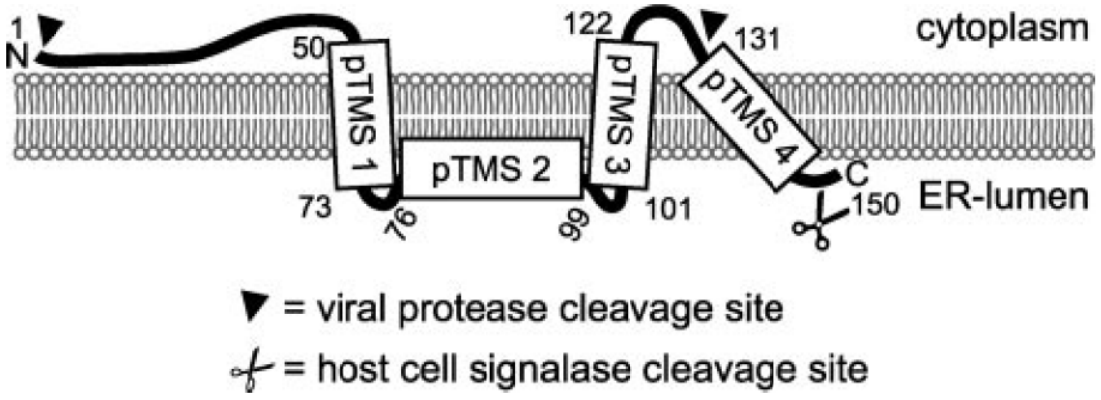

Fig. 1.7 Model for the membrane topology of DV NS4A.

The N-terminal one-third of DV NS4A is localized in the cytoplasm; pTMS 1 and pTMS 4 span the membrane from the cytoplasmic to the luminal site, whereas pTMS 3 seems to span the lipid bilayer from the luminal to the cytoplasmic site. Amino acids around positions 76-99 (pTMS 2) most probably do not span the membrane but are closely associated with the luminal side of the lipid bilayer.

(Miller *et al.*, 2007)

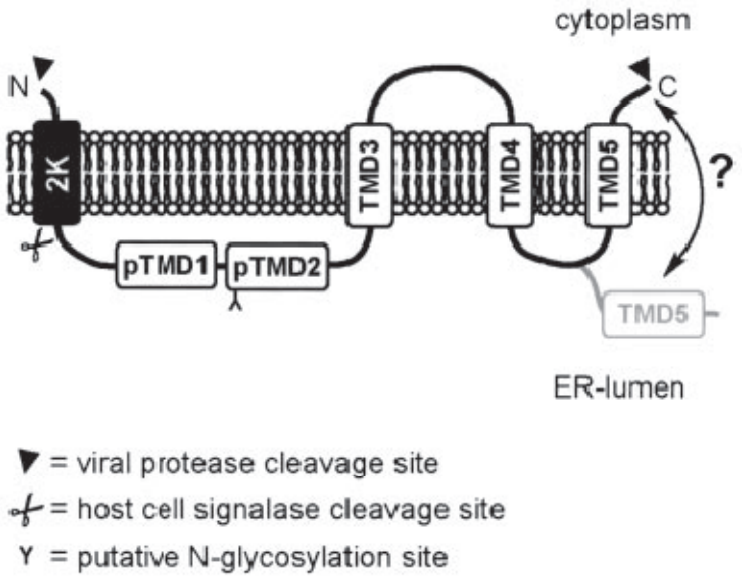

Fig. 1.8 Model for the membrane topology of DV 2K-NS4B.

2K serves as a signal sequence for the translocation of the NH2 terminus of NS4B into the lumen of the ER. It indicated that predicted TMDs 1 and 2 do not span the membrane but rather reside in the ER lumen. TMDs 3, 4, and 5 span the membrane, and serve as internal signal sequences for membrane association. Glycosylation may occur at an internal N-glycosylation site in the predicted TMD 2.

(Miller *et al.*, 2006)

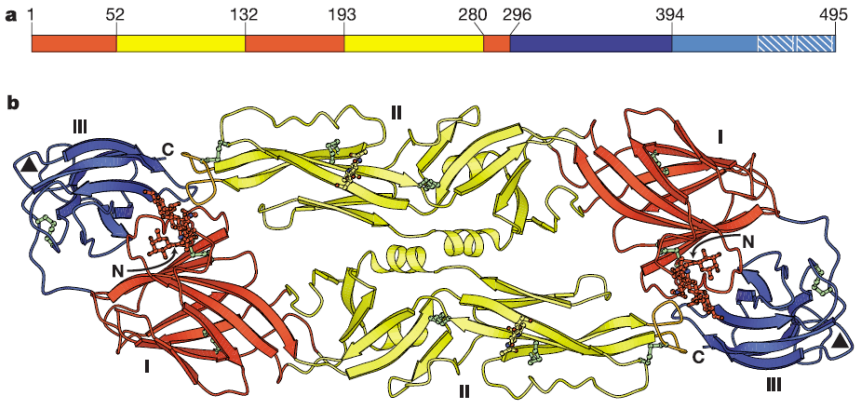

Fig. 1.9 Structure of the dimer of dengue E soluble fragment (sE) in the mature virus particle.

(a) The three domains of dengue sE. Domain I is red, domain II is yellow, domain III is blue. (b) The sE dimer. This is the conformation of E in the mature virus particle and in solution above the fusion pH. (Modis *et al*, 2004)

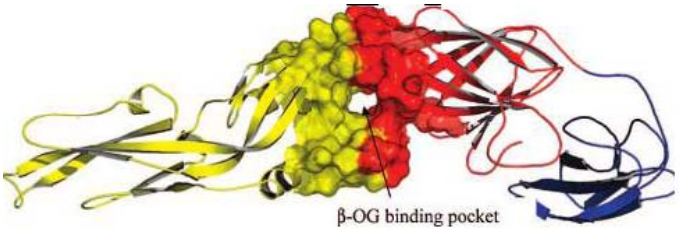

Fig. 1.10 Structure of dengue 2 E protein.

Domain I: red; domain II: yellow; domain III: blue. The β-OG binding pocket is located between domain I and II. (Li *et al.*, 2008)

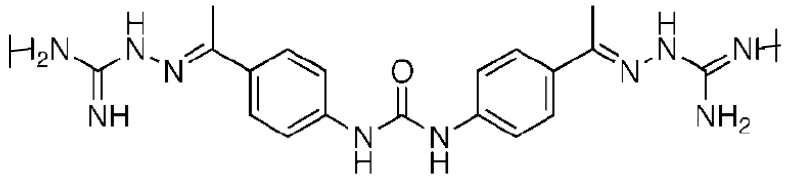

P02

Fig. 1.11 Molecule structure of the compound P02.

(Zhou *et al.*, 2008)

Compound	Core	R1	R2
6	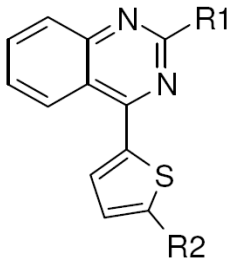	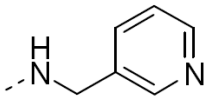	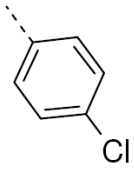

Fig. 1.12 Molecule structure of the compound 6.

(Wang *et al.*, 2009)

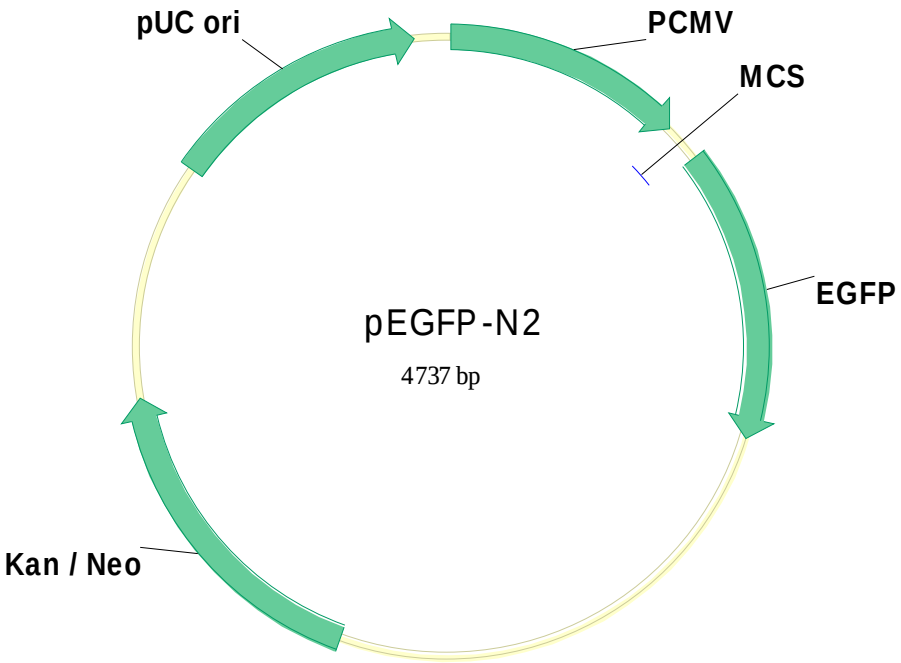

Fig. 3.1 Map of pEGFP-N2. The EGFP fragment was obtained by PCR reaction with primers EGFP-F and EGFP-R.

Kan/Neo: kanamycine, neomycin, resistance gene; pUC ori: *E. coli* replication origin; PCMV: Human cytomegalovirus (CMV) immediate early promoter; MCS: multiple cloning sites; EGFP: enhanced green fluorescent protein.

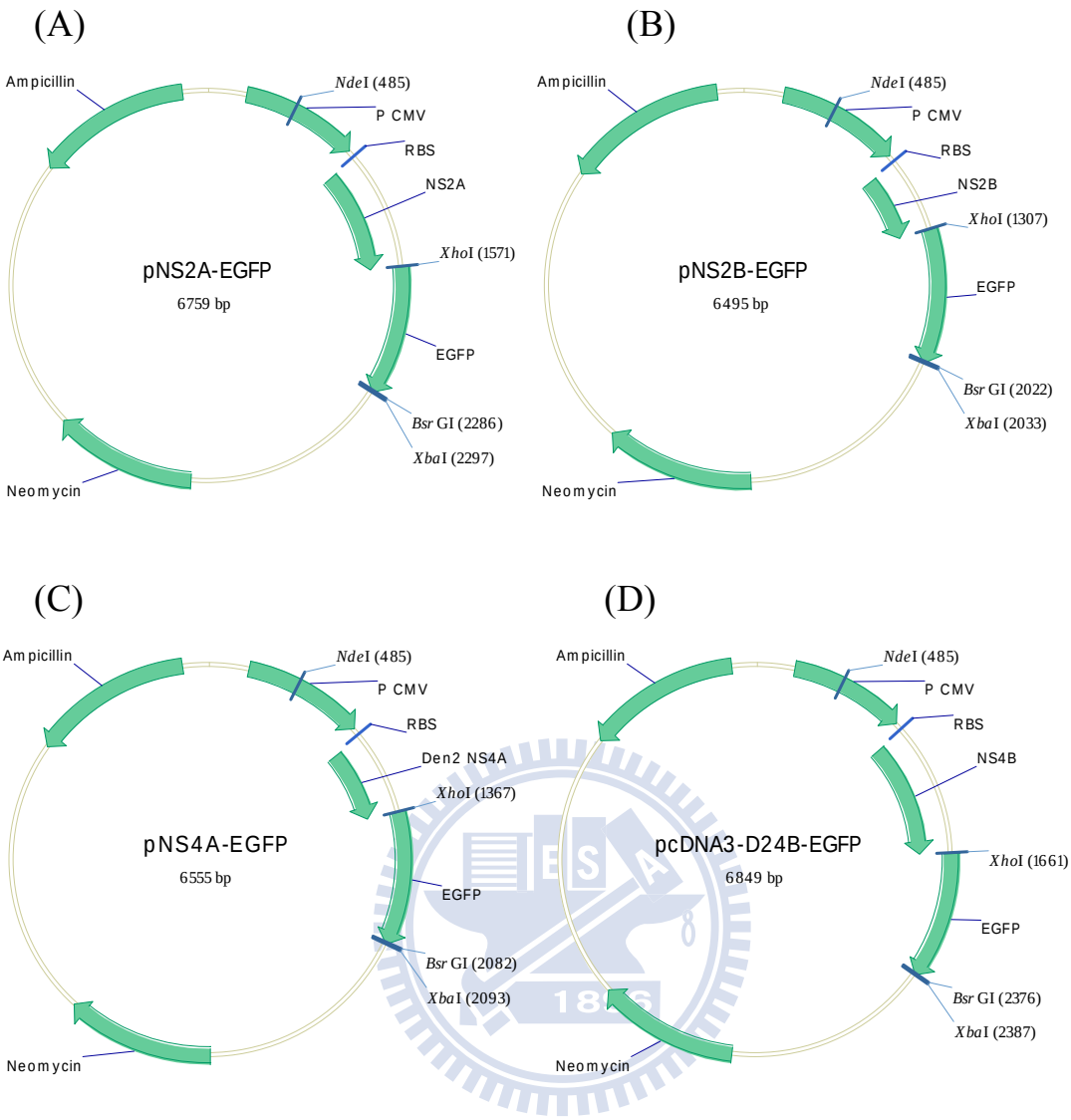

Fig. 3.2 Maps of pNS2A-EGFP, pNS2B-EGFP, pNS4A-EGFP, and pcDNA3-D24B-EGFP.

(A) Map of pNS2A-EGFP. (B) Map of pNS2B-EGFP. (C) pNS4A-EGFP. (D) Map of pcDNA3-D24B-EGFP. Neomycin: Neomycin resistance gene; Ampicillin: Ampicillin resistance gene; P CMV: Human cytomegalovirus (CMV) immediate early promoter; RBS: ribosome binding site; EGFP: enhanced green fluorescent protein; NS2A: nonstructural protein 2A; NS2B: nonstructural protein 2B; NS4A: nonstructural protein 4A; NS4B: nonstructural protein 4B.

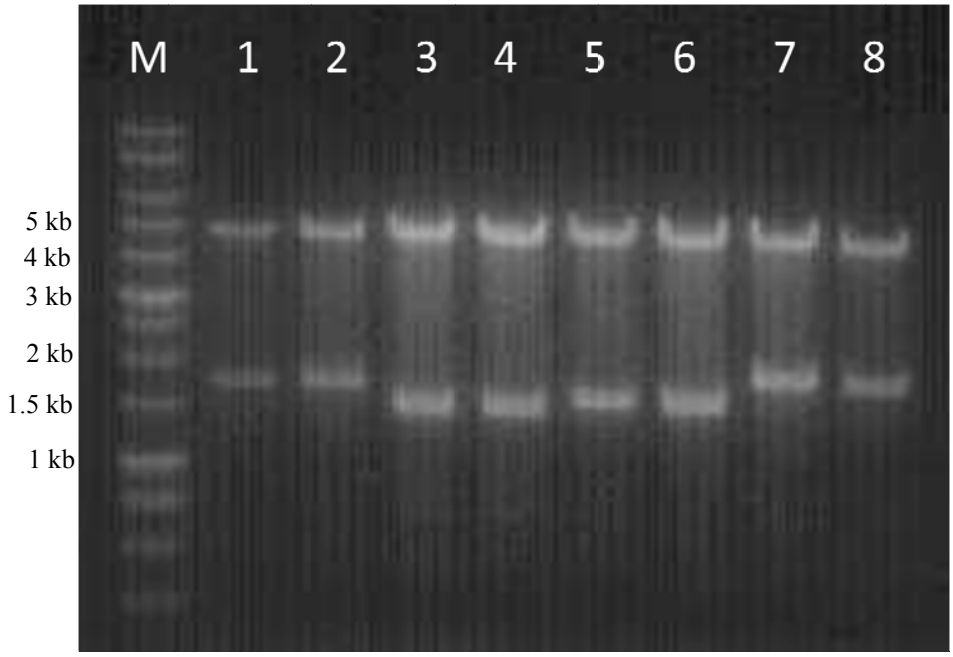

Fig. 3.3 Restriction enzyme digestions of pNS2A-EGFP, pNS2B-EGFP, pNS4A-EGFP, and pcDNA3-D24B-EGFP.

Lane 1 & 2, pNS2A-EGFP was digested by *BsrG*I and *Nde*I into 1801 bp and 4958 bp. Lane 3 & 4, pNS2B-EGFp was digested by *BsrG*I and *Nde*I into 1537 bp and 4958 bp. Lane 5 & 6, pNS4A-EGFP was digested by *BsrG*I and *Nde*I into 1597bp and 4958 bp. Lane 7 & 8, pcDNA3-D24B-EGFP was digested by *BsrG*I and *Nde*I into 1891 bp and 4958 bp.

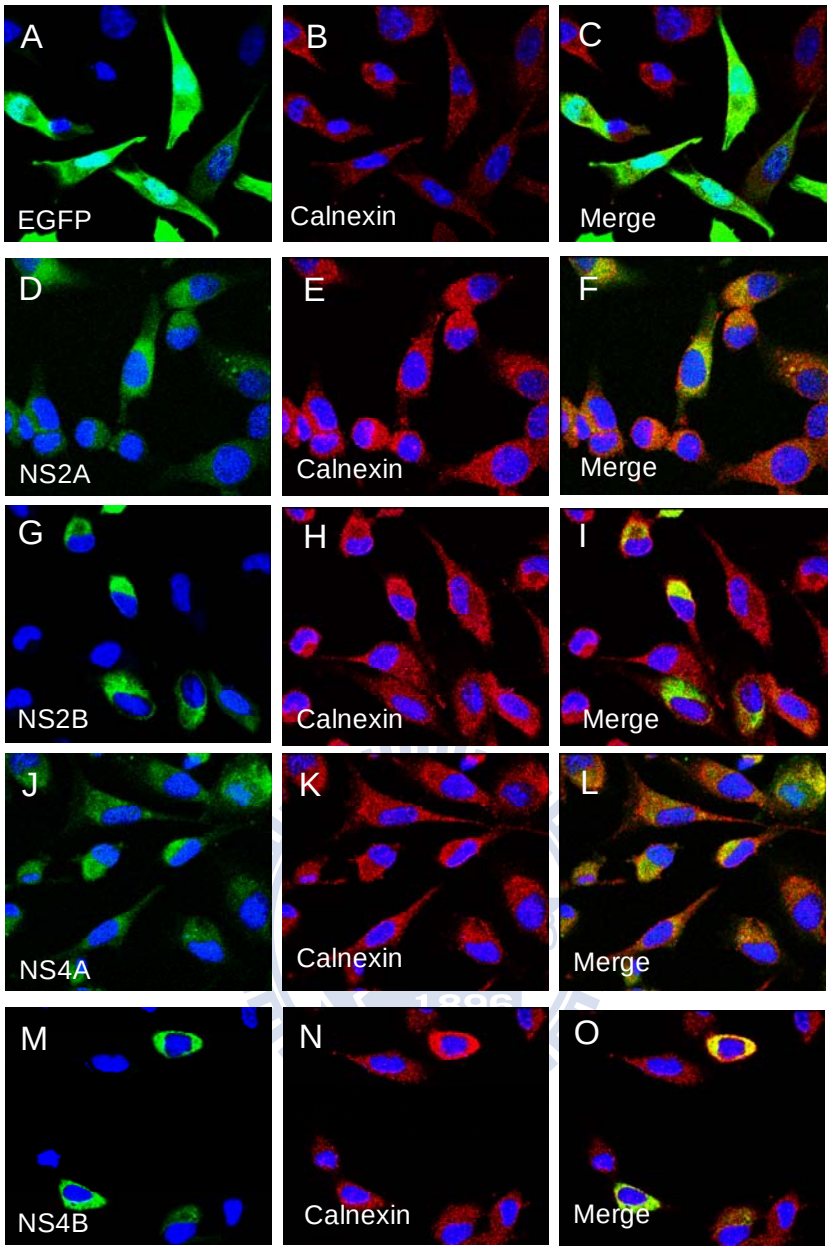

Fig. 3.4 Expression and colocalization of NS2A-EGFP, NS2B-EGFP, NS4A-EGFP, and NS4B-EGFP with the cellular marker protein, calnexin.

24 hr after transfection, cells were fixed with 4% paraformaldehyde, permeabilized with 0.5% Triton X-100, and processed for immunolabeling. Panels to the *left* depict cells expressed the NS2A, NS2B, NS4A, and NS4B with the fluorescence tag (A, D, G, J, and M) and panels in the *middle* depict the immunostaining of cellular marker calexin (B, E, H, K, and N). Merged pictures are shown on the *right* (C, F, I, L, and O). Nuclear DNA was stained with 4',6-diamidino-2-phenylindole dihydrochloride. Slides were analyzed by confocal laser scanning microscopy.

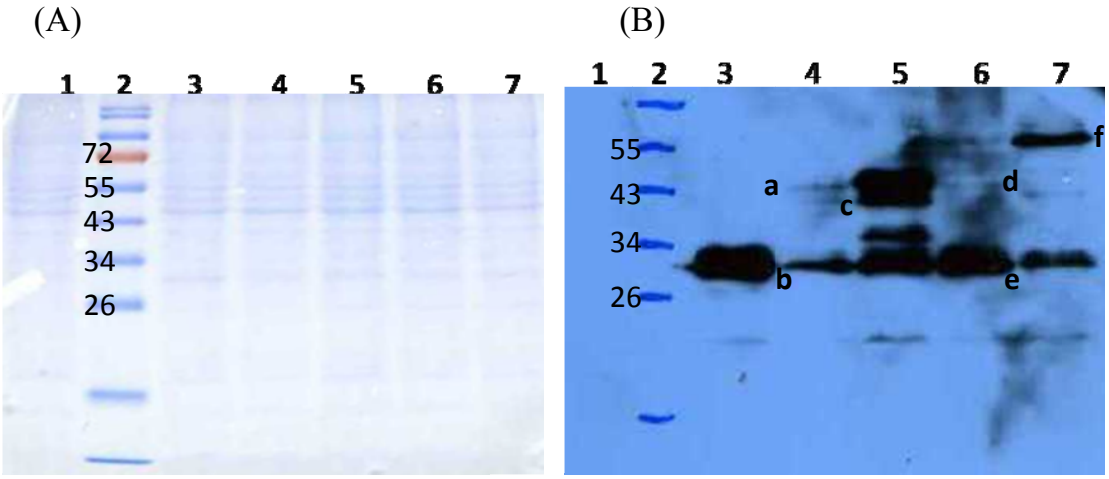

Fig. 3.5 Commassie blue staining and Western blot analysis of transiently expressed nonstructural proteins expressed in BHK-21.

(A) Coomassie blue staining of the supernatant of BHK-21 transfected with different plasmids. (B) Western blot analysis with anti-GFP-HRP antibody against supernatants of BHK-21 transfected with different plasmids. Lane 1, pcDNA3 (negative control); lane 2, prestained protein marker; lane 3, EGFP (positive control, 27 kDa); lane 4, pNS2A-EGFP, 50.9 kDa; lane 5, pNS2B-EGFP, 41.2 kDa; lane 6, pNS4A-EGFP, 43.7 kDa; lane 7, pcDNA3-D24B-EGFP, 54.0 kDa.

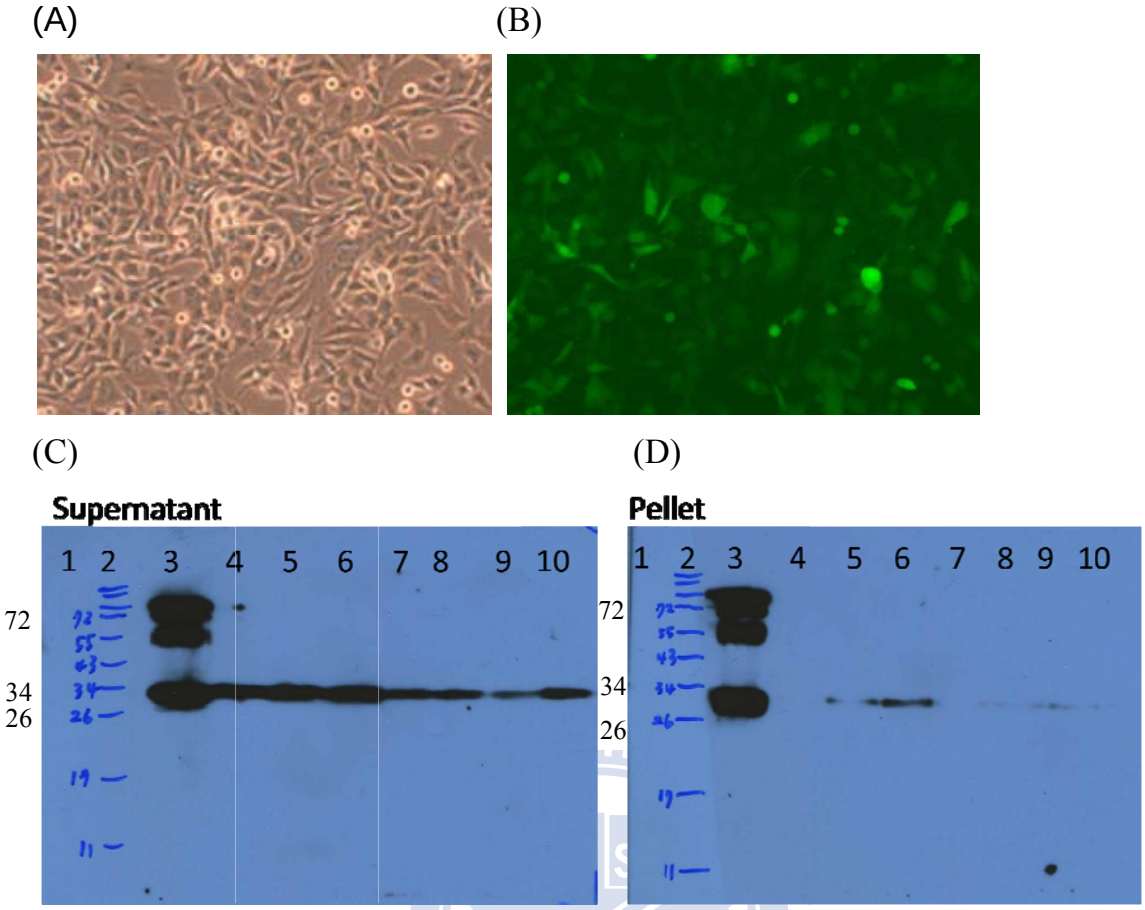

Fig. 3.6 Fluorescence microscopy and Western blot analysis for stable transfected cells (BHK-21) of EGFP.

(A) & (B) The fluorescence microscopy analysis of the stable transfected cells of EGFP. (C) Western blot analysis with anti-GFP-HRP antibody against the supernatant of BHK-21 of selected EGFP colonies (Lane 4-Lane 10, 27 kDa). (D) Western blot analysis with anti-GFP-HRP antibody against the pellet of BHK-21 of selected EGFP colonies (Lane 4-Lane 9, 27 kDa). Lane 1: pcDNA3 (negative control); Lane 2: prestained protein marker; Lane 3: yeast lysate containing Enol-EGFP (positive control, 79 kDa).

(A) (B)

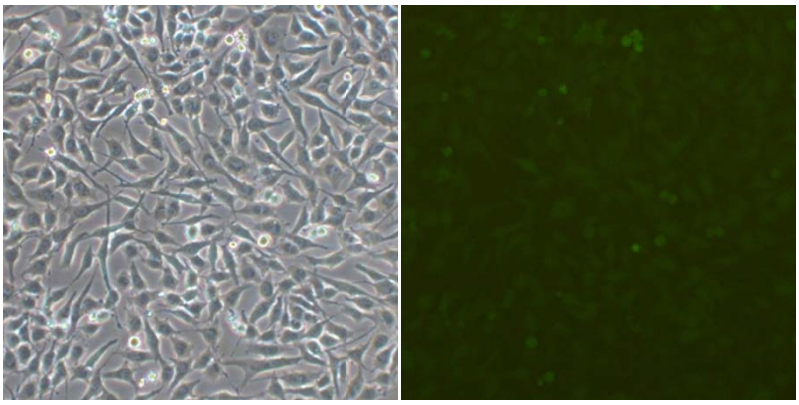

(C)

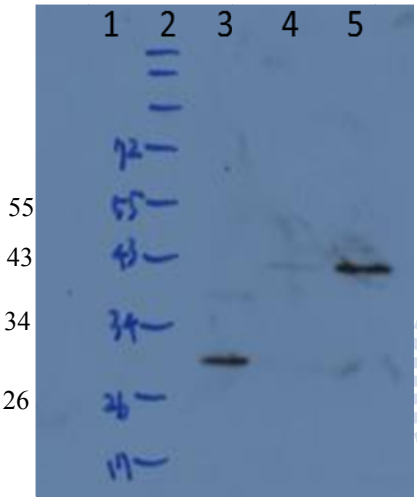

Fig. 3.7 Fluorescence microscopy and Western blot analysis for stable transfected cells (BHK-21) of NS2A-EGFP.

(A) & (B) The fluorescence microscopy analysis of the stable transfected cells of NS2A-EGFP. (C) Western blot analysis with anti-GFP-HRP antibody against the pellet and supernatant of BHK-21 of selected NS2A-EGFP colonies (Lane 4: pellet and Lane 5: supernatant, 50.9 kDa). Lane 1: pcDNA3 (negative control); Lane 2: prestained protein marker; Lane 3: EGFP (positive control, 27 kDa).

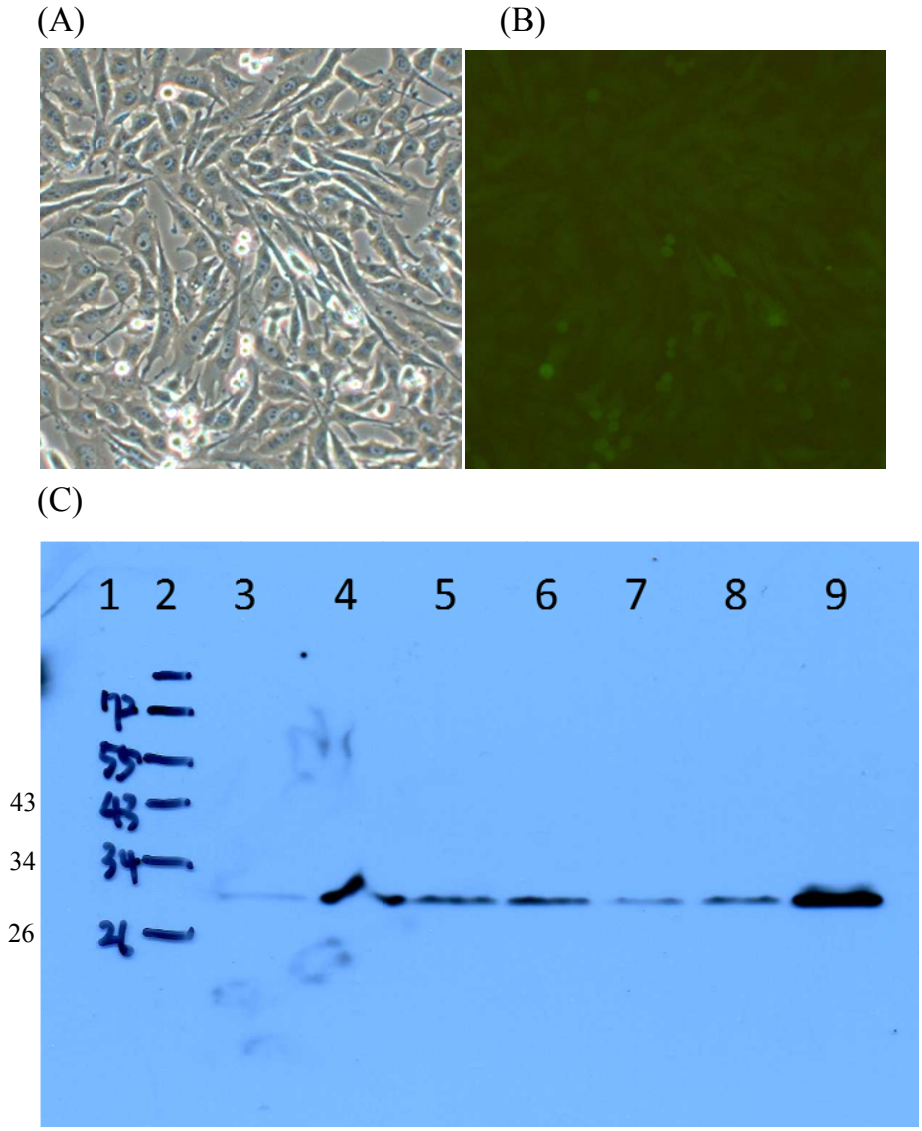

Fig. 3.8 Fluorescence microscopy and Western blot analysis for stable transfected cells (BHK-21) of NS2B-EGFP.

(A) & (B) The fluorescence microscopy analysis of the stable transfected cells of NS2B-EGFP. (C) Western blot analysis with anti-GFP-HRP antibody against the total cell lysate of BHK-21 of selected NS2B-EGFP colonies (Lane 4-Lane 9, 41.2 kDa). Lane 1: pcDNA3 (negative control); Lane 2: prestained protein marker; Lane 3: EGFP (positive control, 27 kDa).

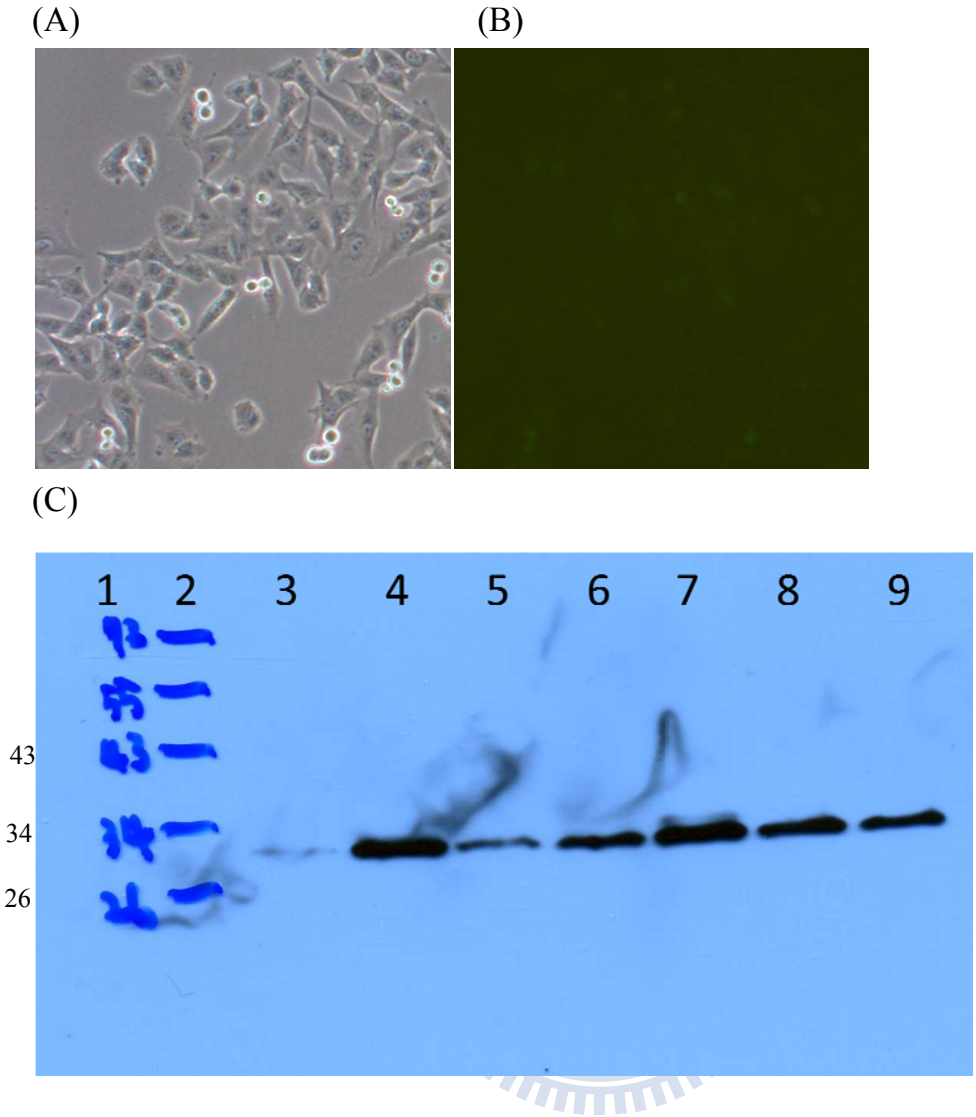

Fig. 3.9 Fluorescence microscopy and Western blot analysis for stable transfected cells (BHK-21) of NS4A-EGFP.

(A) & (B) The fluorescence microscopy analysis of the stable transfected cells of NS4A-EGFP. (C) Western blot analysis with anti-GFP-HRP antibody against the total cell lysate of BHK-21 of selected NS4A-EGFP colonies (Lane 4-Lane 9, 43.7 kDa). Lane 1: pcDNA3 (negative control); Lane 2: prestained protein marker; Lane 3: EGFP (positive control, 27 kDa).

(A) (B)

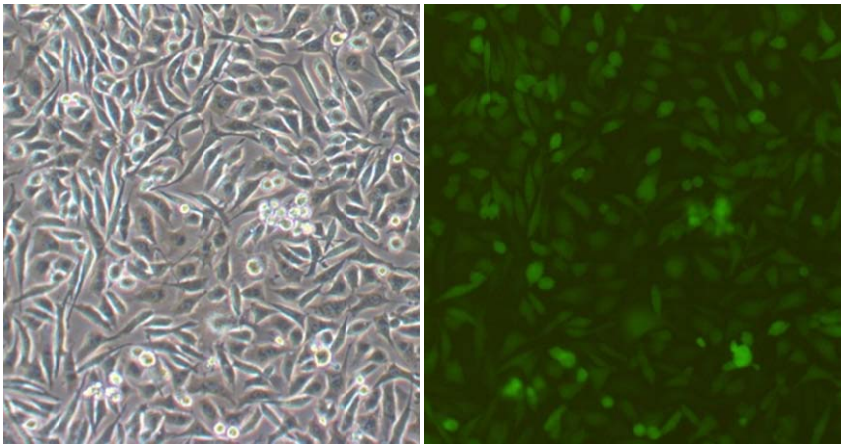

(C)

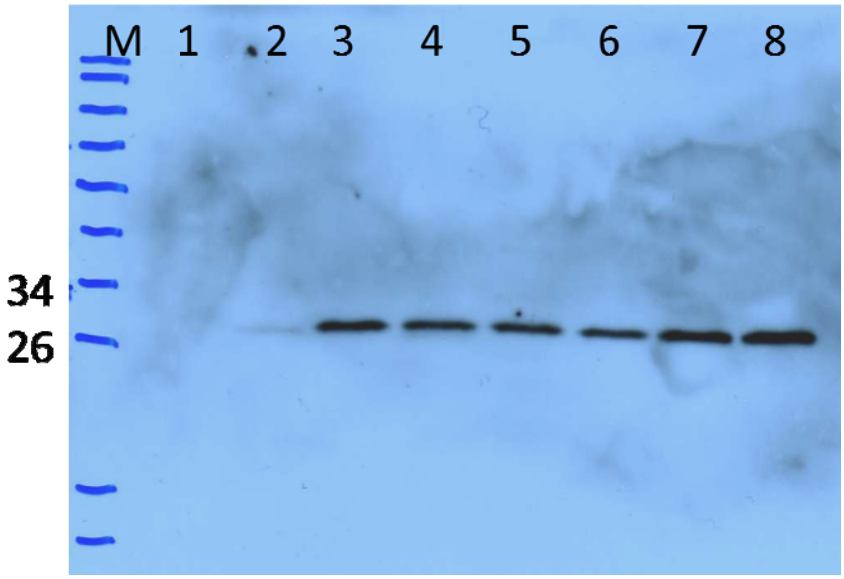

Fig. 3.10 Fluorescence microscopy and Western blot analysis for stable transfected cells (BHK-21) of NS4B-EGFP.

(A) & (B) The fluorescence microscopy analysis of the stable transfected cells of NS4B-EGFP. (C) Western blot analysis with anti-GFP-HRP antibody against the total cell lysate of BHK-21 of selected NS4B-EGFP colonies (Lane 3-Lane 8, 54.0 kDa). Lane 1: pcDNA3 (negative control); Lane 2: EGFP (positive control, 27 kDa).

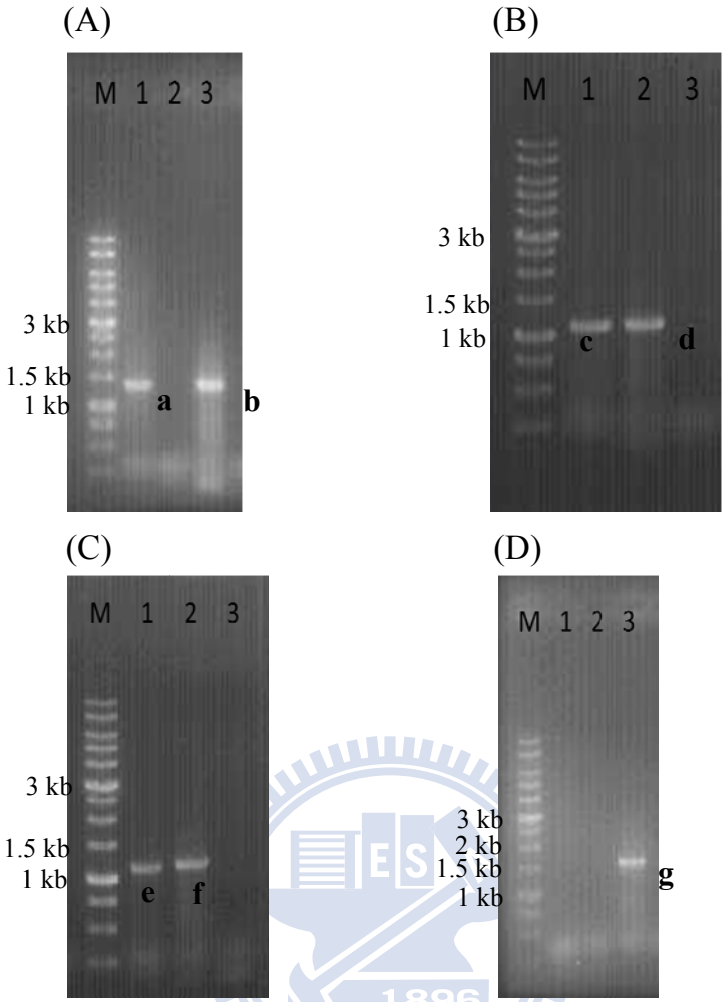

Fig. 3.11 PCR analysis of genomic DNA of the selected stable cell lines of NS2A-EGFP, NS2B-EGFP, NS4A-EGFP, and NS4B-EGFP.

(A) The genomic DNA was extracted from the stable transfected cell line BHK-21 of NS2A-EGFP, and was treated with primers 2AE-F and 2AE-R. Lane1: 2A-EGFP; Lane 2: pcDNA3 (negative control); Lane3: pNS2A-EGFP plasmid (positive control). (B) The genomic DNA was extracted from the stable transfected cell line BHK-21 of NS2B-EGFP, and was treated with primers 2BE-F and 2AE-R. Lane1: 2B-EGFP; Lane2: pNS2B-EGFP plasmid (positive control); Lane 3: pcDNA3 (negative control);. (C) The genomic DNA was extracted from the stable transfected cell line BHK-21 of NS4A-EGFP, and was treated with primers 4AE-F and 2AE-R. Lane1: 4A-EGFP; Lane2: pNS4A-EGFP plasmid (positive control); Lane 3: pcDNA3 (negative control); (D) The genomic DNA was extracted from the stable transfected cell line BHK-21 of NS4B-EGFP, and was treated with primers 4BE-F and 2AE-R. Lane1: 4B-EGFP; Lane 2: pcDNA3 (negative control); Lane3: pcDNA3-D24B-EGFP plasmid (positive control). The expected lengths of NS2A-EGFP, NS2B-EGFP, NS4A-EGFP, and NS4B-EGFP were 1377 bp (a), 1111 bp (c), 1169 bp (e), and 1470 bp (g), respectively.

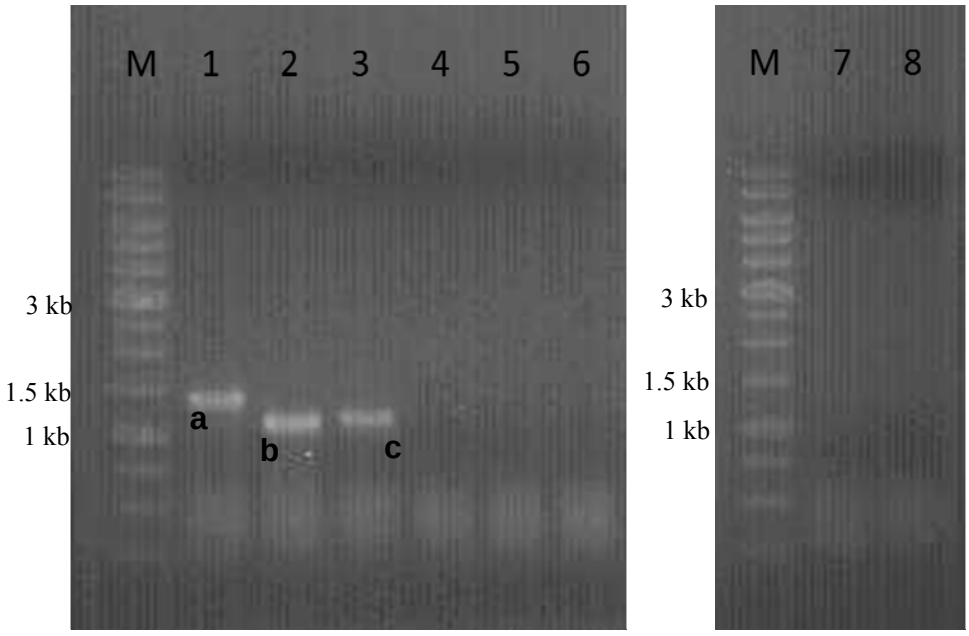

Fig. 3.12 Semi-quantitative RT-PCR of RNA from stable cell lines NS2A-EGFP, NS2B-EGFP, NS4A-EGFP, and NS4B-EGFP.

RNAs were extracted from the selected stable cell lines NS2A-EGFP, NS2B-EGFP, NS4A-EGFP, NS4B-EGFP, and pcDNA3 to perform superscript one-step RT-PCR with individuals primers. Lane1: NS2A-EGFP clone, treated with primers 2AE-F and 2AE-R. Lane2: NS2B-EGFP clone, treated with primers 2BE-F and 2AE-R. Lane3: NS4A-EGFP clone, treated with primers 4AE-F and 2AE-R. Lane7: NS4B-EGFP clone, treated with primers 4BE-FP and 2AE-R. Lane4: pcDNA3 clone, treated with primers 2AE-F and 2AE-R. Lane5: pcDNA3 clone, treated with primers 2BE-F and 2AE-R. Lane6: pcDNA3 clone, treated with primers 4AE-F and 2AE-R. Lane8: pcDNA3 clone, treated with primers 4BE-FP and 2AE-R. Lane4, 5, 6, 8: negative controls. The expected lengths of NS2A-EGFP, NS2B-EGFP, NS4A-EGFP, and NS4B-EGFP were 1377 bp (a), 1111 bp (c), 1169 bp (e), and 1470 bp respectively.

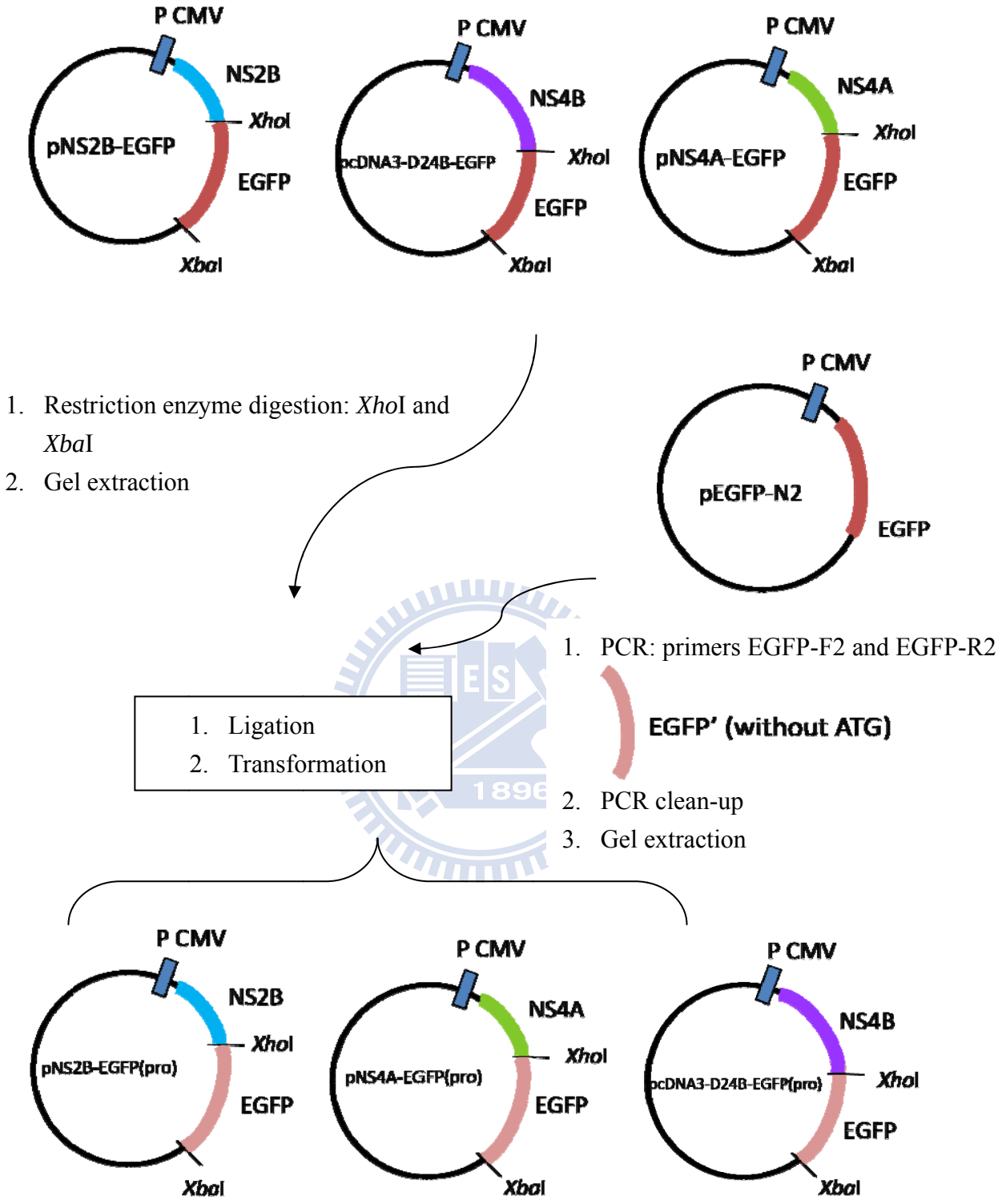

Fig. 3.13 Construction maps of pNS2B-EGFP(pro), pNS4A-EGFP(pro), and pcDNA3-D24B-EGFP(pro).

P CMV: Human cytomegalovirus (CMV) immediate early promoter; NS2A: nonstructural protein 2A; NS2B: nonstructural protein 2B; NS4A: nonstructural protein 4A; NS4B: nonstructural protein 4B; EGFP: enhanced green fluorescent protein; EGFP': enhanced green fluorescent protein without ATG start codon.

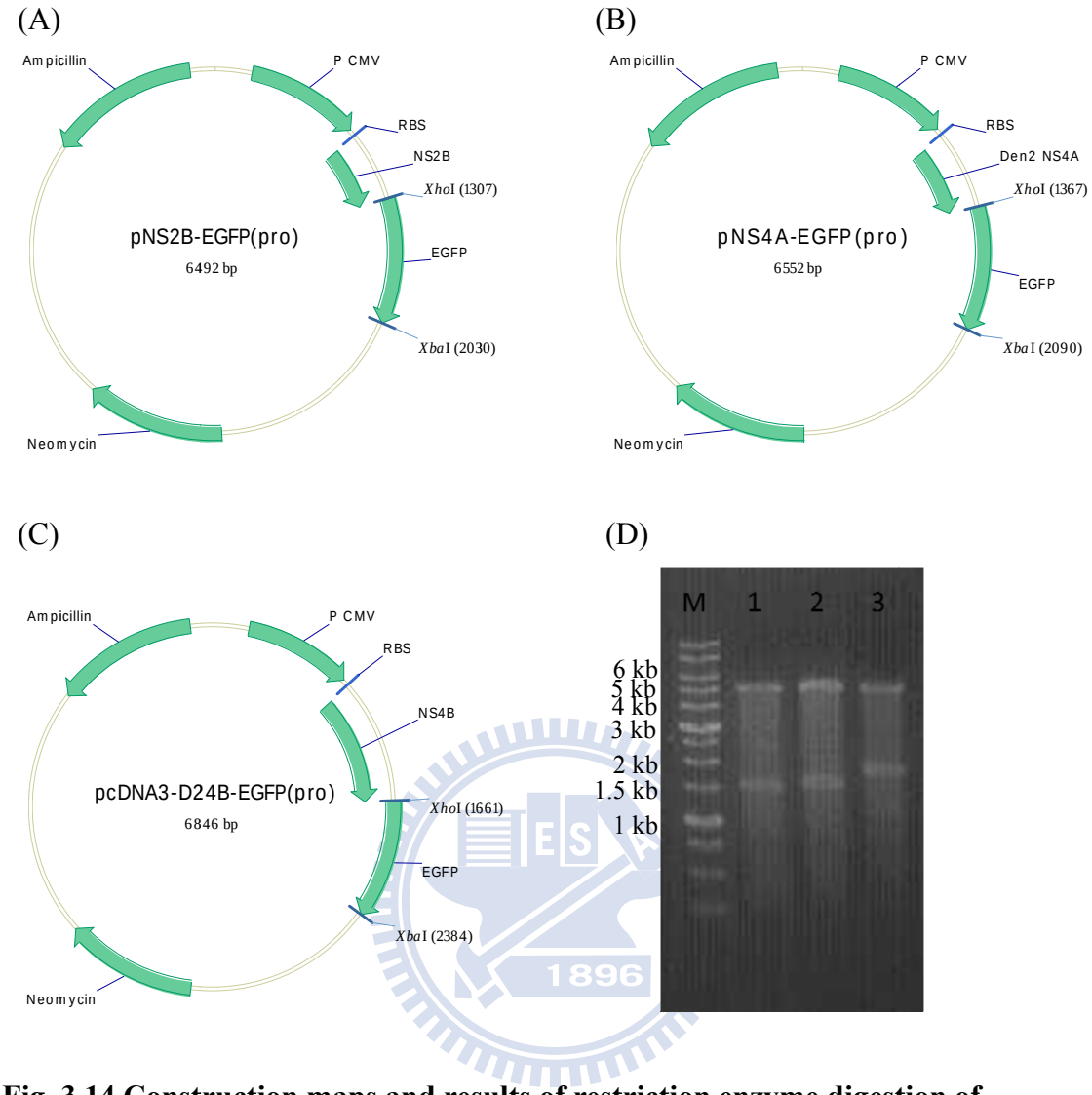

Fig. 3.14 Construction maps and results of restriction enzyme digestion of pNS2B-EGFP(pro), pNS4A-EGFP(pro),and pcDNA3-D24B-EGFP(pro).

(A) Map of pNS2B-EGFP(pro). (B) Map of pNS4A-EGFP(pro). (C) Map of pcDNA3-D24B-EGFP(pro). (D) Lane 1, pNS2B-EGFP(pro) was digested by *BsrG*I and *Nde*I into 1534 bp and 4958 bp. Lane 2, pNS4A-EGFP9(pro) was digested by *BsrG*I and *Nde*I into 1594 bp and 4958 bp. Lane 3, pcDNA3-D24B-EGFP(pro) was digested by *BsrG*I and *Nde*I into 1888 bp and 4958 bp. Neomycin: Neomycin resistance gene; Ampicillin: Ampicillin resistance gene; P CMV: Human cytomegalovirus (CMV) immediate early promoter; RBS: ribosome binding site; EGFP: enhanced green fluorescent protein; NS2A: nonstructural protein 2A; NS2B: nonstructural protein 2B; NS4A: nonstructural protein 4A; NS4B: nonstructural protein 4B.

(A)

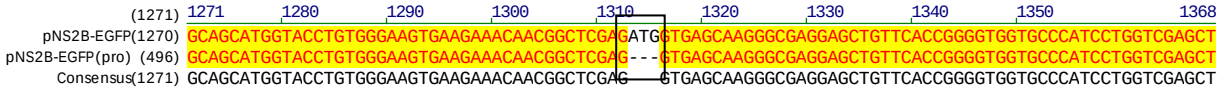

(B)

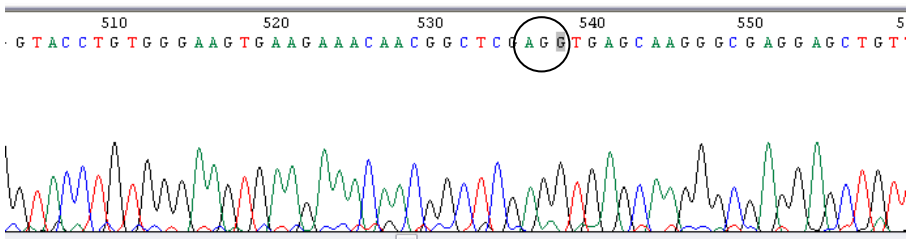

(C)

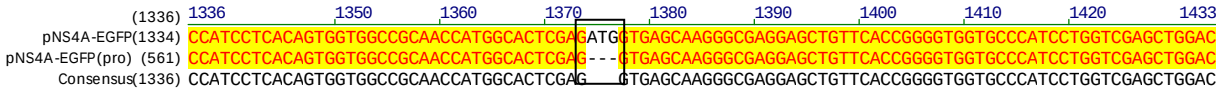

(D)

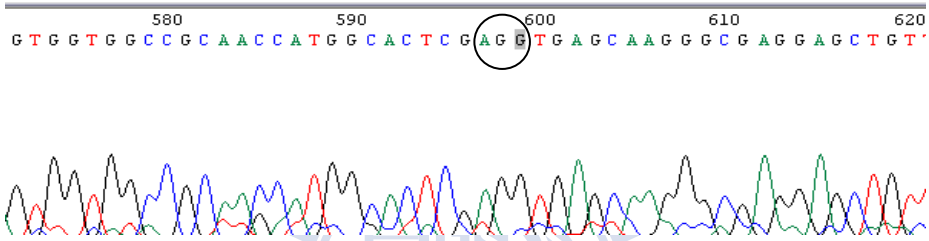

(E)

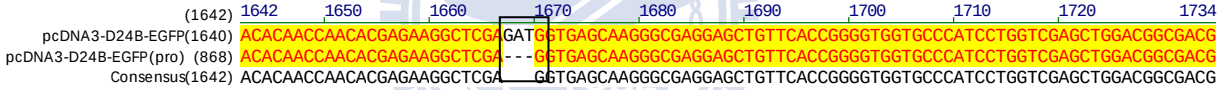

(F)

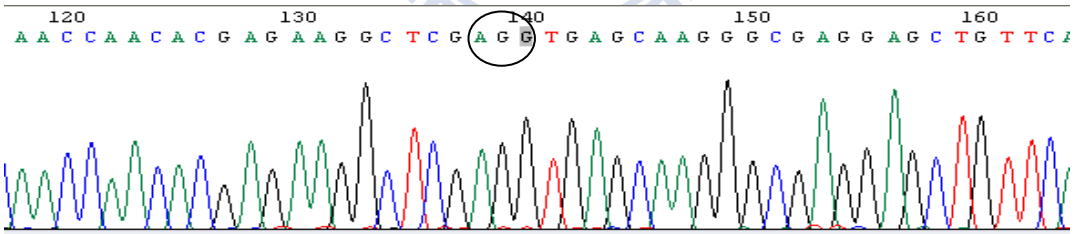

Fig. 3.15 Sequence analysis of pNS2B-EGFP(pro), pNS4A-EGFP(pro), and pcDNA3-D24B-EGFP(pro) at the start of EGFP tag.

(A) & (B) pNS2B-EGFP(pro). (C) & (D) pNS4A-EGFP(pro). (E) & (F) pcDNA3-D24B-EGFP. The deletion ATG were marked with rectangles and circles.

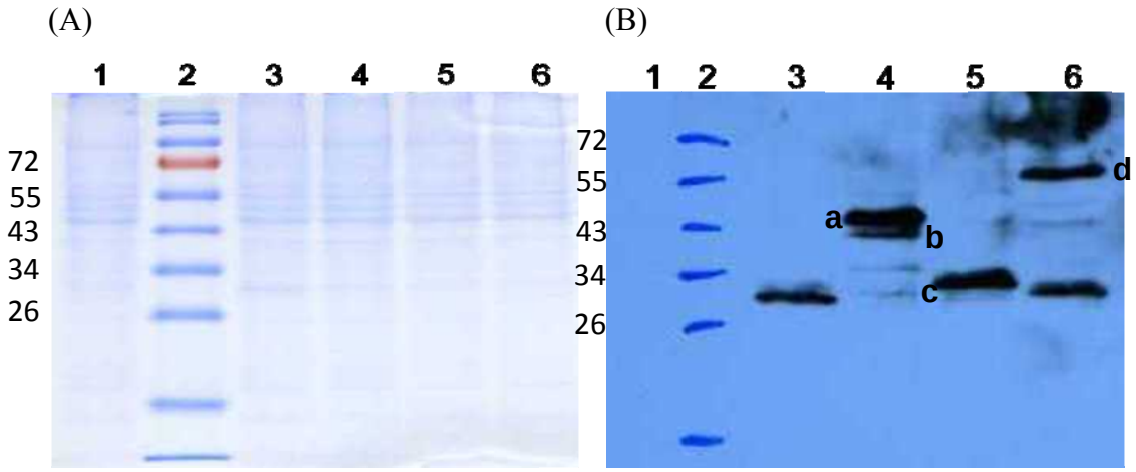

Fig. 3.16 Commassie blue staining and Western blot analysis of proteins pNS2B-EGFP(pro), pNS4A-EGFP(pro), and pcDNA3-D24B-EGFP(pro) expressed in BHK-21.

(A) Coomassie blue staining of the supernatants of BHK-21 transfected with different plasmids. (B) Western blot analysis with anti-GFP-HRP antibody against supernatant of BHK-21 transfected with different plasmids. Lane 1, pcDNA3 (negative control); lane 2, prestained protein marker; lane 3, EGFP (positive control, 27 kDa); lane 4, pNS2B-EGFP(pro), 41.1 kDa; lane 5, pNS4A-EGFP(pro), 43.6 kDa; lane 6, pcDNA3-D24B-EGFP(pro), 53.9 kDa.

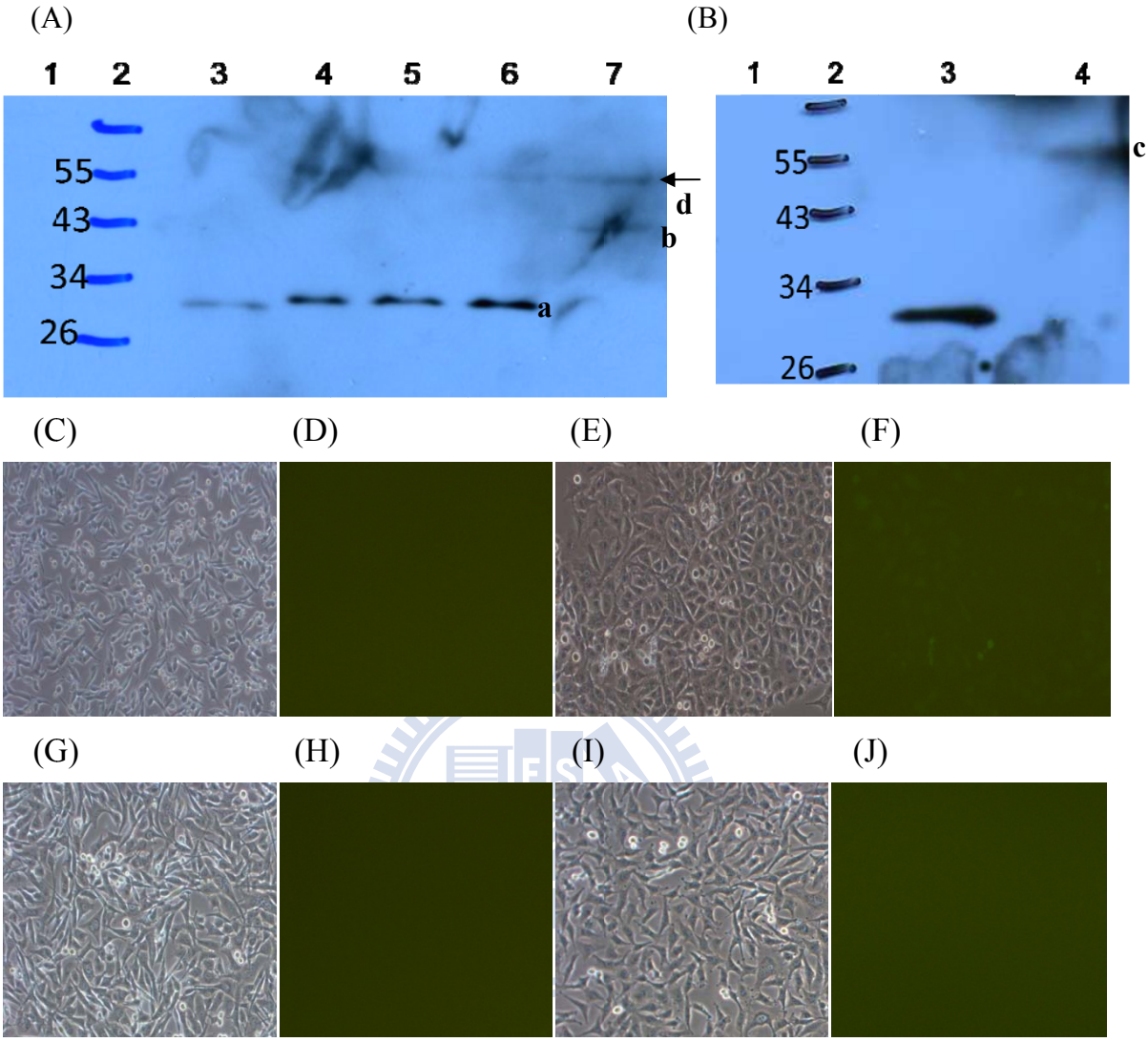

Fig. 3.17 Western blot analysis and fluorescence microscopy for stably transfected cells (BHK-21) of NS2B-EGFP(pro), NS4A-EGFP(pro), and NS4B-EGFP(pro).

(A) Western blot analysis with anti-GFP-HRP antibody against the total cell lysates of BHK-21 of selected NS2B-EGFP(pro) (Lane 7, 41.1 kDa) and NS4A-EGFP(pro) (Lane 4, 5, 6, 41.2 kDa). (B) Western blot analysis with anti-GFP-HRP antibody against the total cell lysate of BHK-21 of selected NS4B-EGFP(pro) (Lane 4, 53.9 kDa). Lane 1: pcDNA3 (negative control); Lane 2: prestained protein marker; Lane 3: EGFP (positive control, 27 kDa). (C) and (D) The fluorescence microscopy analysis of the stable transfected cells of NS2B-EGFP(pro). (E) and (F) The fluorescence microscopy analysis of the stable transfected cells of NS4A-EGFP(pro). (G) and (H) The fluorescence microscopy analysis of the stable transfected cells of NS4B-EGFP(pro). (I) and (J) The fluorescence microscopy analysis of BHK-21 cells.

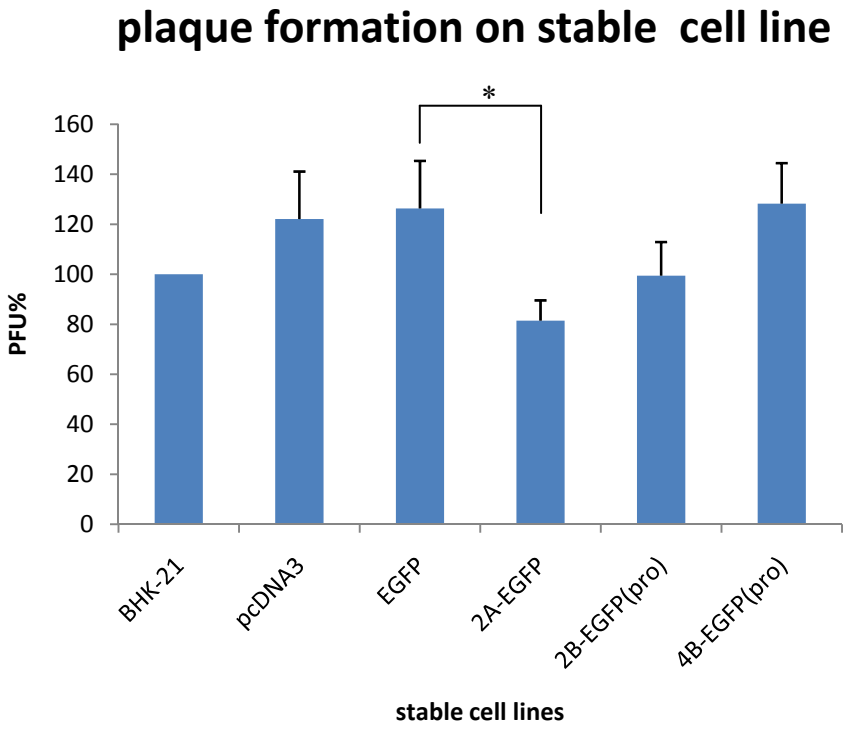

Fig. 3.18 Plaque formation assay on stable cell lines, NS2A-EGFP, NS2B-EGFP(pro), NS4B-EGFP(pro), pcDNA3, and EGFP.

Using the number of PFUs of BHK-21 cells as 100%, the relative percentage of the PFUs were calculated. The y axis shows the percentage of the amount of plaque formation. The x axis denotes the selected stable cell lines and BHK-21. The PFU% of each stable cell lines was compared with that of EGFP using analysis of variation (ANOVA). Six independent samples were analyzed.

* means it was significantly different (P<0.05).

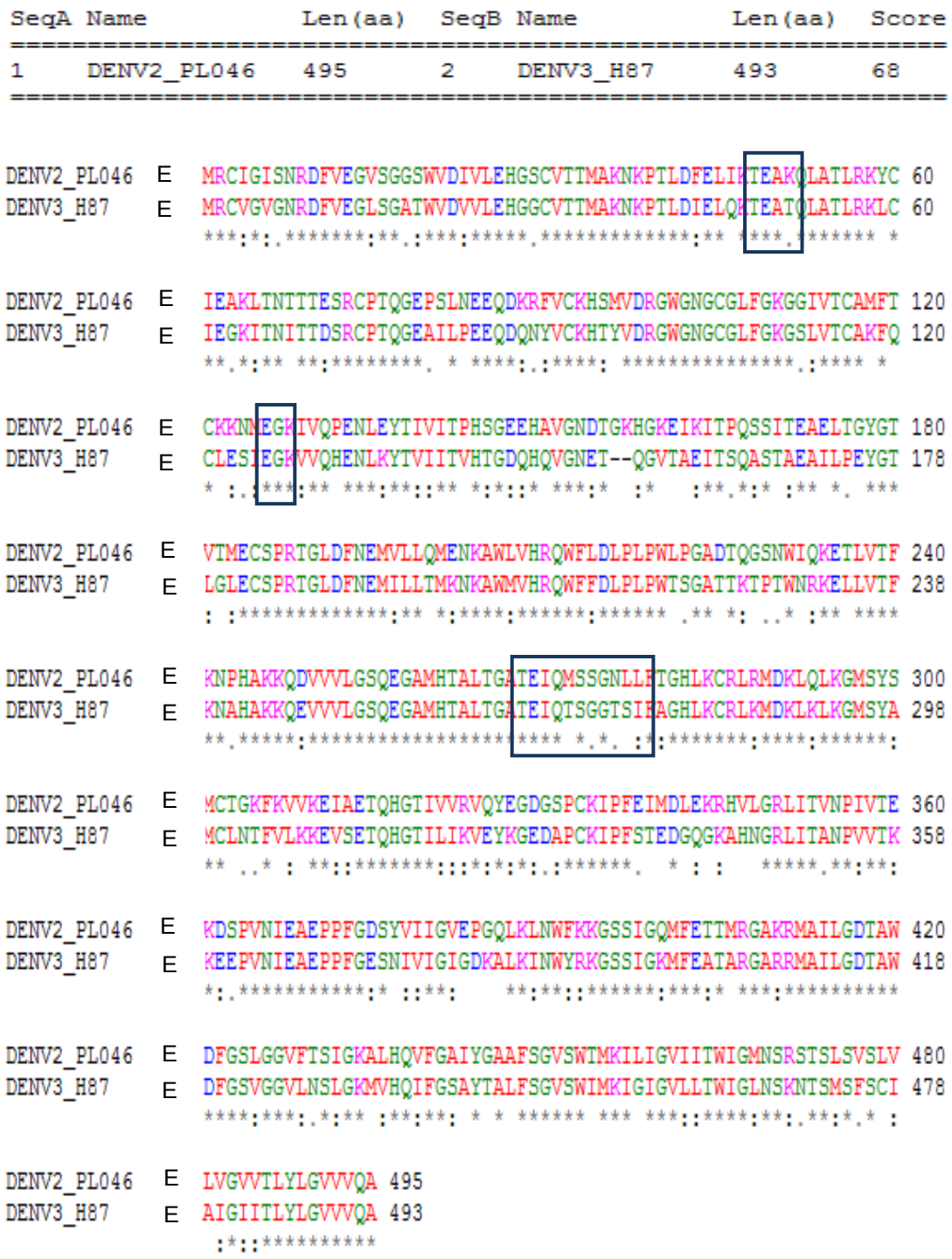

Fig. 4.1 Alignment of amino acids at envelope protein of DV2 PL046 strain and DV3 H87 strain.

The residues lined the β-OG binding pocket were marked with rectangles: residues 48-52, 126-128, and 268-279.

A

Tetracycline	mean	sd	mean±sd
0 μM	100	0.0	100±0.0
10 μM	106.44	7.76	106.44±7.76
50 μM	121.55	4.96	121.55±4.96
100 μM	119.45	7.61	119.45±7.61
300 μM	85.55	18.19	85.55±18.19
500 μM	40.52	22.41	40.52±22.41
700 μM	23.48	20.79	23.48±20.79
1000 μM	12.86	13.02	12.86±13.02

B

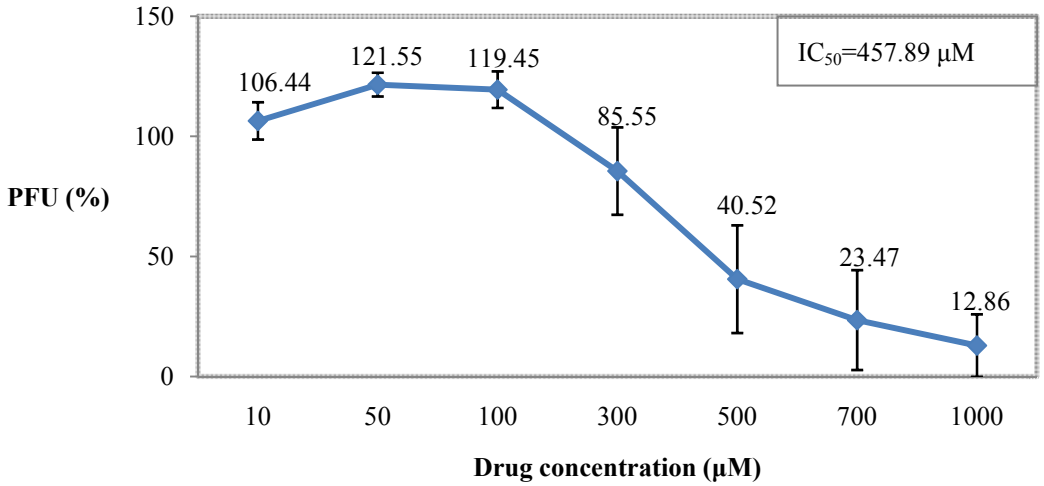

Fig. 4.2 Effect of tetracycline on DV2 plaque formation using BHK-21 mammalian cells. (A) To count the PFUs on each plate in the absence or presence of serial dilutions of tetracycline at a fixed number plaque formation units (PFUs). Using the number of PFUs from the culture plates added 0 μM tetracycline as 100%, the relative percentage of the PFUs were calculated. The result is the average of 3 experiments. (B) The response curve. The IC_{50} value of tetracycline is 457.89 μM. The y axis shows the percentage of the amount of plaque formation compared with control. The x axis denotes the drug concentration. The numbers by the curve indicate the percentage of PFU of individual concentrations.

A

Tetracycline	mean	sd	mean±sd
0 μM	100	0.0	100±0.0
10 μM	95.61	9.66	95.61±9.66
50 μM	100.46	7.54	100.46±7.54
100 μM	100.46	7.83	100.46±7.83
300 μM	54.79	15.26	54.79±15.26
500 μM	26.49	12.86	26.49±12.86
700 μM	27.989	10.96	27.99±10.96
1000 μM	11.33	12.72	11.33±12.72

B

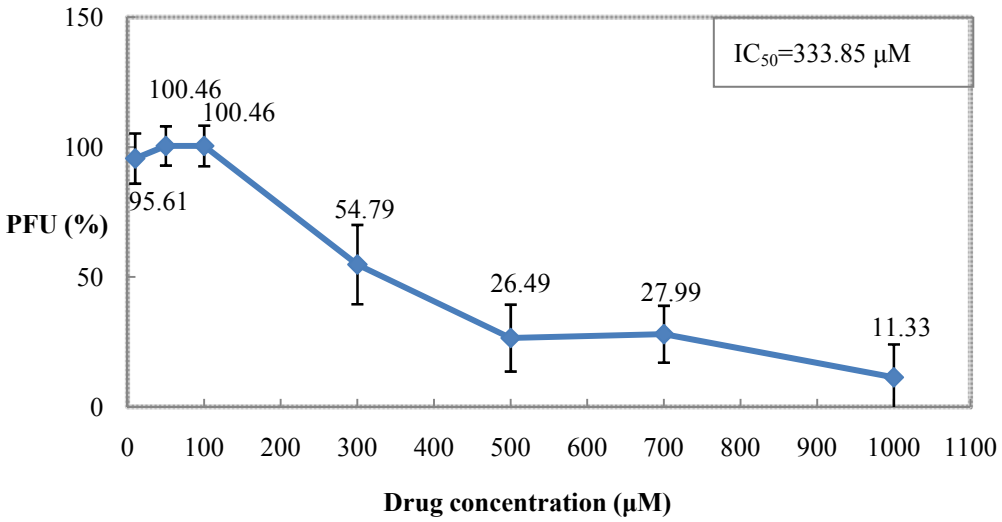

Fig. 4.3 Effect of tetracycline on DV3 plaque formation using BHK-21 mammalian cells. (A) To count the PFUs on each plate in the absence or presence of serial dilutions of tetracycline at a fixed number plaque formation units (PFUs). Using the number of PFUs from the culture plates added 0 μM tetracycline as 100%, the relative percentage of the PFUs were calculated. The result is the average of 3 experiments. (B) The response curve. The IC_{50} value of tetracycline is 333.85 μM. The y axis shows the percentage of the amount of plaque formation compared with control. The x axis denotes the drug concentration. The numbers by the curve indicate the percentage of PFU of individual concentrations.

A

Doxycycline	mean	sd	mean±sd
0 μM	100	0.0	100±0.0
10 μM	126.82	15.13	126.82±15.13
50 μM	45.20	6.92	45.20±6.92
100 μM	14.82	6.92	14.83±6.92
200 μM	5.90	3.00	5.90±3.00
300 μM	1.69	1.35	1.69±1.35
500 μM	0.57	0.54	0.57±0.54
700 μM	0	0	0

B

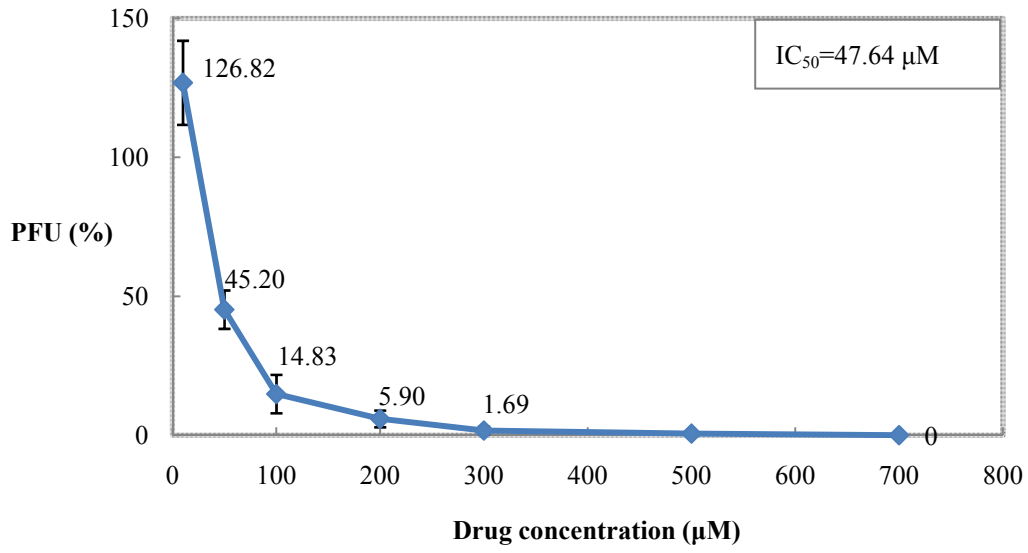

Fig. 4.4 Effect of doxycycline on DV2 plaque formation using BHK-21 mammalian cells. (A) To count the PFUs on each plate in the absence or presence of serial dilutions of doxycycline at a fixed number plaque formation units (PFUs). Using the number of PFUs from the culture plates added 0 μM doxycycline as 100%, the relative percentage of the PFUs were calculated. The result is the average of 3 experiments. (B) The response curve. The IC_{50} value of tetracycline is 47.64 μM. The y axis shows the percentage of the amount of plaque formation compared with control. The x axis denotes the drug concentration. The numbers by the curve indicate the percentage of PFU of individual concentrations.

A

Doxycycline	mean	sd	mean±sd
0 uM	100	0.0	100±0.0
10 uM	116.25	5.57	116.25±5.57
50 uM	156.28	30.98	156.28±30.98
100 uM	84.48	15.5	84.48±15.5
200 uM	48.94	27.16	48.94±27.16
300 uM	25.48	8.21	25.48±8.21
500 uM	16.40	0.79	16.40±0.79
700 uM	6.58	1.14	6.58±1.14

B

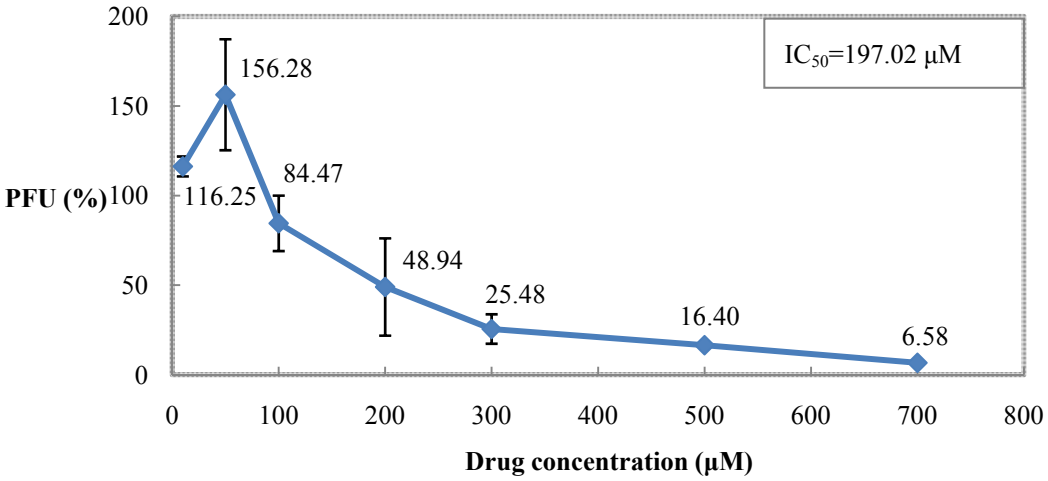

Fig. 4.5 Effect of doxycycline on DV3 plaque formation using BHK-21 mammalian cells. (A) To count the PFUs on each plate in the absence or presence of serial dilutions of doxycycline at a fixed number plaque formation units (PFUs). Using the number of PFUs from the culture plates added 0 µM doxycycline as 100%, the relative percentage of the PFUs were calculated. The result is the average of 3 experiments. (B) The response curve. The IC_{50} value of tetracycline is 197.02 µM. The y axis shows the percentage of the amount of plaque formation compared with control. The x axis denotes the drug concentration. The numbers by the curve indicate the percentage of PFU of individual concentrations.

A

Chlortetracycline	mean	sd	mean±sd
0 μM	100	0.0	100±00
10 μM	101.13	2.65	101.13±2.65
50 μM	48.92	9.98	48.91±9.98
100 μM	27.81	4.08	27.81±4.08
200 μM	13.34	3.62	13.34±3.62
300 μM	6.94	2.59	6.94±2.59
500 μM	6.39	3.21	6.39±3.21
700 μM	2.16	3.12	2.16±3.12

B

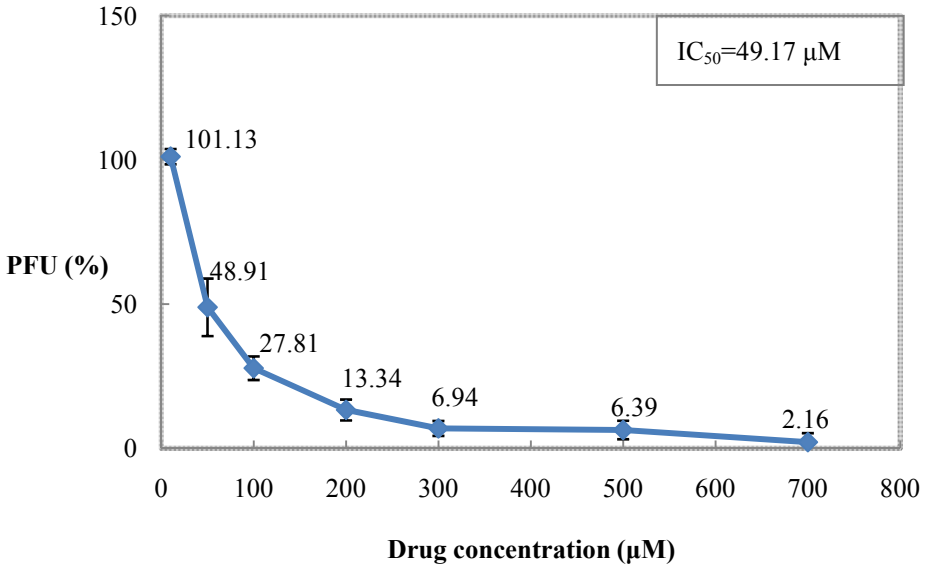

Fig. 4.6 Effect of chlortetracycline on DV2 plaque formation using BHK-21 mammalian cells.

(A) To count the PFUs on each plate in the absence or presence of serial dilutions of chlortetracycline at a fixed number plaque formation units (PFUs). Using the number of PFUs from the culture plates added 0 μM chlortetracycline as 100%, the relative percentage of the PFUs were calculated. The result is the average of 3 experiments. (B) The response curve. The IC_{50} value of chlortetracycline is 49.17 μM. The y axis shows the percentage of the amount of plaque formation compared with control. The x axis denotes the drug concentration. The numbers by the curve indicate the percentage of PFU of individual concentrations.

A

Chlortetracycline	mean	sd	mean±sd
0 μM	100	0.0	100±0.0
10 μM	98.67	10.58	98.67±10.58
50 μM	60.11	11.85	60.11±11.85
100 μM	59.52	8.29	59.52±8.29
200 μM	34.60	13.98	34.60±13.98
300 μM	17.81	9.75	17.81±9.75
500 μM	12.04	9.25	12.04±9.25
700 μM	3.95	2.47	3.95±2.47

B

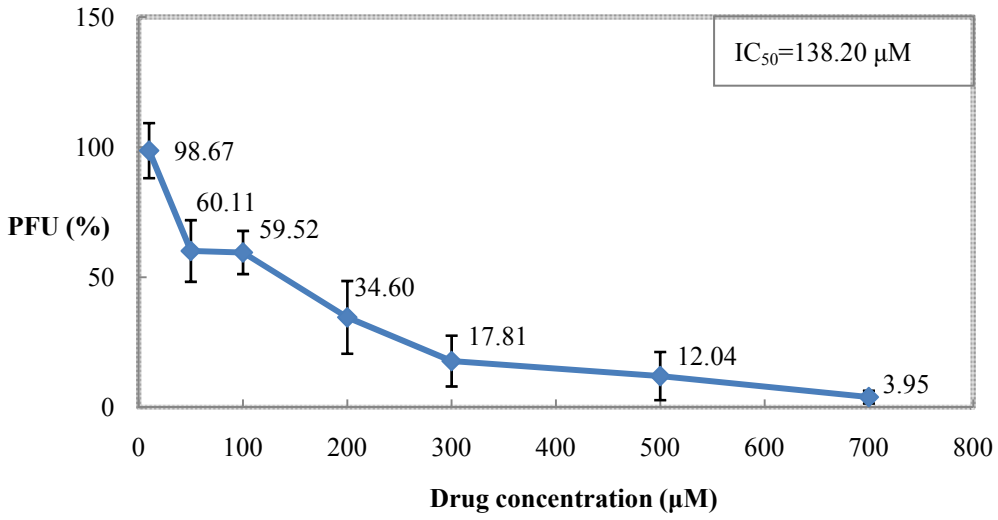

Fig. 4.7 Effect of chlortetracycline on DV3 plaque formation using BHK-21 mammalian cells.

(A) To count the PFUs on each plate in the absence or presence of serial dilutions of chlortetracycline at a fixed number plaque formation units (PFUs). Using the number of PFUs from the culture plates added 0 μM chlortetracycline as 100%, the relative percentage of the PFUs were calculated. The result is the average of 3 experiments. (B) The response curve. The IC_{50} value of chlortetracycline is 138.20 μM. The y axis shows the percentage of the amount of plaque formation compared with control. The x axis denotes the drug concentration. The numbers by the curve indicate the percentage of PFU of individual concentrations.

A

Rolitetracycline	mean	sd	mean±sd
0 μM	100	0.0	100±0.0
10 μM	128.38	19.01	128.38±19.01
50 μM	171.93	30.86	171.93±30.86
100 μM	160.02	35.83	160.02±35.83
200 μM	54.41	15.6	54.41±15.6
300 μM	26.14	13.38	26.14±13.38
500 μM	5.26	2.95	5.26±2.95
700 μM	0.92	1.58	0.92±1.58

B

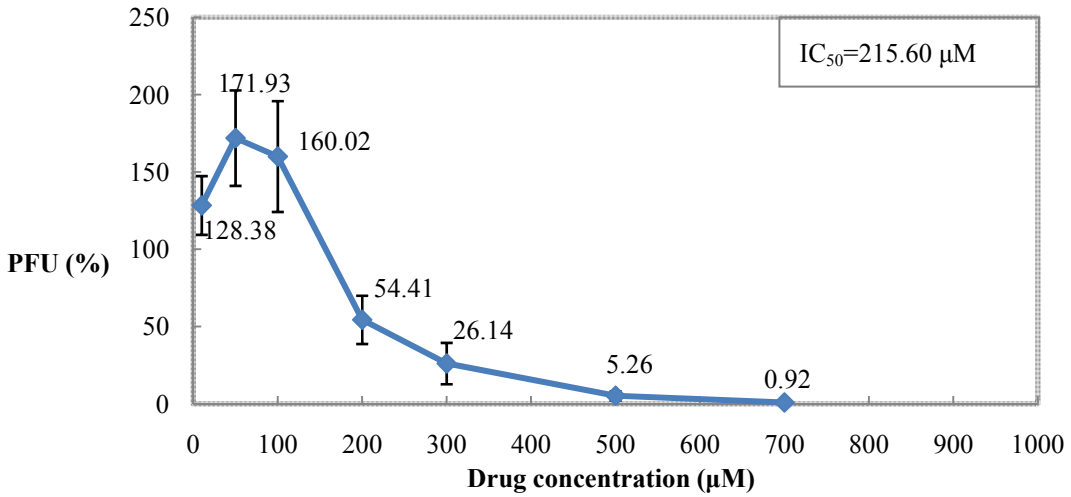

Fig. 4.8 Effect of rolitetracycline on DV2 plaque formation using BHK-21 mammalian cells.

(A) To count the PFUs on each plate in the absence or presence of serial dilutions of rolitetracycline at a fixed number plaque formation units (PFUs). Using the number of PFUs from the culture plates added 0 μM rolitetracycline as 100%, the relative percentage of the PFUs were calculated. The result is the average of 3 experiments. (B) The response curve. The IC_{50} value of tetracycline is 215.60 μM. The y axis shows the percentage of the amount of plaque formation compared with control. The x axis denotes the drug concentration. The numbers by the curve indicate the percentage of PFU of individual concentrations.

A

Rolitetracycline	mean	sd	mean±sd
0 μM	100	0.0	100±0.0
10 μM	100.99	18.50	100.99±18.50
50 μM	119.13	12.03	119.13±12.03
100 μM	110.74	6.84	110.74±6.84
300 μM	68.95	17.21	68.95±17.20
500 μM	40.28	23.56	40.28±23.56
700 μM	13.34	10.34	13.34±10.34

B

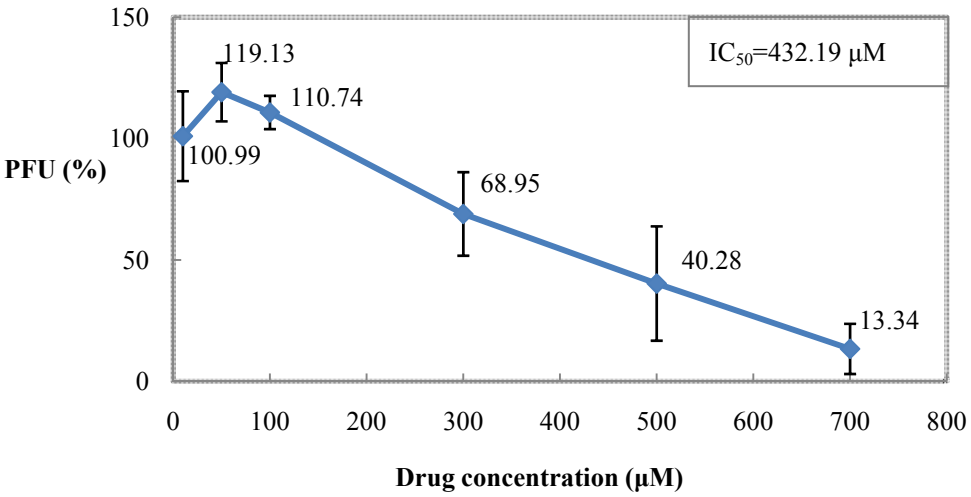

Fig. 4.9 Effect of rolitetracycline on DV3 plaque formation using BHK-21 mammalian cells.

(A) To count the PFUs on each plate in the absence or presence of serial dilutions of rolitetracycline at a fixed number plaque formation units (PFUs). Using the number of PFUs from the culture plates added 0 μM rolitetracycline as 100%, the relative percentage of the PFUs were calculated. The result is average of 2 experiments. (B) The response curve. The IC_{50} value of rolitetracycline is 432.19 μM. The y axis shows the percentage of the amount of plaque formation compared with control. The x axis denotes the drug concentration. The numbers by the curve indicate the percentage of PFU of individual concentrations.

A

Kanamycin	mean	sd	mean±sd
0 μM	100	0.0	100±0.0
10 μM	103.19	17.59	103.19±17.59
50 μM	100.06	5.81	100.06±5.81
100 μM	107.75	5.24	107.75±5.24
300 μM	111.28	13.51	111.28±13.51
500 μM	104.34	6.13	104.34±6.13
700 μM	122.1	24.72	122.10±24.72

B

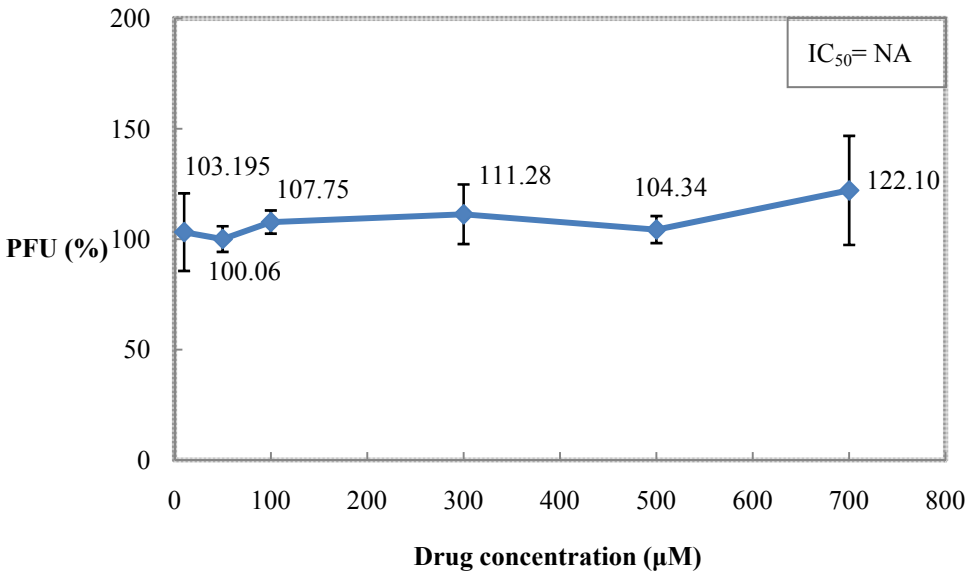

Fig. 4.10 Effect of kanamycin on DV2 plaque formation using BHK-21 mammalian cells. (A) To count the PFUs on each plate in the absence or presence of serial dilutions of kanamycin at a fixed number plaque formation units (PFUs). Using the number of PFUs from the culture plates added 0 μM kanamycin as 100%, the relative percentage of the PFUs were calculated. The result is the average of 2 experiments. (B) The response curve. The y axis shows the percentage of the amount of plaque formation compared with control. The x axis denotes the drug concentration. The numbers by the curve indicate the percentage of PFU of individual concentrations. NA: not applicable.

A

Kanamycin	mean	sd	mean±sd
0 μM	100	0.0	100±0.0
10 μM	88.05	20.07	88.05±20.07
50 μM	85.84	3.01	85.84±3.01
100 μM	90.48	4.73	90.48±4.73
200 μM	83.70	1.60	83.70±1.60
300 μM	91.75	7.70	91.75±7.70
500 μM	87.50	5.36	87.50±5.36
700 μM	86.06	0.94	86.06±0.94

B

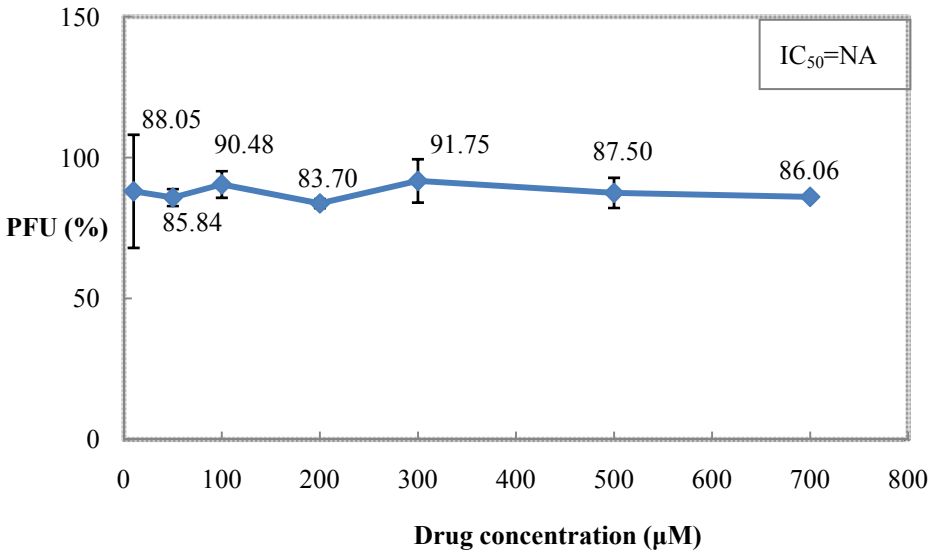

Fig. 4.11 Effect of kanamycin on DV3 plaque formation using BHK-21 mammalian cells. (A) To count the PFUs on each plate in the absence or presence of serial dilutions of kanamycin at a fixed number plaque formation units (PFUs). Using the number of PFUs from the culture plates added 0 μM kanamycin as 100%, the relative percentage of the PFUs were calculated. The result is the average of 2 experiments. (B) The response curve. The y axis shows the percentage of the amount of plaque formation compared with control. The x axis denotes the drug concentration. The numbers by the curve indicate the percentage of PFU of individual concentrations. NA: not applicable.

A

9-amino-1,2,3,4-tetrahydroacridine hydrochloride hydrate	mean	sd	mean±sd
0 μM	100	0.0	100±0.0
10 μM	99.05	1.35	99.05±1.35
50 μM	93.72	4.23	93.72±4.23
100 μM	69.23	17.7	69.23±17.7
200 μM	68.59	3.74	68.59±3.74
300 μM	53.68	4.24	53.68±4.24

B

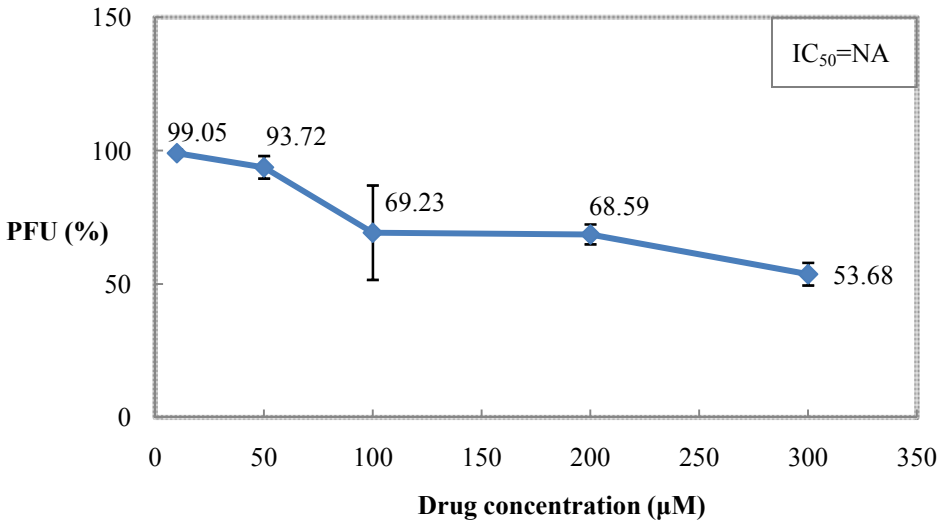

Fig. 4.12 Effect of 9-amino-1,2,3,4-tetrahydroacridine hydrochloride hydrate on DV2 plaque formation using BHK-21 mammalian cells.

(A) To count the PFUs on each plate in the absence or presence of serial dilutions of 9-amino-1,2,3,4-tetrahydroacridine hydrochloride hydrate at a fixed number plaque formation units (PFUs). Using the number of PFUs from the culture plates added 0 μM 9-amino-1,2,3,4-tetrahydroacridine hydrochloride hydrate as 100%, the relative percentage of the PFUs were calculated. The result is the average of 2 experiments. (B) The response curve. The y axis shows the percentage of the amount of plaque formation compared with control. The x axis denotes the drug concentration. The numbers by the curve indicate the percentage of PFU of individual concentrations. NA: not applicable.

A

9-amino-1,2,3,4-tetrahydroacridine hydrochloride hydrate	mean	sd	mean±sd
0 μM	100	0.0	100±0.0
10 μM	88.81	3.22	88.81±3.22
50 μM	86.60	2.43	86.60±2.43
100 μM	74.41	2.73	74.41±2.73
200 μM	74.09	13.78	74.09±13.78
300 μM	68.33	23.19	68.33±23.19
500 μM	63.22	8.83	63.22±8.83

B

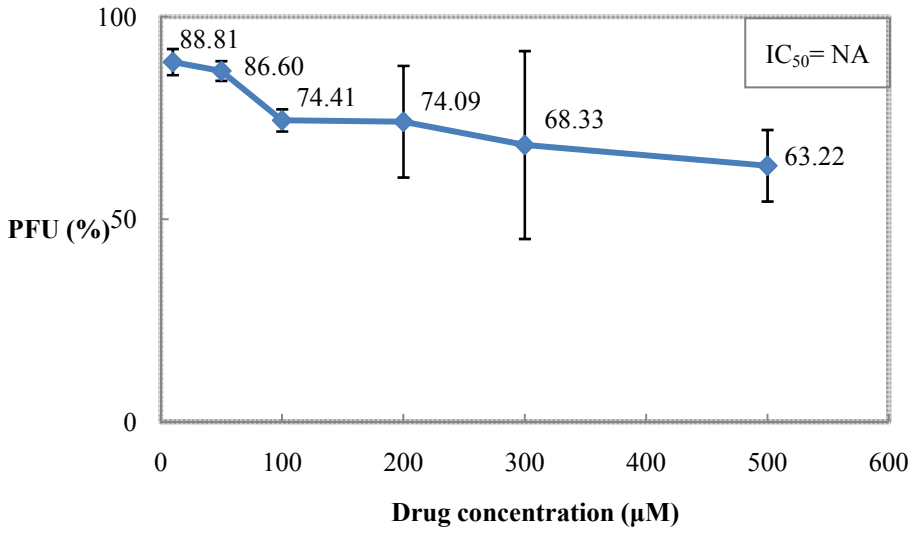

Fig. 4.13 Effect of 9-amino-1,2,3,4-tetrahydroacridine hydrochloride hydrate on DV3 plaque formation using BHK-21 mammalian cells.

(A) To count the PFUs on each plate in the absence or presence of serial dilutions of 9-amino-1,2,3,4-tetrahydroacridine hydrochloride hydrate at a fixed number plaque formation units (PFUs). Using the number of PFUs from the culture plates added 0 μM 9-amino-1,2,3,4-tetrahydroacridine hydrochloride hydrate as 100%, the relative percentage of the PFUs were calculated. The result is the average of 2 experiments. (B) The response curve. The y axis shows the percentage of the amount of plaque formation compared with control. The x axis denotes the drug concentration. The numbers by the curve indicate the percentage of PFU of individual concentrations. NA: not applicable.

A

Berberine	mean	sd	mean±sd
0 μM	100	0.0	100±0.0
10 μM	105.26	8.62	105.26±8.62
50 μM	132.49	6.94	132.49±6.94
100 μM	153.91	12.78	153.91±12.78
200 μM	125.94	17.38	125.94±17.38
300 μM	70.13	3.85	70.13±3.85

B

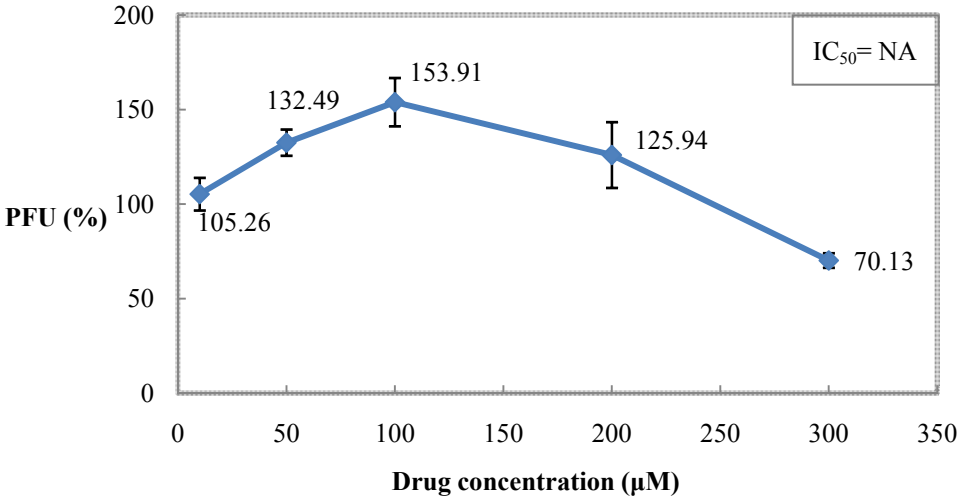

Fig. 4.14 Effect of berberine on DV2 plaque formation using BHK-21 mammalian cells. (A) To count the PFUs on each plate in the absence or presence of serial dilutions of berberine at a fixed number plaque formation units (PFUs). Using the number of PFUs from the culture plates added 0 μM berberine as 100%, the relative percentage of the PFUs were calculated. The result is the average of 2 experiments. (B) The response curve. The y axis shows the percentage of the amount of plaque formation compared with control. The x axis denotes the drug concentration. The numbers by the curve indicate the percentage of PFU of individual concentrations. NA: not applicable.

A

Berberine	mean	sd	mean±sd
0 μM			
10 μM	94.38	14.04	94.38±14.04
50 μM	113.37	4.25	113.37±4.25
100 μM	95.68	12.21	95.68±12.21

B

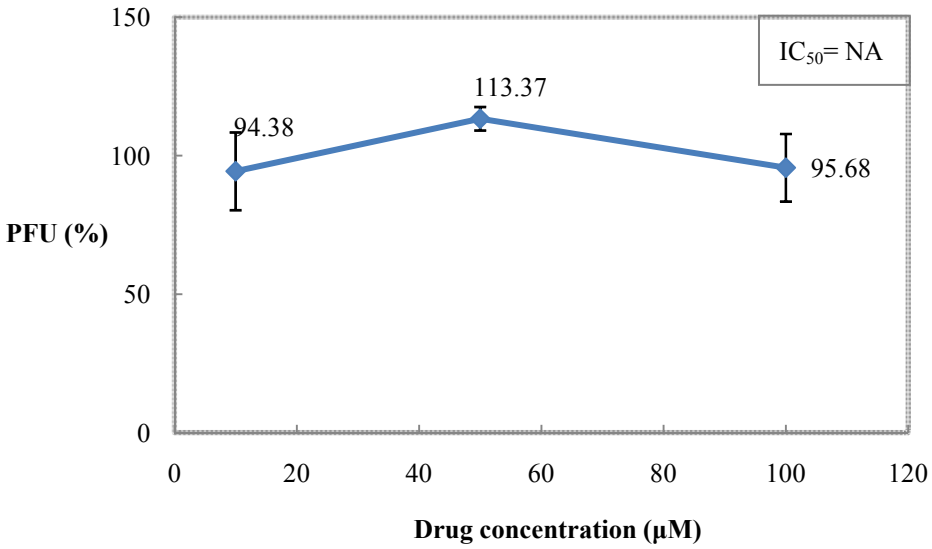

Fig. 4.15 Effect of berberine on DV3 plaque formation using BHK-21 mammalian cells. (A) To count the PFUs on each plate in the absence or presence of serial dilutions of berberine at a fixed number plaque formation units (PFUs). Using the number of PFUs from the culture plates added 0 μM berberine as 100%, the relative percentage of the PFUs were calculated. The result is the average of 2 experiments. (B) The response curve. The y axis shows the percentage of the amount of plaque formation compared with control. The x axis denotes the drug concentration. The numbers by the curve indicate the percentage of PFU of individual concentrations. NA: not applicable.

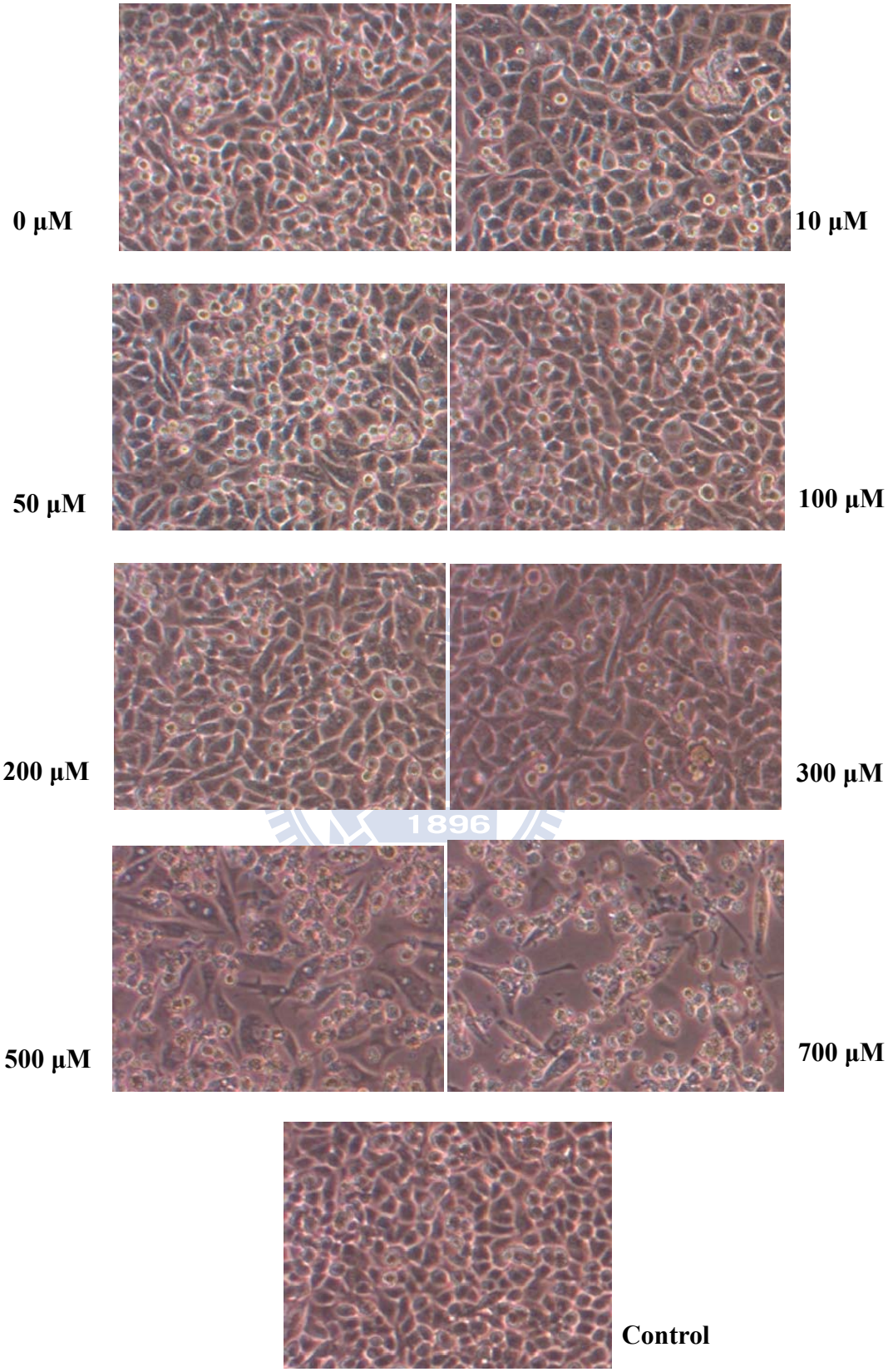

Fig. 4.16 The cell morphology of BHK-21 when adding the different concentrations of 9-amino-1,2,3,4-tetrahydroacridine hydrochloride hydrate with no virus.

Control: no 9-amino-1,2,3,4-tetrahydroacridine hydrochloride hydrate.

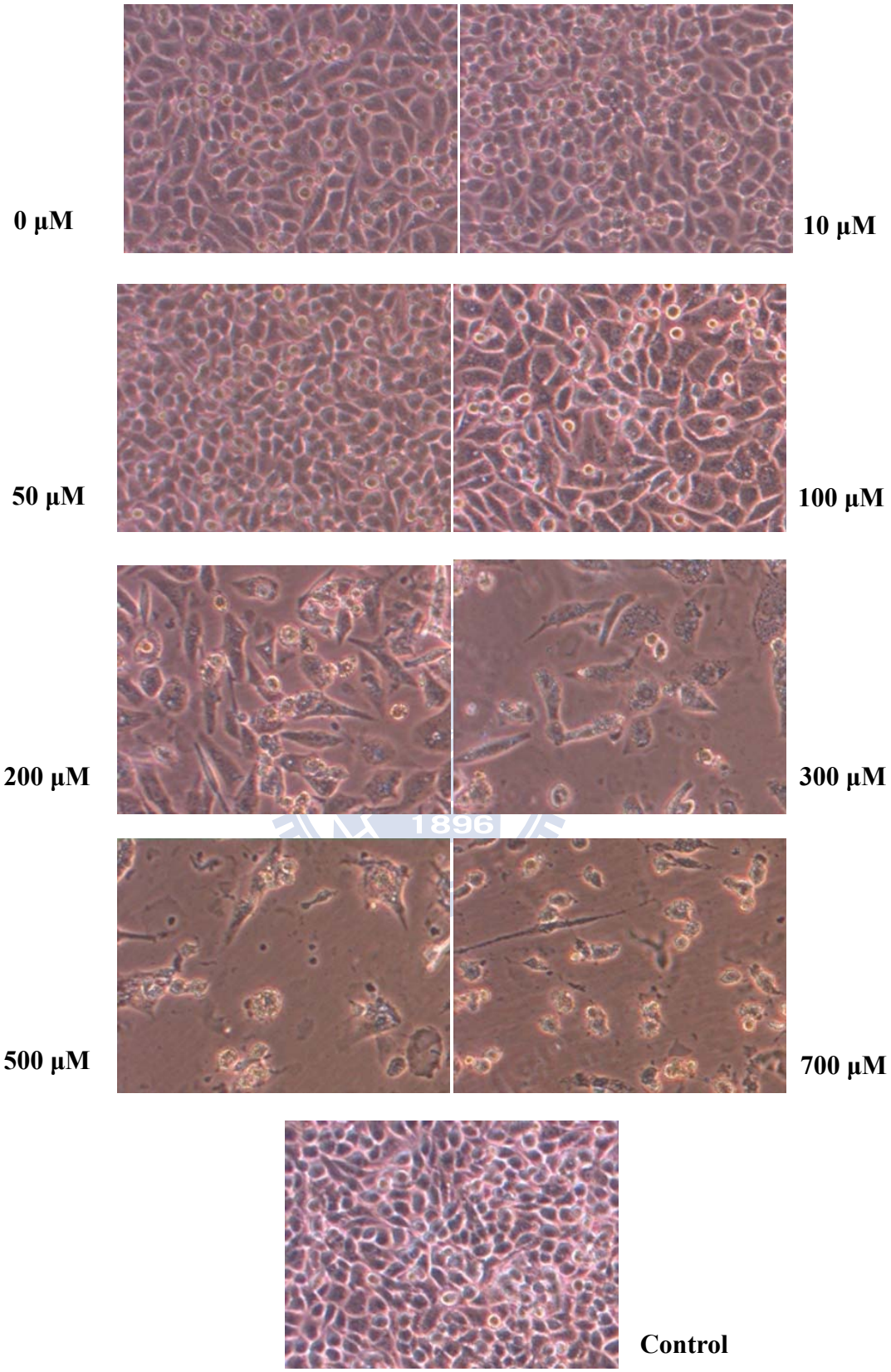

Fig. 4.17 The cell morphology of BHK-21 when adding the different concentrations of berberine.

Control: no berberine.

(A)

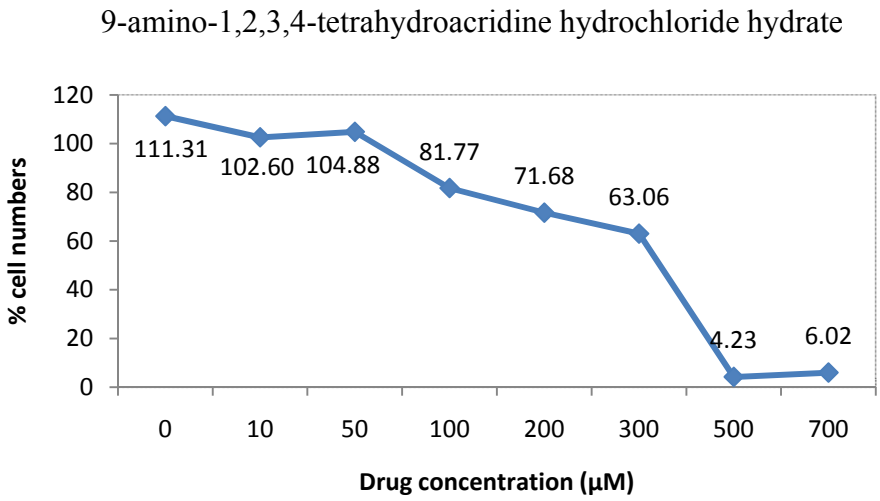

(B)

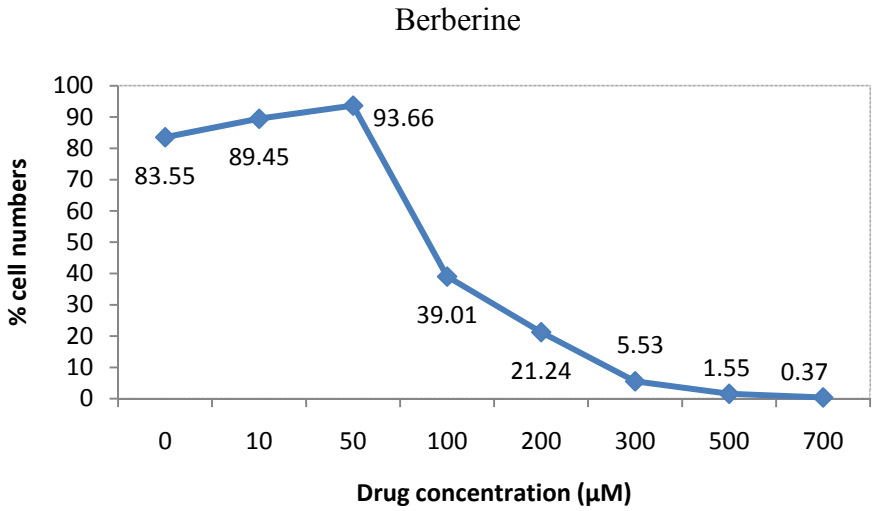

Fig. 4.18 The percentage of cell numbers of BHK-21 when adding the different concentrations of 9-amino-1,2,3,4-tetrahydroacridine hydrochloride hydrate and berberine.

To count the cell numbers on each plate in the absence or presence of serial dilutions of 9-amino-1,2,3,4-tetrahydroacridine hydrochloride hydrate (A) / berberine (B) cultured for 7 days. Using the cell numbers from the culture plates without 9-amino-1,2,3,4-tetrahydroacridine hydrochloride hydrate / berberine as 100%, the relative percentage of the cell numbers was calculated. The y axis shows the percentage of the amount of cell numbers compared with control. The x axis denotes the drug concentration. The numbers by the curve indicate the percentage of cell numbers of individual concentrations.

Appendix 1

Map of pcDNA3

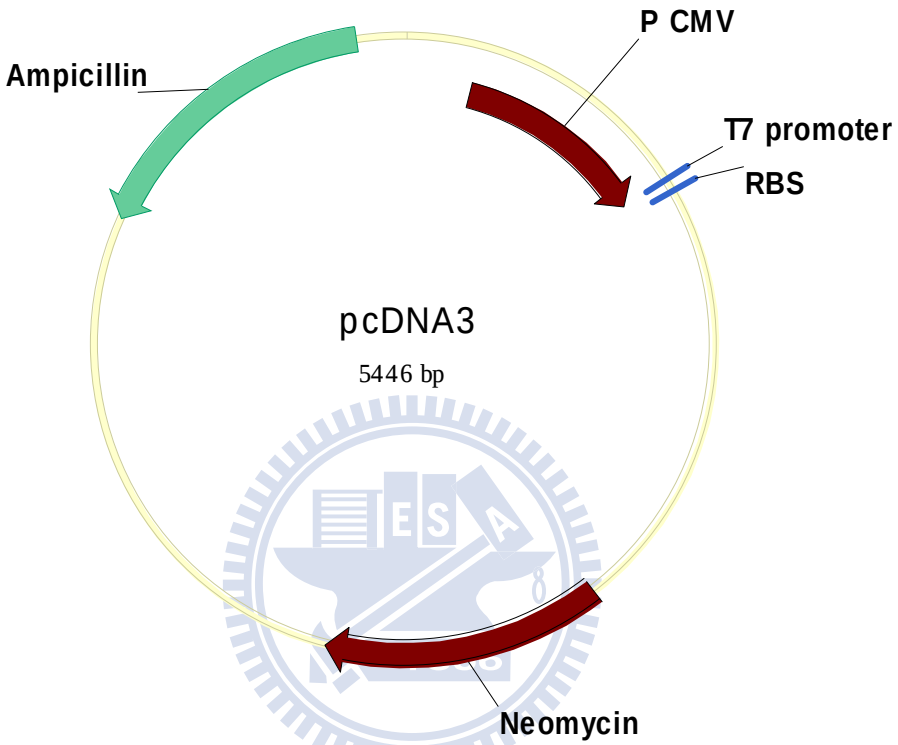

Neo: Neomycin, resistance gene; Amplicillin: Amplicillin resistance gene; PCMV: Human cytomegalovirus (CMV) immediate early promoter; RBS: ribosome binding site; T7 promoter: the T7 transcription promoter.

Appendix 2

Maps of pNS2A-HAHis, pNS2B-HAHis, pNS4A-HAHis, and pcDNA3-D24B-HAHis

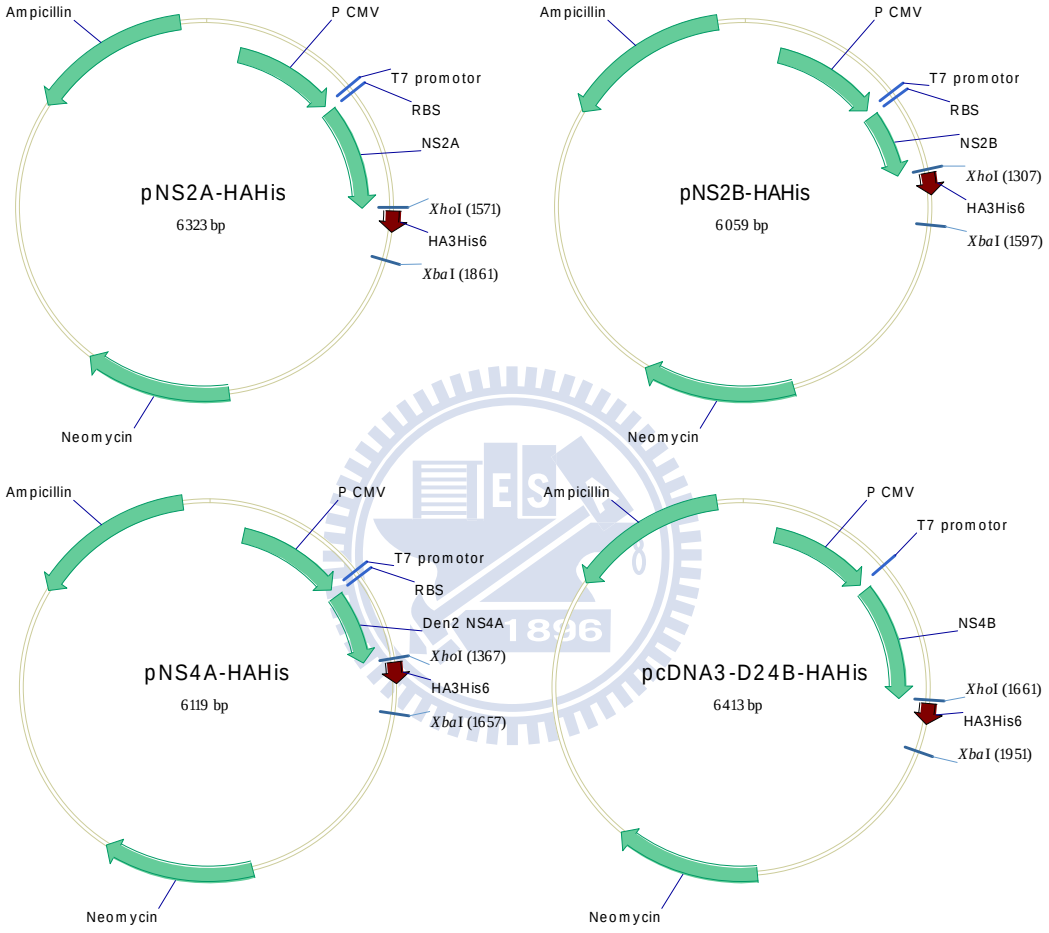

(From 徐婕琳 and 楊馥嘉, Yang laboratory)

Neo: Neomycin, resistance gene; Amplicillin: Amplicillin resistance gene; PCMV: Human cytomegalovirus (CMV) immediate early promoter; RBS: ribosome binding site; T7 promoter: the T7 transcription promoter; NS2A: nonstructural protein 2A; NS2B: nonstructural protein 2B; NS4A: nonstructural protein 4A; NS4B: nonstructural protein 4B. HA3His6: the HAHis tag at the C-terminus.

Appendix 3

Effect of tetracycline on DV2 plaque formation using BHK-21 mammalian cells

(A)

Tetracycline	mean	sd	mean±sd
10 μM	110.18	9.07	110.18±9.07
100 μM	101.19	5.32	101.19±5.32
1000 μM	104.05	4.19	104.05±4.19

(B)

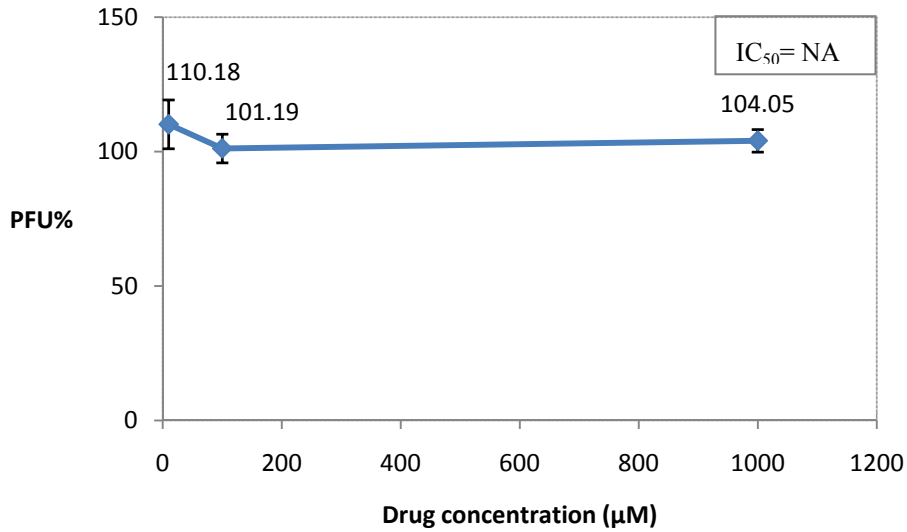

(A) To count the PFUs on each plate in the absence or presence of serial dilutions of tetracycline at a fixed number plaque formation units (PFUs). Using the number of PFUs from the culture plates without tetracycline as 100%, the relative percentages of the PFUs were calculated. The result is the average of 3 experiments. (B) The response curve. The y axis shows the percentage of the amount of plaque formation compared with control. The x axis denotes the drug concentration. The numbers by the curve indicate the percentage of PFU of individual concentrations. NA: not applicable.

(From 杜育穎，Yang laboratory)

Curriculum Vitae

Name	Ching-Yun Chang (張瀞云)
Sex	Female
Date of Birth	10/23/1984
Nationality	Taiwan
Home address	No.8, Ln. 354, Sanhe Rd., Fengyuan City, Taichung Country 420, Taiwan
Telephone No.	+886425318080
Mobile	+886911668540
E-mail	chingyun28@gmail.com

EDUCATION：

Sep/2007 - Sep/2009	M.S. in Department of Biological Science and Technology, National Chiao Tung University, Taiwan (NCTU)
Sep/2003 - Jun/2007	B.S. in Department of Biological Science and Technology, National Chiao Tung University, Taiwan (NCTU)
Sep/2000 - Jun/2003	Taichung Viator High School (台中市私立衛道高級中學)

RESEARCH EXPERIENCES：

Sep/2007 - Jun/2009 **Graduate Research student**

Dr. Yun-Liang Yang Lab, Institute of Biological Science and Technology, National Chiao Tung University

Research topic：

- Functional expression of nonstructural protein NS2A, NS2B, NS4A, and NS4B of dengue virus type 2 PL046 strain.
- Biological assay of inhibitor candidates to dengue virus type 2 and 3.

Jul/2005 - Jun/2007 **Undergraduate Research Student**

Dr. Yun-Liang Yang Lab, Institute of Biological Science and Technology, National Chiao Tung University

Research topic：

- Functional expression of nonstructural protein NS2A, NS2B, NS4A, and NS4B of dengue virus type 2 PL046 strain.

Aug/2006 – Sep/2006 **Teaching assistant**

Biology camp for elementary student, NCTU

To design and teach biology experiments for elementary students.

ACADEMIC ACTIVITY：

Poster Presentation (International)

- **Chang CY,** Huang CC, Huang SF, Tu YY, Yang YL. (2009) Tetracycline derivatives inhibit dengue virus infection of the step of entry. **21st IUBMB and 12th FAOBMB International Congress of Biochemistry and Molecular Biology, Shanghai, China.**
- Huang SF, **Chang CY**, Tu YY, Yang YL. (2008) The mechanism of tetracycline derivatives as Dengue virus inhibitors. **2nd International Conference on Dengue and Dengue Haemorrhagic Fever, Thailand.**

Poster Presentation (Domestic)

- **Chang CY**, Huang SF, Yang YL. (2009) The mechanism of tetracycline derivatives as Dengue virus inhibitors. The poster contests of Department of Biological Science and Technology**,** National Chiao Tung University, Taiwan.

HONORS & SCHOLARSHIP：

Sep/2008 - Jun/2009	Travel fellowship, 21st IUBMB-12th FAOBMB congress
	Second place award, 2009 poster contest of the college of Biological and Technology, NCTU
Sep/2007 - Jan/2008	Academic Achievement Award
Sep/2003 - Jun/2004	Scholarship of Cathay Life Insurance

LEARENED BIOLOGICAL SKILLS：

Cloning, Cell Culture, RNA extraction, RT-PCR, plaque assay, Western Blotting, virus amplification

EXTRACURRICULAR ACTIVITY：

2008-2009	**Representative, Graduates Association**, Department of Biological Science and Technology, NCTU
2005	**Staff**, Biological Science and Technology Camp, NCTU
Sep/2004 - Feb/2005	**Staff**, 5th Life Science Cup, NCTU
Sep/2004 - Jun/2005	**Chief of Public Relation**, Biological Science and Technology Association, NCTU
2003	**Member, inspection committee**, Biological Science and Technology Association, NCTU
2003	**Actress**, president's drama contest